Local thermal non-equilibrium effects
and thermal retardation in natural porous media:
Laboratory experiments and numerical modeling

Manuel Alexander Gossler

Ingenieurfakultät Bau Geo Umwelt

Lehrstuhl für Hydrogeologie

Local thermal non-equilibrium effects and thermal retardation in natural porous media: Laboratory experiments and numerical modeling

Manuel Alexander Gossler

Vollständiger Abdruck der Ingenieurfakultät für Bau Geo und Umwelt der Technischen Universität München zur Erlangung des akademischen Grades eines

Doktor - Ingenieurs (Dr.-Ing.)

genehmigten Dissertation

Vorsitzender: apl. Prof. Dr. rer. nat. habil. Thomas Baumann
Prüfer der Dissertation:
1.   Prof. Dr. rer. nat. Florian Einsiedl
2.   Prof. Dr.-Ing. Markus Disse
3.   Prof. Dr. rer. nat. Peter Bayer

Diese Dissertation wurde am 29.03.2021 bei der Technischen Universität München eingereicht und durch die Ingenieurfakultät Bau Geo Umwelt am 17.08.2021 angenommen.

Abstract

Knowledge about heat transport processes in natural porous media such as aquifers or streambeds is of high interest in various fields of research and engineering applications. Generally, when modeling heat transport, a local thermal equilibrium (LTE) between the fluid and solid phases is assumed. Yet, the mathematical and hydrogeological conditions and implications of the LTE simplification have not been fully established for natural porous media. Additionally, the implications of a deviation from the LTE assumption are so far unknown for heat transport modeling in the field. Furthermore, a widely used concept to determine water fluxes, mean transit times, and other parameters from heat tracer experiments is the use of the thermal retardation factor which, assuming LTE conditions, describes the ratio of the seepage velocity to the thermal velocity. This thermal velocity can be determined by different methods, depending on the input signal, from thermal breakthrough curves (BTCs) which have not been systematically compared yet. As a consequence, this thesis aims to clarify the following research questions: (i) Are local thermal non-equilibrium (LTNE) effects likely to occur in natural porous media? (ii) What are the induced errors and uncertainties if an LTE model is used under conditions in which the LTE assumption is not valid? (iii) Are estimations of parameters, such as the seepage velocity and the heat capacity, determined by using the thermal retardation factor, influenced by LTNE effects and which methods, e.g. utilizing the peak velocity or an analytical model, can be used to evaluate the thermal velocity from thermal BTCs?

To address these questions, in the first part of the thesis, one-dimensional column experiments were performed, and in the second part a numerical parameter study was conducted. More specifically, 43 one-dimensional column experiments with saturated gravel of grain size 7–15 mm were used to compare the transport of a conservative solute tracer with a thermal tracer transport. The measured, effective thermal retardation, possibly influenced by LTNE effects, was compared with the computed thermal retardation predicted by the apparent thermal retardation factor which assumes LTE. The results demonstrate that for scenarios with a step input of the heat tracer (continuous input), the effective thermal retardation for thermal velocities derived by an analytical model, and additionally the mean between injection temperature and initial temperature, can be predicted by the apparent thermal retardation factor. This indicates that possible LTNE effects do not significantly influence the derived velocities within the investigated range of seepage velocity between 5 and 50 m d^{-1} for the

used gravel. This is in accordance with the results of the numerical parameter study which show that LTNE effects do not significantly influence the advective thermal velocity. The other selected methods to derive the advective thermal velocity from thermal BTCs resulted in a constant deviation from the apparent retardation factor at higher seepage velocities. In scenarios with a pulse input of finite duration of the heat tracer, the effective retardation derived by the peak velocity showed deviations from the apparent retardation of up to 35% at seepage velocities lower than 10 m d^{-1}. At higher seepage velocities, the peak velocity could be predicted by the apparent retardation factor.

Subsequently, a numerical parameter study was conducted to extent the investigation of possible LTNE effects to other parameter settings expected in natural porous media. The conditions of forced convective heat transport in porous aquifers, under which the assumption of LTE applies and when it is expected to fail, were examined. To quantify the occurrence and effects of local thermal disequilibrium during heat transport, thermal breakthrough curves from an LTE model with those calculated using an LTNE model, explicitly allowing for different temperatures in the fluid and solid phases, were systematically compared. For the LTNE model, a new correlation for the heat transfer coefficient representative of the conditions in natural porous aquifers was developed using six published experimental results. By conducting an extensive parameter study (>50,000 simulations), it was shown that LTNE effects do not occur for grain sizes smaller than 7 mm or for seepage velocities that are slower than 1.6 m d^{-1}. The limits of LTE are likely exceeded in gravel aquifers or in the vicinity of pumped bores. For such aquifers, the use of an LTE model can lead to an underestimation of the effective thermal dispersion by a factor of 30 or higher, while the advective thermal velocity remains unaffected for most conditions. Thus, the results of the laboratory experiments were confirmed by the result of the numerical simulation. Based on a regression analysis of the simulation results, we provide a criterion which can be used to determine whether LTNE effects are expected for particular conditions.

To summarize, the results of the thesis clarify (i) that the LTE assumption can fail under conditions expected in natural porous media and (ii) that using an LTE model in LTNE favorable conditions results in a significant underestimation of the effective thermal dispersion, while the advective thermal velocity remains mostly unaffected. To the best of our knowledge, for the first time an LTE criterion is presented based on the influence of LTNE effects on a common

modeling parameter, the effective thermal dispersion, rather than theoretical temperature differences between the fluid and solid phases. Furthermore, (iii) it is revealed that methods for determining the advective thermal velocity from thermal BTCs, such as the peak velocity, can lead to significant deviations in flux estimates.

Zusammenfassung

Die exakte Vorhersage und ein genaues Verständnis von Wärmetransportprozessen in natürlichen porösen Medien wie Aquiferen sind in zahlreichen Feldern der Wissenschaft aber auch im angewandten Ingenieurwesen von großer Wichtigkeit. Generell wird dabei fast immer von der Gültigkeit einer fundamentalen Annahme ausgegangen, nämlich einem lokalen thermischen Gleichgewicht (LTE) zwischen der festen und der flüssigen Phase. Dabei wird angenommen, dass die Zeit, die nötig ist, damit sich feste und flüssige Phase thermisch ausgleichen, vernachlässigbar ist. In der Literatur gibt es allerdings Hinweise, dass die Annahme eines thermodynamischen Gleichgewichtes zwischen den beiden Phasen u.a. nicht für alle hydrogeologischen Systeme zutrifft. Des Weiteren beruhen viele Verfahren zur Auswertung von thermischen Tracerversuchen auf dem thermischen Retardationsfaktor, der unter LTE-Bedingungen das Verhältnis zwischen der Abstandsgeschwindigkeit des Fluids und der thermischen Fließgeschwindigkeit beschreibt. Hierbei werden verschiedene Methoden in der Literatur beschrieben, um aus Temperatur-Durchgangskurven thermische Geschwindigkeiten abzuleiten, beispielsweise die Nutzung des Temperaturmaximums oder eines analytischen Modells. Daher ist das Ziel dieser Arbeit zu klären, (i) ob, die LTE-Annahme in natürlichen porösen Medien gültig ist, (ii) welche Konsequenzen und Implikationen sich für die Wärmetransportmodellierung ergeben, falls ein LTE Modell genutzt wird, wenn die LTE Annahme aber nicht gültig ist, und (iii) ob die Parametern, die über thermische Tracerversuche bestimmt werden, durch Abweichungen von LTE Bedingungen beeinflusst sind. Darüber hinaus soll geklärt werde, welche Methoden, wie die Nutzung des Temperaturmaximums oder eines analytischen Modells geeignet sind, um die thermische Geschwindigkeit aus Temperatur-Durchgangskurven zu bestimmen.

Um diese Hypothesen zu überprüfen, wurden zunächst eindimensionale Säulenversuche durchgeführt, die anschließend mit einer numerischen Parameterstudie erweitert wurden. In den Laborversuchen wurden systematisch verschiedene experimentelle Ansätze zur Bestimmung der thermischen Geschwindigkeit miteinander verglichen. Durch eine Gegenüberstellung des effektiven thermischen Retardationsfaktors und des theoretischen thermischen Retardationsfaktors konnte der Einfluss lokaler thermischer Ungleichgewichtseffekte (LTNE) auf die thermische Geschwindigkeit untersucht werden. Hierzu wurden 43 eindimensionale Säu-

lenversuche mit wassergesättigtem Kies mit einer Korngröße im Bereich von 7-15 mm durchgeführt. Uranin wurde als konservativer Tracer genutzt, um die Abstandsgeschwindigkeit zu bestimmen. Diese wurde dann mit der aus den thermischen Durchgangskurven bestimmten Abstandsgeschwindigkeit verglichen. Die Ergebnisse zeigen, dass bei einem kontinuierlichen Eintrag des thermischen Tracers die effektive thermische Retardation mit Hilfe des theoretischen thermischen Retardationsfaktors korrekt vorhergesagt werden kann. Dies gilt, wenn die thermische Geschwindigkeit durch ein analytisches Modell oder durch Ansetzen der mittleren Temperatur zwischen Eingabe- und Ausgangstemperatur als thermischer Durchbruch bestimmt wird. Diese Ergebnisse zeigen, dass LTNE Effekte für die untersuchten Abstandsgeschwindigkeiten von 5-50 m d^{-1} und die untersuchte Korngröße die thermische Geschwindigkeit nicht signifikant beeinflussen. Die Beobachtungen werden auch durch die Ergebnisse der numerischen Parameterstudie bestätigt. Bei thermischen Tracern mit zeitlich begrenzten Temperaturpulsen weicht die effektive thermische Retardation, die durch die Geschwindigkeit des Temperaturmaximums bestimmt wird, um bis zu 35 % von der theoretischen thermischen Retardation bei Abstandsgeschwindigkeiten von weniger als 10 Metern pro Tag ab. Bei höheren Abstandsgeschwindigkeiten konnte die Geschwindigkeit des Temperaturmaximums mit dem erwarteten thermischen Retardationskoeffizienten vorhergesagt werden.

Um mögliche LTNE Effekte für den gesamten Parameterraum poröser Aquifere zu untersuchen, wurde im zweiten Teil eine numerische Parameterstudie durchgeführt. Dabei wurde geprüft, unter welchen Bedingungen die LTE Annahme gültig ist und unter welchen Randbedingungen die Annahme nicht mehr gegeben sind. Um Auftreten und Auswirkungen möglicher LTNE Effekte zu quantifizieren, wurden systematisch thermische Durchgangskurven eines LTE Modells mit denen eines LTNE Modells, das Temperaturunterschiede zwischen fester und flüssiger Phase berücksichtigt, verglichen. Dazu wurde zunächst ein für die Bedingungen von porösen Aquiferen geeigneter Wärmeübergangskoeffizient auf Basis der experimentellen Daten von sechs Veröffentlichungen bestimmt. Die umfangreiche Parameterstudie (> 50 000 Simulationen) zeigt, dass LTNE Effekte bei Korngrößen kleiner als 7 mm und Abstandsgeschwindigkeiten von weniger als 1,6 Metern pro Tag nicht zu erwarten sind. Diese Grenzwerte können allerdings in kiesigen Aquiferen oder in der Nähe von Grundwasserbrunnen überschritten werden. Unter diesen Bedingungen kann die Nutzung eines LTE Modells somit zu einer Unter-

schätzung der effektiven thermischen Dispersion bis zu einem Faktor von über 30 führen, während die advektive thermische Geschwindigkeit durch LTNE Effekte meist unbeeinflusst bleibt. Diese Resultate bestätigen auch die Ergebnisse der durchgeführten Laborversuche. Auf Basis einer Regressionsanalyse der Simulationsergebnisse wurde ein Kriterium entwickelt, das es ermöglicht zu überprüfen, inwieweit LTNE Effekte für die vorherrschenden, hydrogeologischen Verhältnisse zu berücksichtigen sind.

Zusammenfassend konnte gezeigt werden, dass (i) die LTE Annahme bei hohen Fließgeschwindigkeiten und Korngrößen, wie sie zum Beispiel in Kiesaquiferen zu erwarten sind, nicht gültig ist. (ii) Die Nutzung eines LTE Modells kann dann zu einer Unterschätzung der thermischen Dispersion bis zu einem Faktor von über 30 führen, während die advektive Geschwindigkeit kaum beeinflusst wird. Hierzu wird ein Kriterium vorgestellt, dass es erlaubt einfach abzuschätzen, ob LTNE Effekte zu erwarten sind. Während bisherige Kriterien meist auf theoretischen Temperaturdifferenzen zwischen fester und flüssiger Phase basieren, ist dies das Erste, das auf dem Einfluss von LTNE Effekten auf einen üblichen Modellierungsparameter basiert, der effektiven thermischen Dispersion. Außerdem wird gezeigt, (iii) dass manche Methoden zur Bestimmung der thermischen Geschwindigkeit aus Temperaturdurchgangskurven wie die Nutzung des Temperaturmaximums zu signifikanten Abweichungen bei der Berechnung der Grundwasserfließgeschwindigkeit führen können.

Publications

Some text, figures and tables have appeared previously in the following publications:

Experimental investigation of thermal retardation and local thermal non-equilibrium effects on heat transport in highly permeable, porous aquifers

Manuel A. Gossler, Peter Bayer and Kai Zosseder

On the Limitations and Implications of Modeling Heat Transport in Porous Aquifers by Assuming Local Thermal Equilibrium

Manuel A. Gossler, Peter Bayer, Gabriel C. Rau, Florian Einsiedl and Kai Zosseder

Acknowledgements

Table of contents

List of figures

Fig. 6: a) Qualitative temperature development for steady state injection of a fluid, which is injected into a porous medium of different temperature. In the early phase, the temperature between solid and fluid phase is unequal. After a certain amount of time thermal equilibrium is reached. The red dotted line shows the simplification made by the LTE model neglecting any kinetic effects from delayed intra particel diffusion. b) Depiction of the assumption made by the LTE approach in a simplistic aquifer representation. c) Thermal breakthrough curves of an LTE and LTNE model. The LTE

List of tables

List of abbreviations and acronyms

BTC   breakthrough curve

C-S   continuous solid LTNE model

D-C   dispersion concentric LTNE model

LTE   local thermal equilibrium

LTNE   local thermal non-equilibrium

REV   representative elementary volume

Notations

Nomenclature

A	[m²]	cross-sectional area of the column	$Nu = \dfrac{h_{sf} d_p}{\lambda_f}$	[-]	Nusselt number
a_{sf}	[m⁻¹]	specific surface area solid-fluid per unit volume	P_i		i-th root of eq. (46a-d)
c	[J kg⁻¹ K⁻¹]	specific heat capacity	P_D	[-]	dispersion parameter
$D_{l,eff}$	[m² s⁻¹]	effective longitudinal thermal dispersion, eq. (3)	$Pe = \dfrac{qL}{D_{l,eff}}$	[-]	thermal Péclet number L as characteristic length
$D_{l,eff,fit}$	[m² s⁻¹]	effective thermal dispersion fitted with analytical LTE model, eq. (41)	$Pr = \dfrac{\eta c_f}{\lambda_f}$	[-]	Prandtl number
$D_l = \beta \left(\dfrac{\rho_f c_f}{\rho_b c_b} q\right)^2$	[m² s⁻¹]	longitudinal thermal mechanical dispersion model with square velocity relationship	q	[m s⁻¹]	specific discharge
$distance_{Pt100}$	[m]	distance of temperature sensor from inflow	Q	[m³ s⁻¹]	volume flow
d_p	[m]	particle diameter	R_{app}	[-]	expected / apparent thermal retardation eq. (7)
e	[J K⁻¹ m⁻² s⁻⁰·⁵]	thermal effusivity	R_{eff}	[-]	effective thermal retardation
h_{sf}	[W m⁻² K⁻¹]	heat transfer coefficient	r	[m]	radius of the column
L	[m]	characteristic length	$Re = \dfrac{\rho_f v_a d_p}{\eta}$	[-]	Reynolds number
LTNE	[-]	Measure to quantify degree of local-thermal non equilibrium	t	[s]	time
$LTNE_{cat}$	[-]	Criterion to estimate degree of LTNE, eq. (55)	t_{char}	[s]	characteristic time
M	[g]	mass of tracer	t_0	[s]	mean transit time
m_i		i-th root of eq. (45)	T	[-]	normalized temperature eq. (41)
n_{eff}	[-]	effective porosity (fluid volume fraction contributing to fluid flow)	T_b	[°C]	bulk temperature of REV
n_{tot}	[-]	total porosity, fluid volume fraction	T_0	[K]	initial temperature
N	[-]	Number of time steps	$T_{0,Celsius}$	[°C]	initial temperature

T_{degree}	[K]	temperature		η	[kg m^{-1} s^{-1}]	dynamic viscosity
$T_{inj,Kelvin}$	[K]	injection temperature in Kelvin		ρ	[kg m^{-3}]	specific density
$T_{inj,Celsius}$	[°C]	injection temperature in degree Celsius		τ	[s]	time period for analytical solution of LTNE model eq. (42-48); long enough to reach T = T$_{inj}$
T_{end}	[°C]	injection temperature after the pulse		τ_{pulse}	[s]	pulse duration of injection in column experiments
v_a	[m s^{-1}]	seepage velocity				
v_i		Part of analytical solution LTNE see eq. (47)		Subscripts:		
v_t	[m s^{-1}]	advective thermal velocity		s		solid
$v_{t,fit}$	[m s^{-1}]	advective thermal velocity fitted with analytical LTE model eq. (41)		f		fluid
$v_{therm\ peak}$	[m s^{-1}]	thermal peak velocity		b		bulk saturated porous media
$v_{therm\ peak\ dt/dT}$	[m s^{-1}]	thermal velocity of peak of first time derivative		LTE		local thermal equilibrium model
$v_{therm\ T25\ \|T50\|\ T75}$	[m s^{-1}]	thermal velocity corresponding to 0.25|0.50|0.75 of normalized thermal BTC		LTNE		local thermal non-equilibrium model
w		Part of analytical solution LTNE see eq. (43)		eff		referring to volume averaged effective property
w_i		Part of analytical solution LTNE see eq. (48)		method		method used to quantify LTNE
x	[m]	distance		analytical		modeled with analytical model
α_l^s	[m]	longitudinal solute dispersivity		numerical		modeled with numerical model
β	[s^{-1}]	thermal dispersivity				
λ	[W m^{-1} K^{-1}]	thermal conductivity				
κ	[m² s^{-1}]	thermal diffusivity				

Chapter 1 Introduction

1.1 Importance of heat transport modeling in natural porous media

Knowledge of heat transport in aquifers and surface water-groundwater interactions is of primary interest in many areas of hydrogeological research and practice. The following sections give a short overview of the various applications of heat transport modeling in this field to emphasize the importance of a fundamental understanding of its processes, i.e. thermal advection, thermal dispersion, and the heat transfer between the fluid and solid phases.

Shallow geothermal energy systems often use groundwater to exchange heat with the subsurface for domestic or industrial heating or cooling purposes (Fig. 1a). These induced changes in the groundwater temperature are strongly influenced by the relative dominance of heat conduction or advection. In aquifers, especially with high seepage velocities (i.e. pore-water velocity or interstitial velocity), advective heat transport can generate far-reaching thermal plumes (Banks, 2015; Seibertz et al., 2016; Muela Maya et al., 2018). While robust estimation of the governing hydraulic and thermal parameters is crucial for system performance prediction (Hermans et al., 2018), it is also relevant for management of multiple adjacent installations. For example, reliable prediction of thermal plumes in shallow geothermal energy systems is crucial for a sustainable operation, especially in densely used aquifers (Ferguson, 2009; Hähnlein et al., 2013; Böttcher et al., 2019; Attard et al., 2020; Pophillat et al., 2020). Fig. 1b shows the spreading of thermal plumes of groundwater heat pump systems in a scenario analysis for a residential area (Urich et al., 2010). The utilization of the shallow geothermal energy in the groundwater is limited by possible thermal breakthroughs between adjacent systems. Thermal interference can mitigate technological performance and can yield temperature changes in the shallow groundwater beyond environmentally and regulatory critical thresholds (Epting et al., 2017; Böttcher et al., 2019). As the exact values of an environmentally critical increase of groundwater temperatures are still not fully clear (e.g. Brielmann et al., 2009; Bonte et al., 2013a; Casasso and Sethi, 2019) the legislation framework in European countries is also very heterogeneous ranging from minimum distances between such systems from 5-300 m and tolerable temperature changes in the subsurface from 3-10 K (Haehnlein et al., 2010; Tsagarakis et al., 2018; García-Gil et al., 2020). In order to prevent negative influences, a precise prediction of heat transport processes is fundamental to ensure a sustainable usage of these systems.
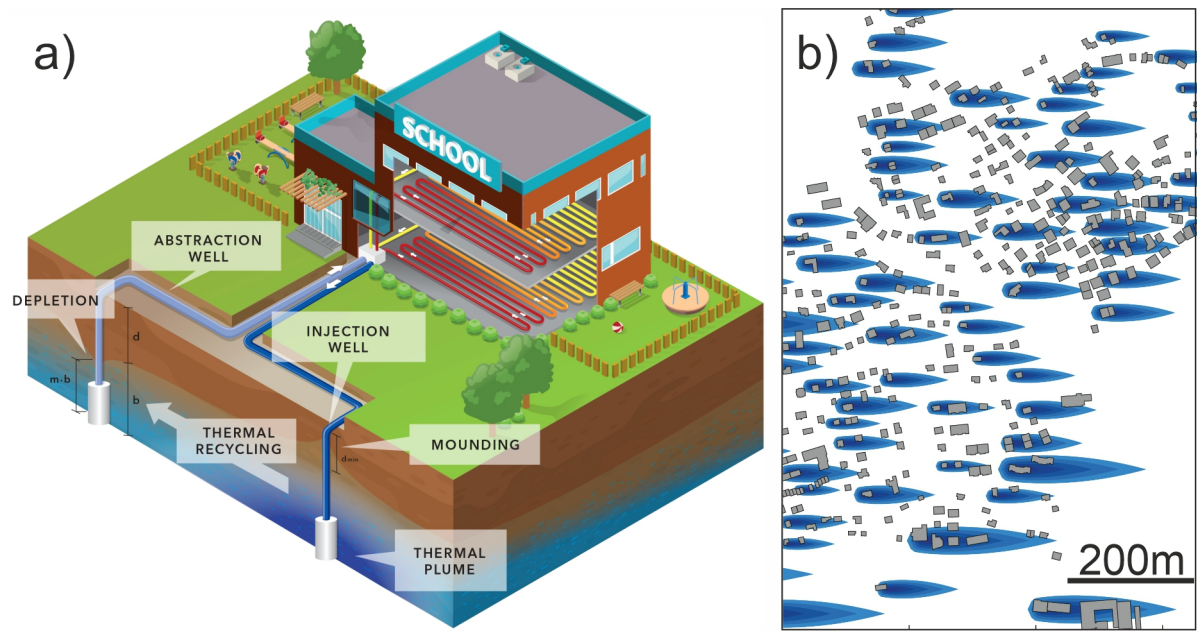
Fig. 1: a) Schematic operation scheme of a groundwater heat pump system. Groundwater is extracted at the abstraction well and used by the heat pump as an environmental energy source for heating or cooling purposes. The heated or cooled groundwater is reinjected into the aquifer, causing a thermal plume (www-01). b) Example of a densely used aquifer with several thermal plumes depicted in blue and buidlings outlined in gray (modified after Urich et al., 2010).

Aside from the rising interest in groundwater effects of geothermal applications, the thermal conditions in aquifers are also studied in other contexts. Using natural or actively stimulated temperature changes in hydrogeological settings as a thermal tracer is a common approach. Thermal tracers commonly utilize the advective heat transport of groundwater flow which affects the temperature distribution. Groundwater fluxes are usually estimated by measuring the deviations of subsurface temperatures from what would be expected under purely conductive conditions (Kurylyk and Irvine, 2019).

Using heat has several benefits as summarized by multiple authors (Anderson, 2005; Constantz, 2008; Rau et al., 2014; Kurylyk et al., 2017; Kurylyk and Irvine, 2019):

- Readily available, often natural temperature signals are present (diurnal, seasonal etc.)

- Inexpensive to measure in high temporal and spatial resolution (e.g. fibre-optic distributed temperature sensing) without time consuming laboratory analysis

- Environmentally benign as no artificial substances are injected

A common field for utilizing heat as a tracer are surface water-groundwater interactions. The mixing zone between groundwater and surface water flow systems, often called hyporheic zone, is of high ecological significance and plays an important role in riverine ecosystem services (Kurylyk et al., 2015; Ren et al., 2018). Furthermore, it is a critical pathway for contaminants and can represent a natural bioreactor for oxic and anoxic biotransformation and exerts a major control on river water quality (Weatherill et al., 2018; Lewandowski et al., 2019). Knowledge about spatial and temporal flow patterns, transient storage and other processes in this zone is especially needed to understand ecological habitats (Findlay, 1995; Kurylyk et al., 2015), to manage water resources (Brunke and Gonser, 1997; Boulton et al., 1998) and can be vital to determine the fate and transport of groundwater contaminants (Conant, 2004). The spatiotemporal variability in the surface water-groundwater exchange fluxes and directions are difficult to characterize and to quantify accurately, which is largely attributed to the high spatiotemporal heterogeneity in streambed hydraulic properties. Heat can serve as one valuable tracer to quantify these surface water-groundwater interactions and is frequently used in this context (Rau et al., 2010, 2012a, 2017; Irvine and Lautz, 2015; Halloran et al., 2016; Kurylyk et al., 2019; Irvine et al., 2020). Heat tracing methods are used in diverse environments and various spatiotemporal scales (Fig. 2) and have become a very valuable tool in many fields (Kurylyk et al., 2019).

a) Local processes   b) Regional processes
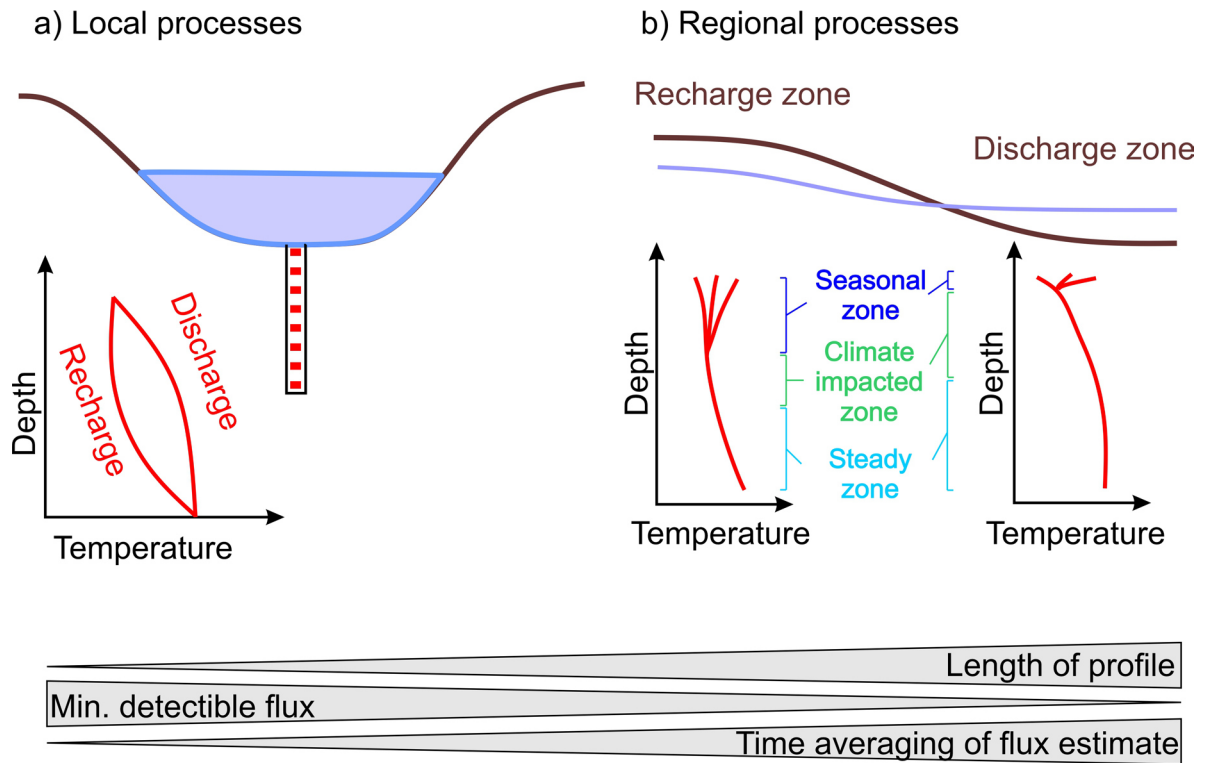
Fig. 2: Heat as a tracer and temperature depth profiles are used in different time and spatial scales. These scales can be local processes (a), e.g., to estimate local short timed, surface-groundwater interactions in a streambed environment, to intermediate and regional scales (b) investigating seasonal effects (modified after Kurylyk et al., 2019).

Besides in surface water-groundwater interaction, temperature patterns are often utilized as thermal tracers in managed aquifer recharge systems and riverbank filtrations. While knowledge of the mean transit time is also important in the afore mentioned applications, it is essential in water resources management for the evaluation and the reduction of the contamination risk, as longer residence times lead generally to higher pathogen inactivation and biodegradation (Toze et al., 2010; Bekele et al., 2014; Ahmed and Marhaba, 2017). The water temperature of the infiltration ponds or the river varies with the ambient temperature. These diurnal or seasonal temperature variations are reflected in the aquifer (Fig. 3). Variations in the amplitude ratios and phase shifts between the pond or river temperature and the groundwater temperature at the observation point can be used to estimate the mean transit time by applying analytical or numerical methods (Laws et al., 2011; Vandenbohede and Van Houtte, 2012; Seibert et al., 2014; Irvine et al., 2017; Moeck et al., 2017).
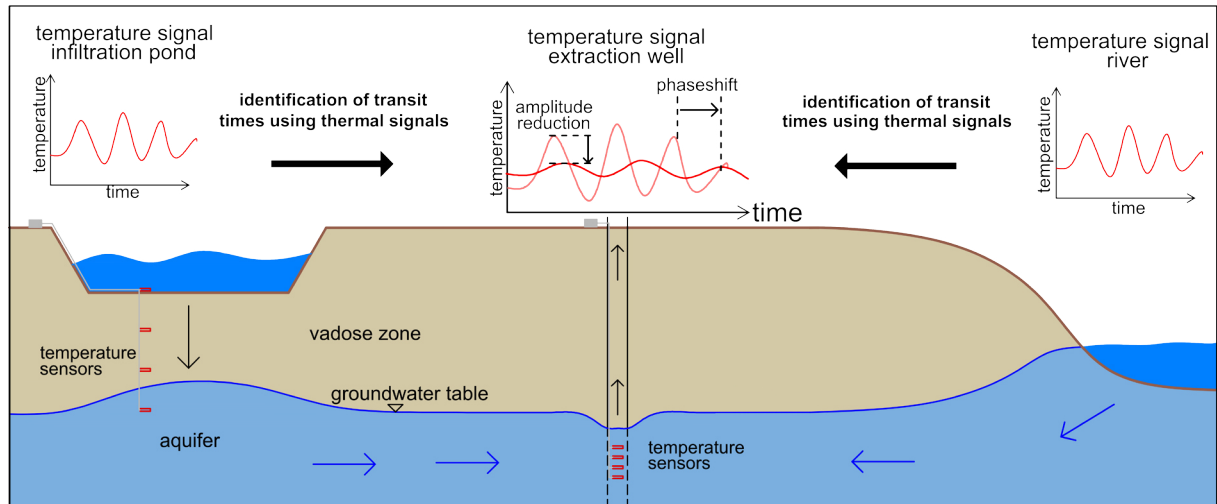
Fig. 3: Simplified schematic of a managed aquifer recharge system and a riverbank filtration. Temperature signals originating from the infiltration pond or the river can be used in the aquifer to estimate mean transit times.

When modeling heat and solute transport in aquifers, the spatial heterogeneity of the hydraulic conductivity distribution is often the most uncertain parameter (Vienken and Dietrich, 2011). Apart from direct measuring methods such as pumping tests, slug tests, borehole flowmeter tests etc., the hydraulic conductivity field can also be inversely estimated as a calibration target in a numerical model. While often hydraulic head data is used for calibration, groundwater temperatures proved also to be an additional or alternative valuable source of information (e.g. Irvine et al., 2013; Colombani et al., 2015; Djibrilla Saley et al., 2016). Furthermore, active thermal tracer experiments showed very positive results in estimating the hydraulic conductivity field in a tomographic setup (Fig. 4) within advection dominated conditions (Seibert et al., 2014; Somogyvári et al., 2016; Somogyvári and Bayer, 2017).
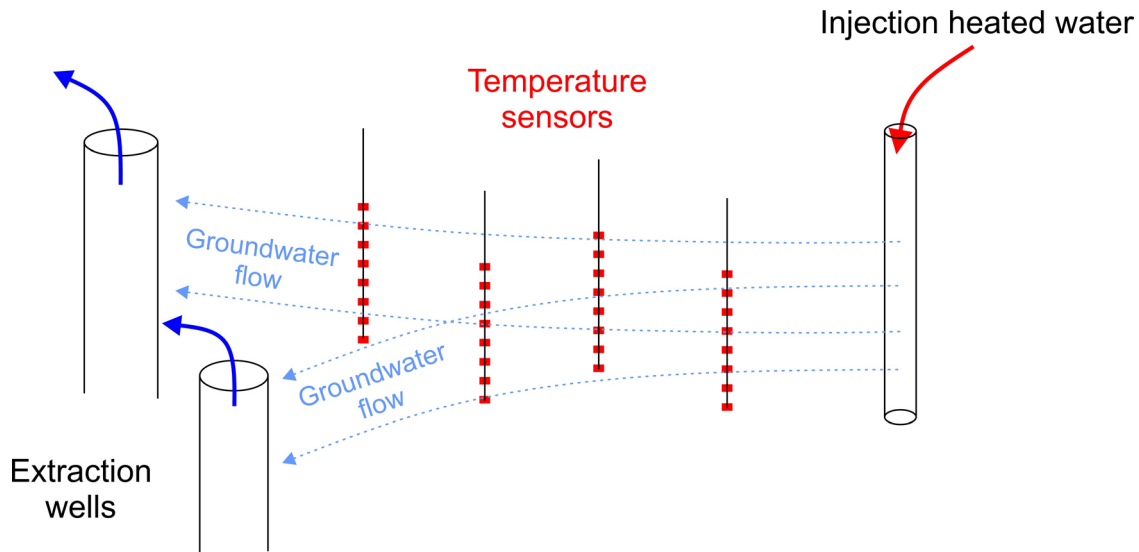
Fig. 4: Experimental design of a thermal tracer field experiment by Somogyvári & Bayer (2017). In this study, the thermal tracer was used to estimate the hydraulic conductivity field. (modified after Somogyvári and Bayer, 2017)

1.2 Modeling approaches (LTE and LTNE)

To summarize, knowledge of heat transport in natural porous media is of high importance in various fields and disciplines in practice and research, as described above. However, in all of the above mentioned applications the fundamental assumption of a local thermal equilibrium (LTE) is generally applied (e.g. Hoehn & Cirpka, 2006; Markle & Schincariol, 2007; Stauffer et al., 2013; Bekele et al., 2014; Irvine et al., 2015; Sarris et al., 2018). LTE is defined as an instant exchange of thermal energy between the solid and the fluid phases of a porous medium, an assumption which neglects potential temperature differences between these phases (Quintard et al., 1997). This means in other words that it is assumed that heat diffusion into the matrix is sufficiently quick at the thermal front, so that any kinetic effects from delayed intra-particle diffusion can be ignored.

Previous work about the general validity of the LTE assumption in porous media focused on engineering applications such as packed bed reactors (Amiri and Vafai, 1998; Al-Nimr and Abu-Hijleh, 2002; Khashan and Al-Nimr, 2005; Al-Sumaily et al., 2013). While several criteria, often theoretically derived formulas using involved parameters such as thermal conductivity of the fluid and solid phase, exist to examine the appropriateness of the LTE assumption for such applications (Amiri and Vafai, 1998; Minkowycz et al., 1999; Kim and Jang, 2002; Khashan and Al-Nimr, 2005; Zhang et al., 2009; Dehghan et al., 2014a; Zanoni et al., 2017; Hamidi et al.,

2019; Novak, 2019), a thorough investigation of the conditions under which LTE is valid for flow in porous aquifers and surface water-groundwater interactions is currently lacking. In fact, adopting the criteria developed for engineering purposes is not straightforward, as the experimental conditions and reference parameters are not representative for those typical of flow in porous aquifers. For example, the required "characteristic length" in technical applications is commonly defined as channel length or width and cannot easily be determined for heat transport in subsurface environments.

Some of the few studies focusing on geotechnical applications showed that the LTE assumption can fail (i) in geothermal systems hosted in fractured rocks (Shaik et al., 2011; Heinze and Hamidi, 2017; Heinze et al., 2017), (ii) in partly saturated systems for example during infiltration of rain or melt water in frozen soil (Heinze and Blöcher, 2019), (iii) in fractured rocks as heterogeneous porous media with large permeability contrasts (Hamidi et al., 2019), and (iv) under streambed conditions with very low Reynolds numbers (Roshan et al., 2014).

In these cases, a local thermal non-equilibrium (LTNE) model should be applied. LTNE models use two separate energy equations to describe the temperature in the fluid and solid phases that are coupled through a heat transfer term, which is dependent on the heat transfer coefficient and the heat transfer area (Sözen and Vafai, 1990). The heat transfer coefficient, commonly described in a dimensionless form as the Nusselt number, is a fundamental physical parameter whose value is usually determined experimentally (Kaviany, 1995). Again, available experimental work stems from the engineering field and the derived parameter values and correlations are valid only under certain conditions (Tavassoli et al., 2013; Sun et al., 2015; Tavassoli et al., 2015; Singhal et al., 2017a, 2017b; Zhu et al., 2019). For instance, these correlations are mostly derived from air or gas as the fluid, using high Reynolds numbers and wider porosity ranges than are commonly found in porous aquifers (Gunn, 1978; Tavassoli et al., 2015; Zhu et al., 2019). In addition, most of these models assume perfect spheres with a single size (Sun et al., 2015) which should not be assumed for a heterogeneous and anisotropic aquifer.

Furthermore, it is difficult to identify and to quantify the errors and uncertainties induced by using an LTE model with the currently available LTNE measures. Standard criteria such as the temperature difference between fluid and solid phases (Khashan and Al-Nimr, 2005; Khashan et al., 2006; Al-Sumaily et al., 2013; Abdedou and Bouhadef, 2015) or the difference between

the local fluid temperatures of both models (Lu and Xiang, 2012; Hamidi et al., 2019) have a technical meaning and the transition to a natural environment is difficult. The implications for heat transport modeling in the field are mostly unknown.

Besides the uncertainty from the LTE assumption, different methods are used to evaluate the above described use cases (section 1.1). In prediction related applications, typically numerical or analytical methods are used (e.g. Zhou et al., 2013; Lo Russo et al., 2016; Ganguly et al., 2017), for example, when assessing the thermal impact induced by geothermal applications. Most of the commonly applied simulation codes only consider LTE models.

When using heat as a tracer to determine water fluxes, mean transit times, or other parameters such as the volumetric heat capacity from heat tracer experiments, thermal breakthrough curves (BTCs) are commonly analyzed (e.g. Becker et al., 2015; Moeck et al., 2017; Somogyvári and Bayer, 2017). In many of these applications, the thermal velocity is of high interest, as it is a proxy for the groundwater flux. The groundwater flux is estimated by applying the thermal retardation factor which describes the ratio of seepage velocity to thermal velocity (Bodvarsson, 1972; Woods and Fitzgerald, 1993, 1997; Shook, 2001). Different methods are available to determine the thermal velocity from thermal BTCs depending on the input signal. For example some studies with pulse input of finite duration use the peak velocity (modal velocity) (e.g. Taniguchi and Sharma, 1990; Lewandowski et al., 2011; Wagner et al., 2014) while others use lag times from maximum cross correlations (Hoehn and Cirpka, 2006; Moeck et al., 2017). Whether these methods give accurate estimates of the advective thermal velocity has not been thoroughly examined, as studies which systematically investigate the seepage velocities derived from heat tracers and solute tracers are scarce (Taniguchi and Sharma, 1990; Rau et al., 2012a, 2012b; Irvine et al., 2013; Bandai et al., 2017). Their results are also not consistent: some works reveal a good agreement (Irvine et al., 2013), while others found systematic over- or underestimation of the derived seepage velocities (Rau et al., 2012a, 2012b; Bandai et al., 2017). Other studies used both heat and solute tracers, but did not make a systematic comparison between heat- and solute-derived velocities (Constantz et al., 2003; Vandenbohede et al., 2009; Ma et al., 2012; Seibert et al., 2014; Wildemeersch et al., 2014; Bakker et al., 2015; Becker et al., 2015; Klepikova et al., 2016; Bonner et al., 2017; Sarris et al., 2018).

1.3 Aims and objectives

Collectively, it is revealed that the commonly applied LTE assumption for heat transport has not yet been thoroughly investigated for natural porous media, especially for highly permeable aquifers. The implications of using an LTE model and the effects to be expected when it fails remain unclear. Suitable Nusselt correlations for conditions expected in porous aquifers to determine the heat transfer coefficient necessary for applying an LTNE model do not exist. Furthermore, methods for the determination of the advective thermal velocity from thermal BTCs have not been systematically compared.

Considering this background, the key questions of this thesis are:

- (i) Are LTNE effects likely to occur in natural porous media such as aquifers and streambeds and under which hydrogeological conditions is the LTE assumption valid?

- (ii) How does a deviation from LTE conditions affect heat transport modeling? What are the arising errors and uncertainties if an LTE model is used but the LTE assumption between fluid and solid phase is not valid?

- (iii) Are estimations of parameters, such as the seepage velocity and the heat capacity, determined by using the thermal retardation factor, influenced by LTNE effects and which methods, e.g. utilizing the peak velocity or an analytical model, can be used to evaluate the thermal velocity from thermal BTCs for different types of injections such as a step input (continuous load) or a pulse input of finite duration?

The scientific approaches to answer these questions are described in the following.

To investigate the influence of LTNE effects on the advective thermal velocity (ii) and, therefore, on estimates of seepage velocities or the bulk heat capacity (iii) one dimensional (1D) column experiments with heat as a tracer, and Uranine as a conservative solute tracer to calculate the hydraulic and sediment parameters are conducted. The role of the applied thermal signal under varying hydraulic conditions is assessed and different methods such as utilizing the peak velocity or fitting of an analytical model are contrasted to determine the thermal velocity (iii). We hypothesize that LTNE effects lead to a deviation between the measured effective thermal retardation and the expected thermal retardation which assumes LTE. To reach this goal the fluorescence dye Uranine was used as conservative tracer to determine the seepage velocity v_a. This true velocity obtained from the tracer experiments with Uranine

was subsequently compared with the advective thermal velocity derived from the thermal breakthrough curves.

To extent this investigation to other parameter settings expected in natural porous media (i) such as different porosities, thermal conductivities, particle sizes etc., a numerical parameter study was conducted. We examine the conditions of forced convective heat transport in natural porous aquifers under which the assumption of LTE applies and determine when it is expected to fail. To achieve this, we systematically compared thermal breakthrough curves calculated using LTE and LTNE models for a range of parameter values that are typical of realistic aquifer conditions and evaluated the influence of LTNE effects (ii). Finding an appropriate Nusselt number (*Nu)* correlation, a dimensionless form of the heat transfer coefficient, for porous aquifers is difficult as the existing correlations are developed for technical applications. Therefore, we developed a new *Nu* correlation to determine the heat transfer coefficient representing the conditions expected in porous aquifers using all available datasets. Finally, we present discrete limits for the conditions under which the commonly used LTE model is applicable when heat transport in porous aquifers is quantified.

1.4   Structure of the thesis

This thesis is organized into five chapters. The first chapter introduces the problem, the research gap, and its significance. The thesis objectives and aims are set out. Chapter two presents the state of the art in heat transport modeling in natural porous media focusing on LTE and LTNE models and existing LTE criterions and heat transfer coefficients. Chapter three describes the methods and the materials used to address the research questions. The first part of chapter three describes the setup, the procedure, and the evaluation methods of the conducted laboratory experiments. Chapter 3.2 lays out the procedure and the approach of the numerical parameter study. The results and discussion of the laboratory experiments and the numerical parameter study are given in the fourth part of the thesis. Chapter five synthesizes the main findings of the results and discusses their implications in a broader scientific context and concludes the thesis with a short outlook on future research objectives.

Chapter 2   State of the art

The following section gives first a short overview of the theoretical basis of heat transport modeling in porous media. Extensive explanations on this broad topic are for example given in Bear (1972), Carbonell and Whitaker (1984), Domenico and Schwartz (1998), Kaviany (1995), Nield and Bejan (2017) and Whitaker (1999). Then the current state of the art on the validity of the LTE assumption, LTNE models and evaluation of thermal breakthrough curves is summarized.

2.1   Volume averaging of a porous medium

A porous medium is generally regarded as a composite medium containing mostly intercon-nected voids and a solid matrix (Nield and Bejan, 2017). In the context of aquifers and streambeds the porous medium usually consists of two or three phases, the solid phase, e.g. gravel and a gaseous (air) and or a liquid phase (water) (Bear, 1972). On the pore scale level a description of the heat transport and fluid dynamics is very complex requiring an exact de-scription of the geometry of the pore structures and solid surfaces (Bear, 1972). To overcome this difficulty, simplifying approaches are used to describe fluid flow and heat transport in porous media (Quintard, 2015). One of the most common methods used is volume averaging with homogenization to reach a macroscopic continuum domain. This requires a definition of volume averaged expressions of the relevant parameters such as velocity, pressure, temper-ature of the fluid and solid phases etc. (Kaviany, 1995; Obembe et al., 2016). This is usually done by starting with the pore scale equations and spatially averaging over volumes or areas to reach a macroscopic scale (Nield and Bejan, 2017). A prominent example would be the derivation of Darcy's law by the methods of volume averaging over the velocity field in pore space described by the Navier-Stokes' equations (e.g. Whitaker, 2000). This necessitates the definition of a representative elementary volume (REV) which allows to describe a pore scale variable as an appropriate mean over a sufficiently large volume, the REV. The length scale of the REV should be much larger than the pore scale but significantly smaller than the length scale of the macroscopic flow domain (Fig. 5). The scale of the REV is highly dependent on the heterogeneity of the porous medium, usually increasing with the heterogeneity of the phase distribution and particle size (Bear, 1972).
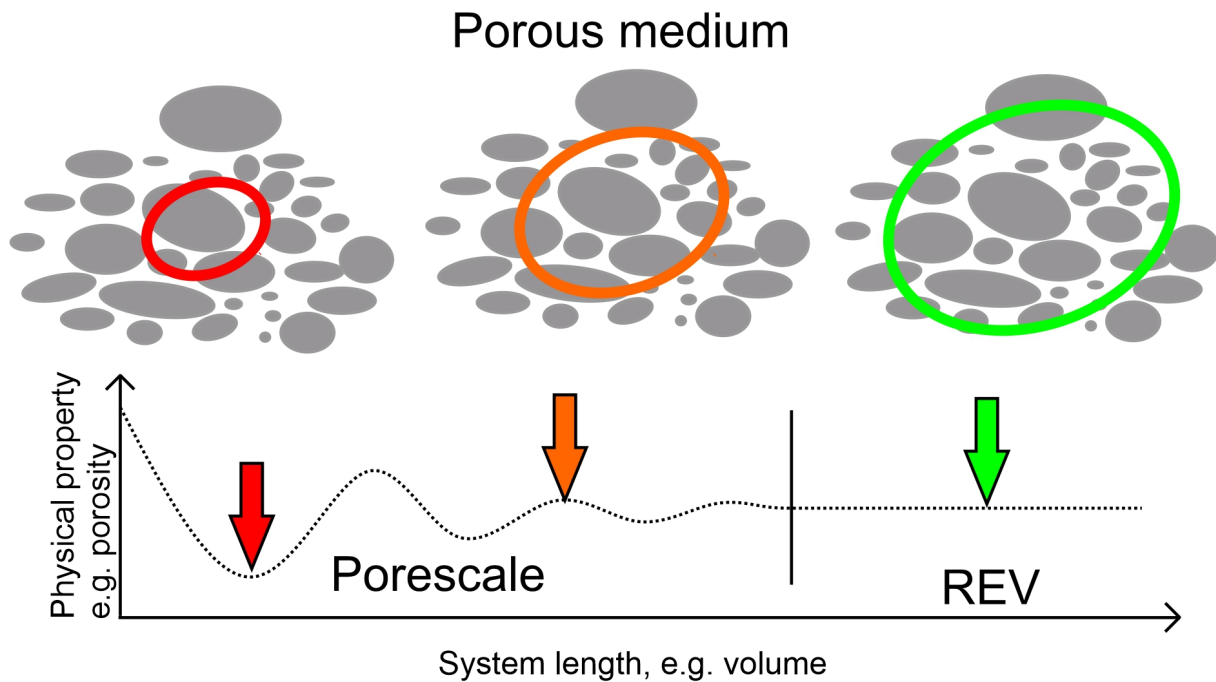
Porous medium

Fig. 5: Concept of the representative elementary volume for a heterogeneous phase distribution of a natural porous media. In the microscopic domain, the property varies strongly, with increasing system length reaching an apropriate mean value in the REV domain (modified after Rau et al., 2014).

When an appropriate REV is defined, the macroscopic heat flow can be described by effective volume averaged parameters such as the thermal and hydraulic conductivities, porosity, heat capacity etc. (Kaviany, 1995). These effective parameters can be influenced by several factors, the effective thermal conductivity of the solid phase for example depends on its structure and continuity, the contact resistance between adjacent particles, the material itself etc. Therefore, defining appropriate effective parameters is not straightforward and often relies on laboratory experiments or simplified approaches.

2.2   Local thermal equilibrium model

Generally, at the pore level there will be a difference at a point in the REV between the fluid temperature and the solid temperature ΔT_{sf}. The same applies to temperatures across the REV ΔT_{REV}. The local thermal equilibrium approach assumes that these temperature differences are much smaller than the temperature over the whole system ΔT_{system} (Kaviany, 1995) and can be neglected:

$$\text{LTE:} \quad \Delta T_{sf} \ll \Delta T_{REV} \ll \Delta T_{system}$$

$$T_{LTE} = T_s = T_f \tag{1}$$

The LTE assumption allows for merging of the two separate energy equations describing temperature in the fluid and solid phases into one, simplifying the modeling procedure by volumetric averaging (Whitaker, 1991). In other words, instead of describing the temperature development in the fluid and solid phase separately, the LTE approach uses one temperature for both phases by assuming a negligible temperature difference between the solid and fluid phases. The LTE model is sometimes also referred to as homogenous model, one-temperature model or one-equation model (Rees and Pop, 2005; Singh et al., 2006; Obembe et al., 2016).

Three processes influence heat transport in a porous medium, conduction, radiation and advection which is in the engineering literature often named convection (Nield and Bejan, 2017). Conductive heat transport can be described by Fourier's law where heat from regions of high temperatures is transferred to those of low temperatures analogue to the molecular diffusion process described by Fick's law in solute transport (Domenico and Schwartz, 1998). Advective heat transport is the thermal energy transported with the moving fluid which can be macroscopically described by Darcy's law in a porous medium (Bear, 1972). Radiative heat transport is generally neglected in heat transport processes in the subsurface due to the very low part in the overall heat transport (Halloran et al., 2016). Advective heat transport also induces thermal mechanical dispersion which acts macroscopically similar to thermal conduction (Anderson, 2005). Thermal mechanical dispersion is thought of as a result of the pore level temperature and velocity variations due to the nonuniformity of the flow field (Özgümüš et al., 2013). The role of thermal mechanical dispersion in heat transport processes in porous media is not fully clear (Bear, 1972; Hopmans et al., 2002; Stonestrom and Constantz, 2003; Irvine et al., 2013; Park et al., 2015, 2018). Specifically, this is the case regarding its relationship to the specific discharge (linear or power law) and with respect to scale dependency (Yagi et

al., 1960; Metzger et al., 2004; Anderson, 2005; Vandenbohede et al., 2009; Rau et al., 2012b; Bandai et al., 2017; Afshari et al., 2019). Rau et al. (2012b) investigated the thermal dispersion with extensive coupled solute and heat tracer experiments and concluded that a power law relationship is suited for describing the thermal dispersion behavior in porous media. Following these suggestions, the propagation of thermal energy in a porous medium under local thermal equilibrium can be described by the advection-conduction equation (Kaviany, 1995; Nield and Bejan, 2017). The equations are as follows:

$$\frac{\partial T}{\partial t} = D_{l,eff} \frac{\partial^2 T}{\partial x^2} - v_{t,LTE} \frac{\partial T}{\partial x} \tag{2}$$

$$D_{l,eff} = n_{tot} \left(\frac{\lambda_f}{\rho_b c_b} + D_l \right) + \frac{(1 - n_{tot})\lambda_s}{\rho_b c_b} \tag{3}$$

$$D_l = \beta \left(\frac{\rho_f c_f}{\rho_b c_b} q \right)^2 \tag{4}$$

$$\kappa = \frac{\lambda}{\rho c} \tag{5}$$

$$\lambda_b = n_{tot}\lambda_f + (1 - n_{tot}) \lambda_s \tag{6}$$

The first part on the right side of eq. (2) is the effective thermal dispersion coefficient $D_{l,eff}$ [m² s⁻¹] (eq. 3) consisting of the thermal diffusivity κ [m² s⁻¹] (eq. 5) and thermal mechanical dispersion coefficient D_l [m² s⁻¹] (eq. 4) described by a power law with the specific discharge q [m s⁻¹], the thermal dispersivity β [s⁻¹], $\rho_{f,s,b}$ [kg m⁻³] as the specific density of the fluid, solid or bulk porous media, $c_{f,s,b}$ [J kg⁻¹ K⁻¹] as the specific heat capacity of the fluid, solid or bulk porous media, and n_{tot} [-] as the total porosity (Rau et al., 2012b).

The thermal diffusivity κ [m² s⁻¹] (eq. 5) is the ratio of thermal conductivity λ [W m⁻¹ K⁻¹] to volumetric heat capacity ρc [J m⁻³ K⁻¹]. The thermal conductivity is here based on an arithmetic mean model of the effective thermal conductivity (eq. 6) which is frequently used (e.g. Whitaker, 1991; Quintard and Whitaker, 1995; Nield and Bejan, 2017) with λ_b [W m⁻¹ K⁻¹] as the effective thermal conductivity of the saturated porous medium and $\lambda_{f,s}$ [W m⁻¹ K⁻¹] as the effective thermal conductivity of the fluid and solid phase. As described above, defining appropriate effective parameters is not straightforward and influenced by many factors such as

the structure and continuity of the solid phase, the contact resistance between adjacent particles, the material itself etc. (Van Antwerpen et al., 2010). Numerous other models to derive an effective thermal conductivity exist e.g. the geometric mean or harmonic mean model etc. An extensive overview showing over 30 other mixing law models to determine an effective thermal conductivity is given in Abdulagatova et al. (2009).

The second part on the right side of eq. (2) describes the advective heat transport process based on (eq. 7 and 8):

$$v_{t,LTE} = \frac{v_a}{R_{app}} = \frac{n_{tot}\rho_f c_f}{\rho_b c_b}\frac{q}{n_{tot}} = \frac{q\rho_f c_f}{\rho_b c_b} \tag{7}$$

$$R_{app} = \frac{\rho_b c_b}{n_{tot}\rho_f c_f} = 1 + \frac{(1 - n_{tot})\rho_s c_s}{n_{tot}\rho_f c_f} \tag{8}$$

with $v_{t,LTE}$ [m s^{-1}] as the advective thermal velocity, v_a [m s^{-1}] as the seepage velocity and R_{app} [-] as the apparent thermal retardation factor.

2.3 Validity of the LTE approach in porous media

When LTE is assumed for heat transport, the temperature difference between the solid and the fluid phase within a representative elementary volume (REV) is considered negligible. Numerous studies investigated the validity of this assumption mostly focusing on engineering applications. A thorough investigation of the conditions under which LTE is valid for flow in porous aquifers and surface water-groundwater interactions is currently lacking. Besides general packed beds (Whitaker, 1991; Kuznetsov, 1998; Lee and Vafai, 1998; Al-Nimr and Abu-Hijleh, 2002; Kim and Jang, 2002; Singh et al., 2006; Zhang et al., 2009), often special conditions are examined like: LTNE in pulsatile flow over a cylinder embedded in a porous channel (Al-Sumaily et al., 2013); LTNE in the presence of internal heat generation in the solid phase (Nouri-Borujerdi et al., 2007; Yang and Vafai, 2010; Fathi-kelestani et al., 2020); LTNE effects at the porous media – fluid boundary (Aguilar-Madera et al., 2011; Yang and Vafai, 2011); LTNE in microchannels filled with porous media (Buonomo et al., 2014), LTNE in condensing flow of a gas through a porous medium (Sözen and Vafai, 1990); LTNE in forced convection with non-Newtonian fluids through porous channels (Khashan and Al-Nimr, 2005); LTNE in free surface flow through porous media (Alazmi and Vafai, 2004); LTNE in packed beds with

conduction only (Carbonell and Whitaker, 1984; Quintard and Whitaker, 1995; Virto et al., 2009); LTNE in conditions with free convection in porous media (Bortolozzi and Deiber, 2001); LTNE in highly transient conditions in porous media (Minkowycz et al., 1999) and others (Dehghan et al., 2014a). Many of these studies are based on theoretical considerations or on analytical or numerical modeling with only a few using laboratory experiments (Wong and Dybbs, 1976; Levec and Carbonell, 1985a, 1985b; Yokoyama et al., 1997; Singh et al., 2006; Virto et al., 2009).

A few studies investigated LTNE effects for geotechnical applications mainly focusing on fractured rock, unsaturated conditions and the influence of heterogeneity. Heinze and Hamidi (2017) proposed a dual porosity LTNE model for fractured porous media for geothermal applications. Heinze et al. (2017) developed a dynamic heat transfer coefficient for an LTNE model of fractured rock which accounts for spatial heterogeneity and temporal changes in the flow and temperature field. Lu and Xiang (2012) investigated LTNE effects for a single fracture impermeable rock by analyzing the temperature difference between the LTE temperature and the LTNE fluid temperature using semi-analytical models. They concluded that significant temperature differences can occur at locations close to the heat source and at early times of the process. Shaik et al. (2011) investigated the role of LTNE effects on the economic potential of geothermal systems in a fractured host rock using a numerical model. They showed that an LTE model can lead to an underestimation of the hot water production temperatures. Yokoyama et al. (1997) used laboratory experiments and numerical modelling to investigate LTNE effects on aquifer thermal energy storage systems in free aquifers taking water level fluctuations into account. They concluded that LTNE effects resulted in an enlargement of the thermal block with less density of heat. Heinze and Blöcher (2019) developed an LTNE model for dynamic partly saturated porous media, for example for the infiltration of rainwater into cold soil. Novak (2019) studied LTNE effects during evaporation in soils defining a new LTE criterion for these conditions. The role of heterogeneity on LTNE effects was studied by Hamidi et al. (2019). They concluded that large permeability contrasts can lead to a deviation between the LTE temperature and LTNE fluid temperature of up to 7 %. Roshan et al. (2014) investigated the validity of the LTE assumption for streambed conditions with very slow flow conditions. They concluded that inferred pore water velocities assuming LTE conditions can be significantly overestimated due to LTNE effects and that this will be limited to very low seepage velocities. They reasoned that increasing seepage velocities lead to higher advective fluxes,

which increase the LTNE between the fluid and solid phase, but that this effect is significantly smaller than the increase of the heat transfer coefficient which comes along with increasing seepage velocities leading to LTE conditions.

To summarize, LTNE effects have been investigated for engineering applications and for special conditions in natural porous media. But the validity of the LTE assumption in common aquifer and streambed conditions and the consequences of a deviation from the LTE conditions are still unclear.

Some of the above-mentioned studies proposed criterions to examine the appropriateness of the LTE assumption. An overview is given in Table 1. These criteria are based on different constraints like a maximum allowed temperature difference between the fluid and solid phase, a maximum ratio between the time needed to reach thermal equilibrium and the problem time scale or a maximum allowed error in the determination of a heat transfer coefficient. While these criteria can be relevant for engineering applications the consequences for modeling results like a temperature plume of a thermal groundwater use remain unknown. Whether a temperature difference in the solid and fluid phase leads to an overestimation of the plume length or has other implications is not clear. Furthermore, adopting the criteria, which were developed for engineering applications to aquifers or streambeds is difficult, as the experimental conditions and reference parameters are not representative for natural conditions. The commonly required "characteristic length" usually defined as length or height of the packed bed (Table 1) cannot be easily determined for heat transport in the subsurface.

Table 1: Overview of different LTE criterions found in literature.

Author	LTE Criterion	
(Whitaker, 1980)	$$LTE_{crit} = Pe \frac{r_h}{L^2}\left(1 + \frac{\lambda_{f,eff}d_p}{\lambda_{s,eff}r_h}\right); \ll 1$$ with: $r_h = $ pore hydraulic radius and L as height of channel	General criterion for LTE LTE if $LTE_{crit} \ll 1$
(Whitaker, 1991)	$$LTE_{crit} = \left\{\frac{n(n-1)[\rho_f c_f - (\rho_s c_s L^2_{cond})]}{[n\lambda_{f,eff} + (n-1)\lambda_{s,eff}]t^*}\right\}\Lambda; \ll 1$$ $$LTE_{crit} = \left\{n(n-1)Pe\left(\frac{L_{cond}}{d_p}\right)\left(\frac{L_{cond}}{L_{conv}}\right)\left(\frac{\lambda_{f,eff}}{n\lambda_{f,eff} + (n-1)\lambda_{s,eff}}\right)\right\}\Lambda; \ll 1$$ $$LTE_{crit} = \left\{\frac{[n(n-1)](\lambda_{f,eff} - \lambda_{s,eff})}{[n\lambda_{f,eff} + (n-1)\lambda_{s,eff}]}\right\}\Lambda; \ll 1$$ with: L_{cond} or L_{conv} as characteristic conductive or convective length t^* as characteristic time; Λ see (Whitaker, 1991)	General criterion for LTE based on theoretical consideration of the volume averaging approach; LTE if all $LTE_{crit} \ll 1$

Author	LTE Criterion	
(Lee and Vafai, 1998)	$$LTE_{crit} = \frac{\lambda_{f,eff}}{\lambda_{s,eff}} + \frac{Bi}{4}; \gg 10$$	Validity of LTE for Nusselt estimation for a packed bed with heated walls LTE if $LTE_{crit} \gg 10$
(Minkowycz et al., 1999)	$$LTE_{crit} = \frac{Sp}{Pe} = \frac{Nu \frac{\lambda_{f,eff}}{\lambda_{b,eff}} \left(\frac{L}{r_h}\right)^2}{Pe}; \ll 100$$ with: $r_h = $ pore hydraulic radius and L as height of channel	Porous medium subjected to rapid transient heating or cooling as a sinusoidal boundary condition; LTE if $LTE_{crit} \ll 100$
(Bortolozzi and Deiber, 2001)	$$LTE_{crit} = Da; \ll 10^{-5}$$	Heat transfer under natural convection in porous media; LTE if $LTE_{crit} \ll 10^{-5}$
(Al-Nimr and Abu-Hijleh, 2002)	$$LTE_{crit} = e^{-\left(\frac{Bi}{C_R(1-n)}\right)(t_{dim}-nx_{dim})} I_0 \left[2\left(\frac{Bi^2 x_{dim}}{C_R(1-n)}(t_{dim}-nx_{dim})\right)^{0.5}\right]$$ $$\ll \frac{Bi}{C_R(1-n)} \Psi$$ with: $Bi = $ Biot number; L as width of channel I_0 as modified Bessel function of first kind and zero order dimensionless time $t_{dim} = \frac{tq}{L}$ and space $x_{dim} = \frac{x}{L}$; $$\Psi = \int_0^{t_{dim}-nx_{dim}} e^{-\left(\frac{Bi}{C_R(1-n)}\right)q} I_0 \left[2\left(\frac{Bi^2 x_{dim}q}{C_R(1-n)}\right)^{0.5}\right] du$$	Packed bed under transient forced convection
(Kim and Jang, 2002)	$$LTE_{crit} = Pr_{f,eff} Re_{dp} Da^{1/2} \frac{n}{Nu}; \ll 1$$	General criterion, tested for packed beds with heated top wall and cooled bottom wall; LTE if $LTE_{crit} \ll 1$
(Byun et al., 2006)	$$LTE_{crit} = \frac{(1-n)\rho_s c_s w}{h_{sf} a_{sf}}; \ll 1$$ with: w as the frequency of the oscillating flow	LTE criterion for a semi-infinite porous medium under oscillating flow from a cold side to a hot side and reverse. Based on the ratio of the problem timescale to the thermal inertia time scale: LTE if $LTE_{crit} \ll 1$
Zhang et al. (2009)	$$LTE_{crit} = Pr_{f,eff} Re_{dp} Da^{\frac{1}{2}} \frac{\frac{\lambda_{s,eff}}{\lambda_{f,eff}}}{1 - \frac{\lambda_{s,eff}}{\lambda_{f,eff}}} Nu^{-1} \frac{1}{6(1-n)}; \ll 1$$ with: $Da = \frac{d_p^2}{L^2}$; $L = $ length of packed bed	General criterion, tested for packed beds with constant wall temperature; LTE if $LTE_{crit} \ll 1$

Author	LTE Criterion	
(Dehghan et al., 2014a, 2014b)	$LTE_{crit} = \left\| \dfrac{(\theta_s - \theta_f)h_{sf}a_{sf}2L^2}{\lambda_{b,eff}Nu} \right\| ; \ll 1$ with: $\theta_{s,f}$ as dimensionless temperature fluid or solid, L as radius of tube	Based on a perturbation analysis, for a porous media in a tube heat exchanger; allows to estimate importance of LTNE; LTE if $LTE_{crit} \ll 1$
(Zanoni et al., 2017)	$LTE_{crit} = \dfrac{6h_{sf}}{q\rho_s c_s} ; \gg 1$	Packed bed with sand and air in convection dominated conditions; LTE if $LTE_{crit} \gg 1$

2.4   LTNE models

When the LTE approach is not suitable, a local thermal non-equilibrium (LTNE) model, sometimes also named non local thermal-equilibrium model, heterogeneous model, two-temperature model or two-equation model (Rees and Pop, 2005; Singh et al., 2006; Obembe et al., 2016) can be used. LTNE models are rarely used the environmental field and more common in engineering applications. These models apply two separate energy equations to describe the temperature in the fluid and solid phases (Fig. 6) and allow temperature differences between them, loosening the required assumptions (eq. 9):

$$\text{LTNE:} \quad \Delta T_{REV} \ll \Delta T_{system}$$

$$T_s \neq T_f$$

(9)

with ΔT_{REV} [-] as the normalized temperature difference in the REV and ΔT_{system} [-] as the normalized temperature difference in the whole investigated system.

While the LTE model disregards any kinetic disequilibrium effects, the LTNE model allows to account for these dynamic processes induced by the temporal temperature differences (Fig. 6). Similar to the LTE model, they are typically derived by volume averaging and assume that each phase is continuous and can be represented by appropriate effective parameters (Kaviany, 1995). The thermal coupling between the fluid phase and the solid phase is controlled by a heat transfer coefficient h_{sf}. The accurateness of the results is highly dependent on an appropriate value of this parameter, which is either derived by the examination of a simplified microstructure like a grid of spherical particles or based on empiric relationships derived in laboratory experiments or particle resolved direct numerical modelling (Wakao et al., 1979; Tavassoli et al., 2015).
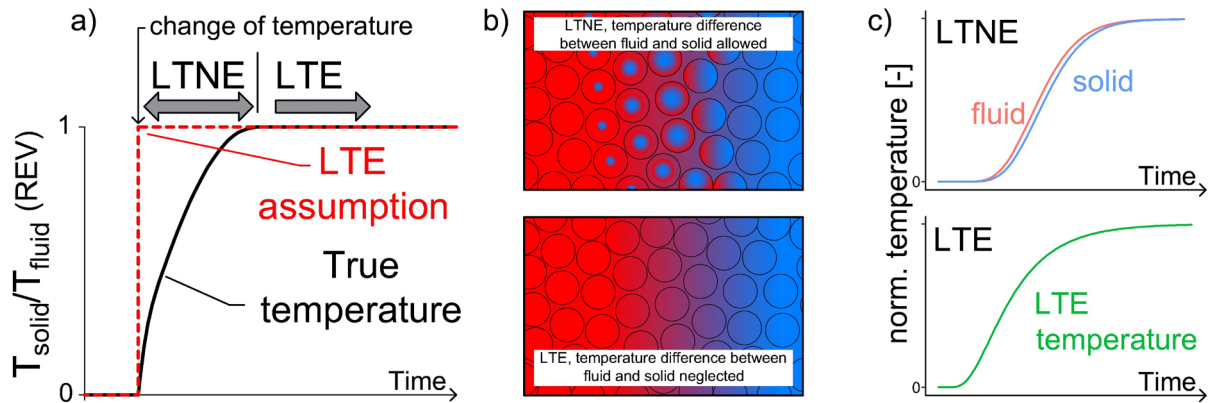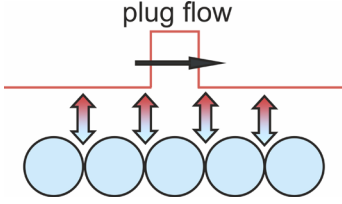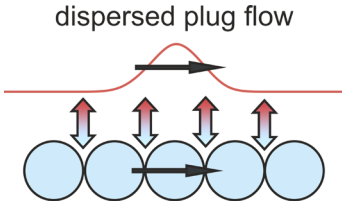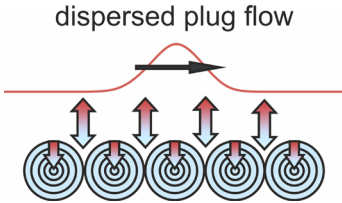
Fig. 6: a) Qualitative temperature development for steady state injection of a fluid, which is injected into a porous medium of different temperature. In the early phase, the temperature between solid and fluid phase is unequal. After a certain amount of time thermal equilibrium is reached. The red dotted line shows the simplification made by the LTE model neglecting any kinetic effects from delayed intra particel diffusion. b) Depiction of the assumption made by the LTE approach in a simplistic aquifer representation. c) Thermal breakthrough curves of an LTE and LTNE model. The LTE model constitutes an averaged temperature between the fluid and solid phase while the LTNE model provides the temperature development of both phases.

Different LTNE models exist, the three most common LTNE models are the Schumann model, the continuous solid phase model (C-S) and the dispersion-concentric model (D-C) (Table 2). The Schumann model and the C-S model are easier to handle and analyze as both fluid and solid phase temperature equations are only functions of distance and time while the D-C model introduces another dimension, the center symmetric radial position inside the particle (Kaguei et al., 1976; Levec and Carbonell, 1985a). The Schumann model is the simplest model, only considering plug flow in the fluid phase neglecting fluid and solid heat conduction and thermal mechanical dispersion (Wakao et al., 1979). The C-S model describes both the fluid and solid temperatures as a continuum, considering thermal mechanical dispersion and heat conduction in the fluid phase and axial heat conduction in the solid phase. The D-C model also accounts for thermal mechanical dispersion and heat conduction in the fluid phase, but the temperature in the solid phase is radial symmetric in the particle, neglecting axial heat conduction of the solid phase (Kaguei et al., 1976; Wakao and Kaguei, 1982). The most common LTNE model is the C-S model as it accounts for the axial heat conduction in the solid phase.

Table 2: Overview of different LTNE models and their limitations (Kaguei et al., 1976; Wakao et al., 1979; Obembe et al., 2016).

Model	Schematic	Governing equations	Description
Schumann model	plug flow	$$\frac{\partial T_s}{\partial t} = v_a \frac{\partial T_f}{\partial x} + \frac{h_{sf} a_{sf}}{(1-n_{tot})\rho_f c_f}(T_s - T_f)$$ $$\frac{\partial T_s}{\partial t} = \frac{h_{sf} a_{sf}}{(1-n_{tot})\rho_s c_s}(T_s - T_f)$$	- fluid in plug flow, only advection considered, fluid conduction and dispersion neglected - heat exchange between fluid and solid phase - no temperature gradient in particle - no axial heat conduction
Continuous solid phase model (C-S)	dispersed plug flow	$$\frac{\partial T_f}{\partial t} = \left(\frac{\lambda_f}{\rho_f c_f} + D_l\right)\frac{\partial^2 T_f}{\partial x^2} - v_a\frac{\partial T_f}{\partial x}$$ $$+ \frac{h_{sf} a_{sf}}{n_{tot}\rho_f c_f}(T_s - T_f)$$ $$\frac{\partial T_s}{\partial t} = \left(\frac{\lambda_s}{\rho_s c_s}\right)\frac{\partial^2 T_s}{\partial x^2} - \frac{h_{sf} a_{sf}}{(1-n_{tot})\rho_s c_s}(T_s - T_f)$$	- fluid in dispersed plug flow, fluid conduction and dispersion considered - heat exchange between fluid and solid phase - axial heat conduction in solid phase
Dispersion concentric model (D-C)	dispersed plug flow	$$\frac{\partial T_f}{\partial t} = \left(\frac{\lambda_f}{\rho_f c_f} + D_l\right)\frac{\partial^2 T_f}{\partial x^2} - v_a\frac{\partial T_f}{\partial x}$$ $$+ \frac{h_{sf} a_{sf}}{n_{tot}\rho_f c_f}((T_s)_r - T_f)$$ $$\frac{\partial T_s}{\partial t} = \left(\frac{\lambda_s}{\rho_s c_s}\right)\frac{\partial^2 T_s}{\partial r^2} + \frac{2}{r}\frac{\partial T_s}{\partial r}$$ $$at\ r = R_s,\ \left(\frac{\lambda_s}{\rho_s c_s}\right)\frac{\partial T_s}{\partial r} = h_{sf} a_{sf}(T_s - T_f)$$	- fluid in dispersed plug flow, fluid conduction and dispersion considered - heat exchange between fluid and solid phase - radial symmetric particle temperature - no axial heat conduction in solid phase

The resulting partial differential equations for a continuous-solid LTNE model are given in eq. (10) & (11) (Amiri and Vafai, 1994). The two temperatures are interlinked by a coupling term (Wakao et al., 1979) based on the heat transfer coefficient h_{sf} [W m^{-2} K^{-1}] (eq. 12) and the specific surface area a_{sf} [m^{-1}] (eq. 13), here assumed for a bed of spherical particles (Dullien, 1979). The equations are as follows

$$\frac{\partial T_f}{\partial t} = \left(\frac{\lambda_f}{\rho_f c_f} + D_l\right)\frac{\partial^2 T_f}{\partial x^2} - v_a\frac{\partial T_f}{\partial x} + \frac{h_{sf} a_{sf}}{n_{tot}\rho_f c_f}(T_s - T_f) \tag{10}$$

$$\frac{\partial T_s}{\partial t} = \left(\frac{\lambda_s}{\rho_s c_s}\right)\frac{\partial^2 T_s}{\partial x^2} - \frac{h_{sf} a_{sf}}{(1-n_{tot})\rho_s c_s}(T_s - T_f) \tag{11}$$

$$h_{sf} = \frac{Nu\,\lambda_f}{d_p} \tag{12}$$

$$a_{sf} = \frac{\left(6(1 - n_{tot})\right)}{d_p} \tag{13}$$

with d_p [m] as the particle diameter and Nu [-] as the Nusselt number.

The effective thermal dispersion in the fluid phase consisting of the thermal conductivity of the fluid and the thermal mechanical dispersion is described by the first part on the right hand side in eq. (10), the advective part is the second term and the heat transfer between the fluid and solid phase is described by the last part. The temperature development in the solid phase can be described by the axial heat conduction as defined by the first term in eq. (11) and the coupling term between fluid and solid phase temperature.

2.5 Heat transfer coefficients

The heat transfer coefficient (eq. 12) is a vital parameter for LTNE models, as it describes the heat transfer rate between the fluid and solid phases. As seen above h_{sf} [W m^{-2} K^{-1}] depends on Nu [-], the particle size d_p [m] and the thermal conductivity of the fluid λ_f [W m^{-1}K^{-1}] (Wakao et al., 1979). While λ_f and d_p are usually known in ideal packed beds, Nu must be estimated using an appropriate correlation which commonly depends on the particle Reynolds number, Re [-] (eq. 14) , and the Prandtl number, Pr [-] (eq.15) (see Table 3 for examples).

$$Re = \frac{\rho_f v_a d_p}{\eta} \tag{14}$$

$$Pr = \frac{\eta c_f}{\lambda_f} \tag{15}$$

With η [kg m^{-1} s^{-1}] as the dynamic viscosity of the fluid.

Generally, such a correlation is empirically derived from laboratory experiments (Shent et al., 1981; Wakao and Kaguei, 1982; Achenbach, 1995; Collier et al., 2004; Nie et al., 2011; Naghash et al., 2016; Zanoni et al., 2017) or more recently by particle resolved direct numerical modeling (Sun et al., 2015; Tavassoli et al., 2015; Singhal et al., 2017b; Chen and Müller, 2019; Zhu et al., 2019). As natural porous aquifers are typified by Re < 50 and a porosity (fluid volume fraction) n < 0.5, the correlations established by previous studies are covering much broader

ranges. Table 3 shows an overview of these correlations and demonstrates that no single model appropriately describes the conditions expected in a porous aquifer.

Table 3: Overview of different Nusselt correlations where Reynolds number and porosity constraints are within the range of conditions typical of porous aquifers.

Author	Correlation	Data in range	
Nelson and Galloway (1975)	$$Nu = \frac{2\zeta + \left(\frac{2\zeta^2(1-n_{tot})^{\frac{1}{3}}}{\left[1-(1-n_{tot})^{\frac{1}{3}}\right]^2} - 2\right)tanh\zeta}{\frac{\zeta}{1-(1-n)^{1/3}} - tanh\zeta}$$ with $\zeta = 0.3\left[\frac{1}{(1-n_{tot})^{\frac{1}{3}}} - 1\right]Re^{1/2}Pr^{1/3}$	$0.01 < Re$ <100	developed new model with no lower boundary limit for Nusselt and test this vs existing data (air/gas as fluid)
Wakao et al. (1979)	$Nu = 2 + 1.1\,Pr^{\frac{1}{3}}Re^{0.6}$	$15 < Re <$ 8500 $n_{tot} = 0.4$	widely used, reevaluated most of the correlations and data up to that date; but fluid always gas/air
Achenbach (1995)	$Nu = [(1.18\,Re^{0.58})^4 + \left(0.23\left(\frac{1}{1-n_{tot}}Re\right)^{0.75}\right)^4]^{1/4}$	$1 < Re < 10^4$ $0.26 < n_{tot} <$ 0.9	experimentally determined by mass transfer experiments, naphthalene sublimation in air, spherical particles
Nie et al. (2011)	$Nu = (0.049 \pm 0.0236)\,Re^{0.8572 \pm 0.0937}\,Pr^{\frac{1}{3}}$	$5 < Re < 280$ $0.327 < n_{tot} <$ 0.418	experimentally determined by fitting a numerical model to transient step responses for airflow through different beds of particles (glass, lead, and steel)
Roshan et al. (2014)	$Nu = 2.4x10^{-5} + 285.6(\,Pr^{\frac{1}{3}}Re^{2.7})$	$0.001 < Re <$ 0.01 $0.34 < n_{tot} <$ 0.44	based on data from Kunii and Smith (1961) (water – sand based), but this data of Kunii & Smith is criticized by e.g. Wakao and Kaguei (1982) due to an improper mathematical model
Tavassoli et al. (2015, 2013)	$Nu = (7 - 10n_{tot} + 5n_{tot}^2)\left(1 + 0.1Re^{0.2}\,Pr^{\frac{1}{3}}\right) + (1.33 - 2.19n_{tot} + 1.15n_{tot}^2)Re^{0.7}\,Pr^{\frac{1}{3}}$	$0 < Re < 100$ $0.35 < n_{tot} < 1$	modified the Gunn (1978) correlation based on particle resolved direct numerical simulations for gas - solid for monodispersed spheres and non-spherical particles (by choosing proper effective diameter)
Sun et al. (2015)	$Nu = \frac{(-0.46 + 1.77n_{tot} + 0.69n_{tot}^2)}{n_{tot}^3} + (1.37 - 2.4n_{tot} + 1.2n_{tot}^2)Re^{0.7}\,Pr^{\frac{1}{3}}$	$1 < Re < 100$ $0.5 < n_{tot} <$ 0.9	based on particle resolved direct numerical simulations for gas - solid (monodispersed spheres)

Author	Correlation	Data in range	
Naghash et al. (2016)	$Nu = (0.00119 \pm 0.00273)$ $\left[Re\left(\dfrac{2n_{tot}}{3(1-n_{tot})}\right)\right]^{1.647\pm0.501} Pr^{\frac{1}{3}}$	$40 < Re < 100$ $0.33 < n_{tot} < 0.66$	experimentally determined by fitting a numerical model to transient step responses for airflow through a bed of microporous silica gel particles
Zanoni et al. (2017)	$Nu = 0.001(Pr^{\frac{1}{3}} Re^{1.97})$	$0.5 < Re < 31$ $0.36 < n_{tot} < 0.37$	based on laboratory experiments (air-sand) fitted to a numerical model (Comsol)
Singhal et al. (2017)	$Nu = 2.67(\pm1.48) + 0.53(Pr^{0.53} Re^{0.77})$	$9 < Re < 180$ $0.351 < n_{tot} < 0.367$	based on particle resolved direct numerical simulations for gas - solid (monodispersed spheres)
Chen and Müller (2019)	$Nu = 2 + 0.77(1 - n_{tot}) + 0.64(1 - n_{tot})^2 + \big(0.6 + 1.1(1 - n_{tot})\big)Re^{0.5}Pr^{\frac{1}{3}}$	$Re < 100$ $0.5 < n_{tot} < 1$	numerically determined Nu with a thermal lattice Boltzmann method for gas-solid (monodispersed spheres)
Zhu et al. (2019)	$Nu = (-0.83 + 16.21n_{tot} - 14.67n_{tot}{}^2)\big(1 - 0.01Re^{0.2} Pr^{\frac{1}{3}}\big) + (1.5 - 2.6n_{tot} + 1.31 n_{tot}^2)Re^{0.7} Pr^{\frac{1}{3}}$	$0 < Re < 550$ $0.35 < n_{tot} < 1$	review and reevaluation of Nu correlations based on particle resolved direct numerical modelling

2.6 Quantification of LTNE

Different methods have been used to describe and quantify LTNE effects on heat transport in porous media. One type of LTNE measures is based on the normalized temperature difference between the fluid and solid phase (Amiri and Vafai, 1998; Khashan and Al-Nimr, 2005; Khashan et al., 2006; Al-Sumaily et al., 2013; Abdedou and Bouhadef, 2015). This LTNE measure can be either defined as the maximum (eq. 16) or the average (eq. 17) of the temperature difference at a point in the packed bed (Amiri and Vafai, 1998; Virto et al., 2009) or across the whole packed bed (Khashan and Al-Nimr, 2005; Khashan et al., 2006; Al-Sumaily et al., 2013; Abdedou and Bouhadef, 2015)

$$LTNE_{fluid\ solid,max,x} = max_N \left| T_{LTNE,f,x} - T_{LTNE,s,x} \right| \tag{16}$$

and

$$LTNE_{fluid\ solid,mean,x} = \frac{\sum_1^N \left| T_{LTNE,f,x} - T_{LTNE,s,x} \right|}{N} \tag{17}$$

With N as the number of time steps, $T_{LTNE,f,x}$ [-] as the normalized fluid temperature of the LTNE model at the distance x [m], and $T_{LTNE,s,x}$ [-] as the normalized solid temperature of the LTNE model at the distance x.

Another approach to measure the LTNE intensity is to compare the maximum and average temperature difference between the normalized temperature obtained using the LTE model $T_{LTE,x}$ [-] and the fluid temperature of the LTNE model (Lu and Xiang, 2012; Hamidi et al., 2019) for each evaluated distance x (N= number of timesteps).

$$LTNE_{LTE-LTNE,max,x} = max_N |T_{LTE,x} - T_{LTNE,f,x}|$$
(18)

and

$$LTNE_{LTE-LTNE,mean,x} = \frac{\sum_1^N |T_{LTE,x} - T_{LTNE,f,x}|}{N}$$
(19)

The threshold value which defines the boundary between LTE and LTNE conditions is commonly set to a difference of 5 % in the above explained measures (Khashan and Al-Nimr, 2005; Khashan et al., 2006; Al-Sumaily et al., 2013; Abdedou and Bouhadef, 2015). This value is chosen rather arbitrarily, the consequences for heat transport modeling in the field if one of these measures exceed this value are not clearly stated.

2.7 Prediction modeling

When heat transport in porous media has to be predicted, e.g. in geothermal applications, numerical and analytical solutions of the heat transport equations are used. Analytical solutions have the advantage of usually being faster to solve, numerically exact and continuous in time and space (Anderson et al., 2015). But as analytical solutions typically require simple geometry and simple boundary conditions, their application is very limited. In addition, analytical solutions do not exist for all problems (Olver, 2016). Therefore, often numerical models are used in prediction related applications.

Numerical models use an approximate form of the governing heat transport equation. This allows to solve fully transient, 3D, heterogeneous and anisotropic problems under complex initial and boundary conditions (Anderson et al., 2015). Different numerical methods exist, the

most common ones are the finite-element, finite-differences and finite-volume methods (Diersch, 2014). As the finite-element technique is very often used in groundwater related numerical approaches and thought of as the most general and powerful method (Diersch, 2014), the following section gives a short overview of the basic principles of this method. Detailed explanations of the fundamentals of numerical modeling are for example given in Reddy and Gartling (2010), Diersch (2014), and Olver (2016). Following Bear (1972) and Reddy and Gartling (2010) the major steps in the finite element formulation are as follows:

1. The problem domain is divided into a finite number of elements that are defined by nodes. Arbitrary and irregular geometries can be represented by finite elements which makes the method readily applicable to various problems. The dependent variable is defined as a continuous solution within the elements, this means, that the value of the dependent variable can be obtained by the values of the variable at the nodes of the element and the position.

2. Generation of the approximation function, often a weighted integral or a weak-form statement of the differential equation over a typical element and development of the finite element model by taking the derivative with respect to the dependent variable at all nodes of the element. Different finite element models can exist for the same differential equation based on the method of approximation, e.g. Galerkin, least-squares etc.

3. Merging of the equations of all elements to obtain a global system of algebraic equations.

4. Definition of the boundary conditions in terms of nodal values.

5. Integration of the boundary conditions into the equations and solution of the equations.

Different simulation codes are frequently used to solve heat transport problems numerically in natural porous media like aquifers. These are for example the finite-element codes Feflow (Diersch, 2014), Comsol Multiphysics and OpenGeoSys (Kolditz et al., 2012), the finite-differences codes SEAWAT (Langevin et al., 2008) and TOUGH2 (Pruess et al., 1999) and some finite-volume codes like ANSYS FLUENT and PFLOTRAN (Mills et al., 2007). An overview of available simulation codes is for example given in (Hecht-Méndez et al., 2010). While some of these

codes are capable of solving LTNE problems e.g. Comsol, to the authors knowledge LTE models are nearly always used in prediction modeling in natural porous media. This demonstrates that LTNE effects have not been considered in depth for prediction modeling in natural porous media.

2.8   Evaluation of thermal breakthrough curves

Naturally occurring or anthropogenically induced thermal signals in the groundwater or in the streambed can be used to estimate different parameters such as groundwater fluxes and mean transit times (e.g. Becker et al., 2015; Moeck et al., 2017; Somogyvári and Bayer, 2017). This can be done by comparing thermal signals at different observation wells or by using temperature depth profiles to estimate vertical fluxes and similar approaches. In many of these applications the thermal velocity is of high interest as it is a proxy for the groundwater flux. The advective thermal velocity is related to the seepage velocity by an effective thermal retardation factor R_{eff} which describes the ratio between the seepage velocity to the advective thermal velocity (Shook, 2001; Stopa and Wojnarowski, 2006). If LTE is valid, R_{eff} equals an apparent retardation factor R_{app} (eq. 8), that is estimated by relating the ratio of heat capacities between the bulk porous media and the fluid (Bodvarsson, 1972; Woods and Fitzgerald, 1993, 1997; Shook, 2001).

Determining the advective thermal velocity is therefore often a key component when using heat as a tracer. Neglecting effective thermal dispersion would result in a breakthrough curve with a sharp temperature front, which can easily be used to determine the advective thermal velocity (Shook, 2001). However, in previous experimental studies, measured thermal BTCs are influenced by conduction and thermal mechanical dispersion, resulting in a differently shaped BTC, depending on the used temperature signal. So, these differences should be accounted for, when thermal BTCs from heat tracer experiments are evaluated.

Different methods are available to determine the thermal velocity from thermal breakthrough curves depending on the input signal. Typical input signals are a step input, which can be described as a continuous input of a constant load, a pulse input of finite duration, where a constant load is applied for a finite duration, and a periodic signal, often diurnal or seasonal temperature changes in a sinusoidal form. A common approach independent of the input signal is

to use an appropriate analytical model with the advective thermal velocity as a fitting parameter (e.g. Bakker et al., 2015; Bandai et al., 2017; Caissie and Luce, 2017; Rau et al., 2012a). In scenarios with a pulse input of finite duration, the thermal peak velocity, defined by the movement of the maximum of the temperature signal, is frequently utilized (e.g. Constantz et al., 2003; Lewandowski et al., 2011; Somogyvári and Bayer, 2017). When periodic signals are analyzed, characteristic peak and trough matching (e.g. Markle and Schincariol, 2007; Laws et al., 2011; Becker, Clark and Johnson, 2015) and lag times from maximum cross correlations (e.g. Hoehn and Cirpka, 2006; Bekele et al., 2014; Taylor, Banks and Watson, 2016) are used to evaluate the thermal velocity. An overview of the used approaches in experimental studies is given in Table 4.

Table 4: Methods for different source signal types used to derive the thermal velocity, $v_{therm\ fit}$ as the velocity obtained by fitting an analytical model to a BTC, the peak velocity $v_{therm\ peak}$ and the peak velocity of the first time derivative $v_{therm\ peak\ dT/dt}$ from heat tracer experiments.

Source signal type	Methods to determine v_{therm}	Examples from literature
Finite duration pulse signal	Fitting parameter in analytical model ($v_{therm\ fit}$)	Bakker et al. (2015)
	Peak time ($v_{therm\ peak}$)	Constantz et al. (2003); Lewandowski et al. (2011); Somogyvári & Bayer (2017); Taniguchi & Sharma (1990); Wagner et al. (2014)
	Peak of first time derivative ($v_{therm\ peak\ dT/dt}$)	Somogyvári & Bayer (2017)
Step signal	Fitting parameter in analytical model ($v_{therm\ fit}$)	Bandai et al. (2017); Rau et al. (2012a)
	Self-defined value between initial and injection temperature	Park et al. (2015)
	Mean value between initial and injection temperature	Irvine et al. (2013)
	Peak of first time derivative ($v_{therm\ peak\ dT/dt}$)	Somogyvári et al. (2016)
Periodic signal	Fitting parameter in analytical model ($v_{therm\ fit}$)	Caissie and Luce (2017); Halloran et al. (2016); Rau et al. (2017, 2012b); Schneidewind et al. (2016)
	Lag time from maximum cross correlation	Bekele et al., (2014); Hoehn and Cirpka (2006); Markle and Schincariol (2007); Moeck et al. (2017); Taylor et al. (2016); Vandenbohede and Van Houtte (2012)
	Characteristic peak and trough matching	Becker et al. (2015); Laws et al. (2011); Markle and Schincariol (2007)

Whether these methods give accurate estimates of the advective thermal velocity has not been thoroughly examined, as studies which systematically investigate the seepage velocities derived from heat tracers and solute tracers are scarce (Taniguchi and Sharma, 1990; Rau et al., 2012a, 2012b; Irvine et al., 2013; Bandai et al., 2017). Their results are also not consistent: some works reveal a good agreement (Irvine et al., 2013), while others found systematic over- or underestimation (Rau et al., 2012a, 2012b; Bandai et al., 2017). Other studies used both heat and solute tracers, but did not make a systematic comparison between heat- and solute-derived velocities (Constantz et al., 2003; Vandenbohede et al., 2009; Ma et al., 2012; Seibert et al., 2014; Wildemeersch et al., 2014; Bakker et al., 2015; Becker et al., 2015; Klepikova et al., 2016; Bonner et al., 2017; Sarris et al., 2018).

Chapter 3   Material and methods

3.1   One-dimensional column experiments to estimate LTNE effects on thermal retardation

The following section lays out the experimental setup of the laboratory experiments which were used to compare different methods to evaluate the thermal velocity from thermal BTCs and assess the influence of LTNE effects on the advective thermal velocity. This chapter is based on the methods section of Gossler et al. (2019) but has been extended and adapted.

3.1.1   Experimental method

3.1.1.1   Experimental setup

The laboratory setup illustrated in Fig. 7 was developed to study one-dimensional (1D) heat and solute tracer transport through a cylinder-shaped sample at seepage velocities of v_a = 1 - 50 m d^{-1} and at temperatures of 5 – 70 °C.

The experiments were considered as one-dimensional because the heated water and the solute tracer were injected throughout the whole cross section of the column perpendicular to the flow direction which is a frequently applied assumption (Leibundgut et al., 2009; Maier et al., 2015; Bandai et al., 2017). Furthermore, even if the inflow into the column is not perfectly uniform, influences of non-uniform boundary conditions in laboratory soil columns should dissipate at 3/2 of the radius of the column (Barry, 2009). Assuming that the inflow into the column is uniform across the whole cross section, the heat and solute concentration gradients in the y and z directions equal zero:

$$\frac{\partial T}{\partial y} = \frac{\partial T}{\partial z} = 0 \quad | \quad \frac{\partial C}{\partial y} = \frac{\partial C}{\partial z} = 0 \tag{20}$$

which allows to reduce the three-dimensional heat transport and solute transport equations to the one-dimensional equations given in Chapter 2. This means that the effective thermal dispersion and the effective solute dispersion in the z and y axis perpendicular to the flow direction x are neglected because neither a temperature gradient respectively a concentration gradient nor an advective flux which could cause mechanical dispersion exist in these directions.

To enable an instant change between hot-water injection and cold-water injection, two refrigerated bath circulators (Witeg WCR-P22) were used. The two devices have an accuracy of ± 0.1 K. They can be used independently for heating and cooling and served here as cold and hot water tanks. An eight-channel peristaltic pump (Ismatec Ecoline) was used to control the volume flow into the column. A three-way valve was installed at each of the inflow tubes close to the column to allow tempering of the tubes without injection into the column. Furthermore, the three-way valves were used to inject a solute tracer.
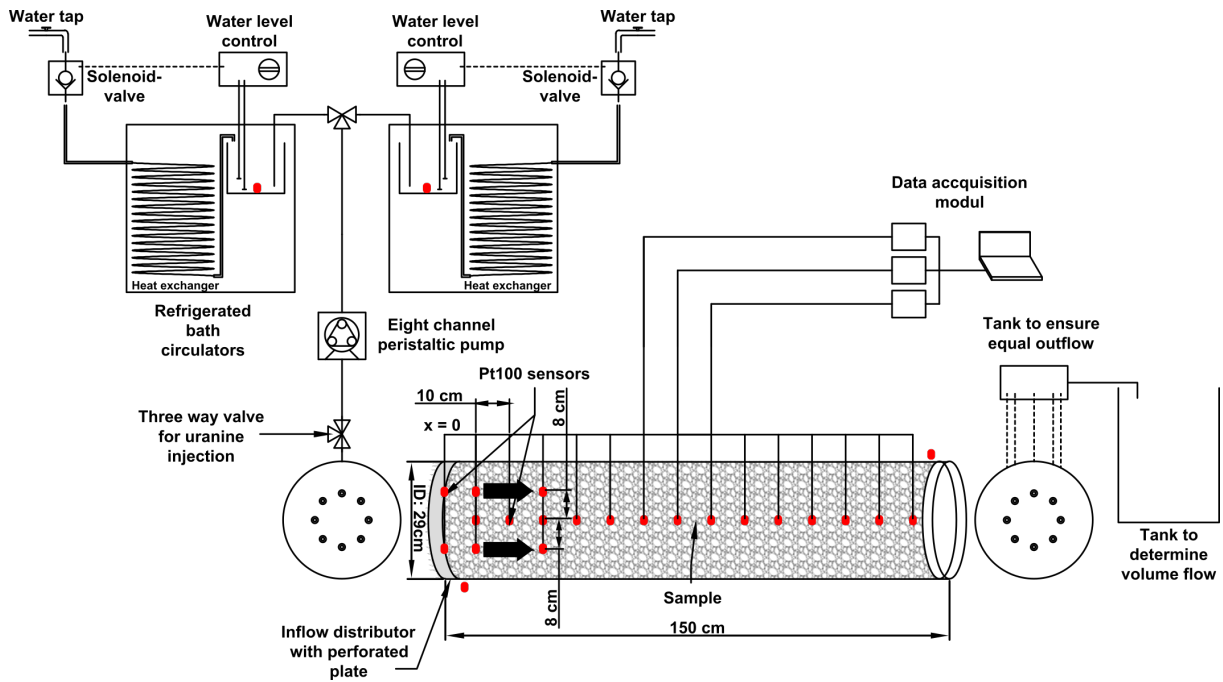
Fig. 7: Schematic experimental setup of the laboratory experiments. The refrigerated bath circulators served as a hot and cold water storage. The volume flow was controlled by an eight-channel peristaltic pump. The red dots mark the positions of the Pt100 temperature sensors. The column can be installed in a vertical and horizontal configuration.
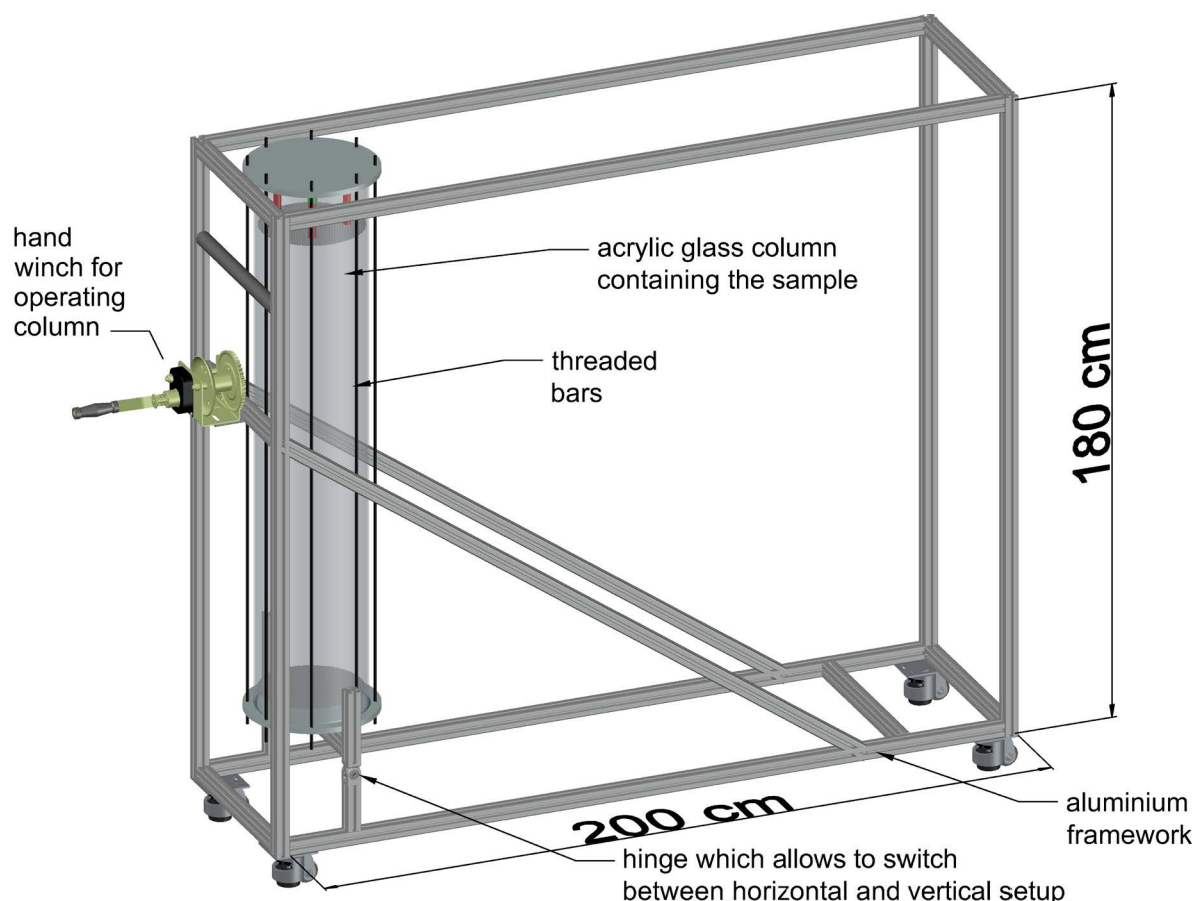
Fig. 8: Aluminium framework of the laboratory setup containing the acrylic glass column, here in the vertical setup. The thermal insulation is not displayed. The construction allows to change between a horizontal and a vertical experiment setup.

The sample was inserted in an acrylic glass column with an inner diameter of 0.29 m and a length of 1.5 m within an aluminum framework (Fig. 8). Uniform inflow and outflow of the column was ensured by eight radially arranged inlets (CPC couplings) in the lid and the bottom of the column (Fig. 9), and by an inflow distributor consisting of a perforated plate with a distance of 4 cm after the lid. A vertically movable perforated stabilization plate mounted on the lid prevented shifting of the sample during tilting of the column (Fig. 9) The column was thermally insulated by a 5-cm-thick layer of K-Flex 25 (λ = 0,034 W m^{-1} K^{-1}) insulation. In addition, the inflow tubes were thermally insulated by a K-Flex tube (wall thickness 10 mm). A tank at the end of the outflow tubes was installed to ensure the same pressure level at each outflow tube. A tank at the outflow was used to determine the volume flow through the column.
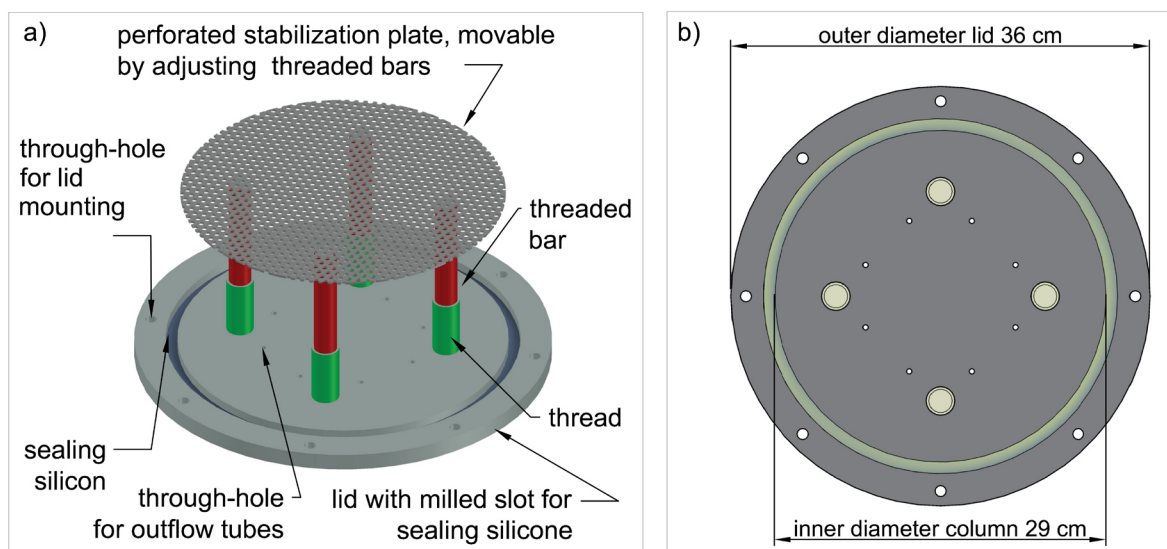
Fig. 9: a) lid of the column with a movable perforated stabilization plate to prevent shifting of the sample during tilting of the column. b) top view of the lid with dimensions. The bottom lid of the column is similar without the threaded bars and threads.

3.1.1.2 Data acquisition system for heat and solute

The temperature development of the fluid in the laboratory setup was monitored with four-wire Pt100 sensors (Omega Engineering) with an accuracy class 1/10 of IEC 751 / EN 60751 resulting in an accuracy of ±0.03 K. Two kinds of Pt100 sensors were used: sheathed ones with a total length of 18 cm and a diameter of 3 mm, and hermetically sealed wire sensors with a diameter of 1 mm. During the packing of the column, these sensors were inserted from the outside of the column with thermo fittings. The sheathed sensors were positioned at the center of the column. Calibration was done using high precision bath circulators. In addition to the column itself, the temperature in the circulation thermostats and the room temperature were monitored. The positions of the sensors are shown in Fig. 7. The data acquisition at a 3 s interval was handled by Pt104A modules (Omega Engineering).

To determine seepage velocities and solute dispersivity, the fluorescence dye uranine (color index 45350) was used. It is assumed that uranine has conservative properties in the experimental setting as adsorption processes mainly take place in environments containing abundant organic matter and uranine showed very low adsorption in batch experiments with limestones (Smart and Laidlaw, 1977). Uranine has been proven to be thermally very stable with a decay of less than 10 % for a duration of one month in geothermal reservoirs up to 210 °C

(Adams and Davis, 1991). Furthermore, it was successfully used as a tracer in geothermal systems with temperature above 150°C (Rose et al., 2001). Nevertheless, as the solubility is temperature dependent, the measured intensity can also be affected (Smart and Laidlaw, 1977). The calibration curve to determine the uranine concentrations from the measured intensities was created at room temperature of around 20 °C. The maximum temperature difference is therefore around 10 °C. Using the correction formula and coefficients for temperature dependency for uranine (Smart and Laidlaw, 1977; Leibundgut et al., 2009), the resulting relative difference in intensity is less than 5 %.

The tracer was injected into the column with the fluid using syringes which were connected to the inflow tube to the column using three-way valves (Fig. 10). The samples were taken at the outflow of the column in varying time intervals depending on the applied volume flow. The solute tracer was analyzed with a fluorescence spectrometer (Perkin Elmer LS 45). To each fluid sample, 20 µl of 20 wt.% EDTA was added to reach a pH-value of approximately 9 to prevent influences of the pH-value on the fluorescence (Smith and Pretorius, 2002) and to avoid precipitation of interfering particles. A dilution series from a known concentration was measured to create a calibration curve using the measured intensities and the concentration (Appendix Fig. B 1). A linear regression of the calibration curve was used to calculate the concentration from the measured intensity. The measurement setup of the fluorescence spectrometer was: fluorescence excitation wavelength of 491 nm and fluorescence emission wavelength of 512 nm (Leibundgut et al., 2009).
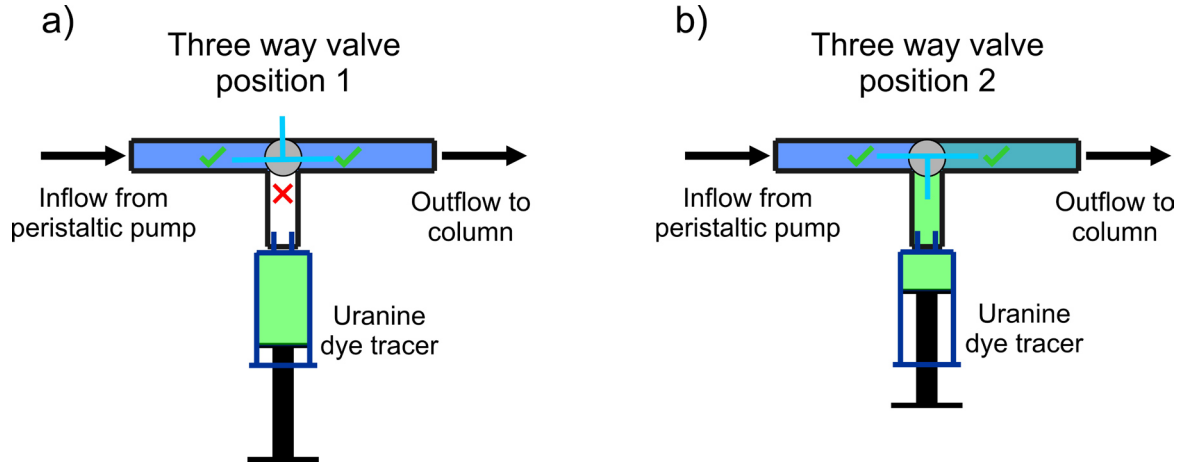
Fig. 10: a) Three way valve for uranine injection in position 1 which allows a throughflow from the peristaltic pump to the column and blocking the connection for the uranine injection. b) Three way valve in position 2 allowing the injection of the uranine tracer into the inflow to the column.

3.1.1.3 Properties of the porous media

The gravel used as the sample in the laboratory setup was sieved Carrara Marble, with a grain size distribution in the range of 7-15 mm. The following properties are needed to calculate the apparent thermal retardation for the porous medium: The total porosity n_{tot} [-] (fluid volume fraction) of the saturated gravel was experimentally determined three times in a two-step procedure. First, the specific density of the marble was obtained by measuring the volume (water displacement) and the weight. In the second step, a circular vessel with a diameter of 26 cm and a height of 25 cm was filled with gravel and compacted with the same method as during column packing. The weight of the gravel (around 8.5 kg) was measured. Then, water was added until the surface of the topmost gravel was covered, and the total weight was determined. The specified parameter values were used to derive the volume of the gravel and the water and thereby, n_{tot}. The temperature during the experiments was 24.5 °C, the accuracy of the scale was ± 0.1 g. The resulting calculated total porosity was n_{tot} = 36 ± 1 %. The effective porosity n_{eff} [-] (fluid volume fraction contributing to fluid flow) was determined by solute tracer experiments, as described below in section 3.1.2.4. The volumetric heat capacity $\rho_s c_s$ of the gravel was estimated by a modified transient plane source method with a commercial device (C-therm) by:

$$\rho_s c_s = \frac{e_s^2}{\lambda_s},$$

(21)

whereas the solid thermal effusivity, e_s [J K^{-1} m^{-2} s$^{-0.5}$], and thermal conductivity λ_s [W m^{-1} K^{-1}] of the saturated solid phase were measured (He 2005). The used contact agent was distilled water and the measurement time was 1 s. Three pieces of gravel with a diameter of approximately 40 mm were cut in half, resulting in 6 samples. The surface was polished until smooth to assure optimal contact to the sensor. Before the measurement, the pieces of gravel were saturated in water for 24 hours.

The bulk volumetric heat capacity of the saturated porous media $\rho_b c_b$ [J m^{-3} K^{-1}] is defined as (Buntebarth and Schopper, 1998; Schärli and Rybach, 2001):

$$\rho_b c_b = n_{tot} \rho_f c_f + (1 - n_{tot}) \rho_s c_s \qquad (22)$$

The thermal conductivity of the saturated gravel λ_b can for example be estimated by the arithmetic mean model (Whitaker, 1991):

$$\lambda_b = n_{tot} \lambda_f + (1 - n_{tot}) \lambda_s \qquad (23)$$

Table 5: Parameter values of the porous medium, measured or taken from literature.

Parameter	Unit	Value	Procedure / Source
Particle size d_p	[mm]	7-15	based on vendor information (purchased material)
Total porosity n_{tot}	[%]	36 ± 1	measured
Effective porosity n_{eff}	[%]	35 ± 2	measured (solute tracer experiments eq. 35)
Vol. heat capacity of solid $\rho_s c_s$	[MJ m^{-3} K^{-1}]	2.06 ± 0.02	according to eq. (21)
Thermal conductivity of solid λ_s	[W m^{-1} K^{-1}]	3.2 ± 0.2	measured (modified transient plane source)
Thermal effusivity of solid e_s	[J K^{-1} m^{-2} s$^{-1/2}$]	2584 ± 93	measured (modified transient plane source)
Thermal conductivity of fluid λ_f (20 °C)	[W m^{-1} K^{-1}]	0.598	taken from literature (VDI, 2013)
Thermal conductivity of sat. porous media λ_b	[W m^{-1} K^{-1}]	1.75	according to eq. (23)
Vol. heat capacity of fluid (20 °C) $\rho_f c_f$	[MJ m^{-3} K^{-1}]	4.18	taken from literature (VDI, 2013)
Vol. heat capacity of sat. porous media $\rho_b c_b$	[MJ m^{-3} K^{-1}]	2.87 ± 0.02	according to eq. (22)
Resulting R_{app}	[-]	1.88	according to eq. (25)

3.1.1.4 Experimental preparation

The column was set up vertically for the filling procedure. The gravel was packed in the column in layers of approximately 5 cm from bottom to top. Each layer was compacted by mechanical force using a metal plate. The Pt100 sensors were installed during the column packing by inserting the sensors through fittings into the column. A thin, perforated aluminum plate was placed on top of the gravel after filling. This plate was attached to the lid by threaded rods, allowing it to be moved in a vertical direction. This prevented the gravel from shifting during the tilting of the column (Fig. 9). To establish a uniform initial temperature, the column was injected with water until a uniform temperature was reached at all temperature sensors.

Prior to the start of the experiment, the three-way valves close to the inflow were adjusted to block the inflow to the column and to dispose the water. This was done to ensure that the water in the inflow tubes was the same temperature as the inflow temperature. As this was established, the three-way valves were adjusted to enable inflow into the column.

3.1.1.5 Experimental procedure

Two different experimental setups, step input (Fig. 11a) that gives a continuous, constant input of heated water, and a pulse input of finite duration, a continuous input of heated water for a finite duration (Fig. 11b), were used to evaluate which methods can be used to determine the advective thermal velocity for estimation of the apparent retardation factor, R_{app} [-]. For the step input experiments (Fig. 11a), the column was positioned vertically and the injection and flow of the water was from top to bottom. The initial temperature was set to $T_{0,Celsius}$ = 10 °C. The water from the water tap flowed through both heat exchangers into one tank of the second thermostat. When the temperature in the tubes reached T_{inj}, the three-way valves were adjusted to start the injection of the tempered water into the column. This step was defined as the experimental start time (t = 0). The injection temperatures were either set to 30 °C or 15 °C, to evaluate any influence of different injection temperatures. The experiments

were stopped when the center temperature sensor most distant from the inflow reached a constant value close to T_{inj}.
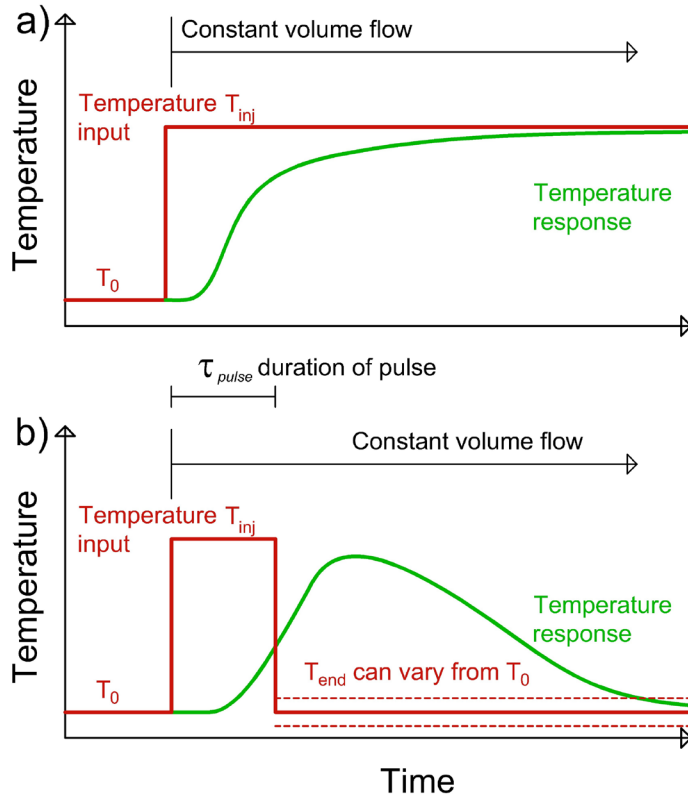
Fig. 11: Experimental procedures for (a) step input and (b) pulse input of finite duration experiments.

The second setup was a pulse input of finite duration (Fig. 11b). A heat pulse was created by injecting hot water (T_{inj}) for a defined time τ_{pulse} into the column. The pulse time τ_{pulse} was 30 minutes for all experiments. This value was chosen, as it allows a sufficiently measurable temperature signal. Furthermore, it does not significantly affect the results. This was investigated prior to the experiments using eq. 13 to calculate BTCs for varying values of τ_{pulse} and v_a. The effective retardation for the peak velocity is only significantly affected, if the ratio τ_{pulse} to the expected mean transit time exceeds values of 0.5 (Fig. 12). The maximum value in the investigated range in the experiments is 0.5 for the experiment with the highest seepage velocity of 35 m d^{-1}. In the range of the experiments with lower seepage velocities ($v_a < 10$ m d^{-1}), the ratio is below 0.2.
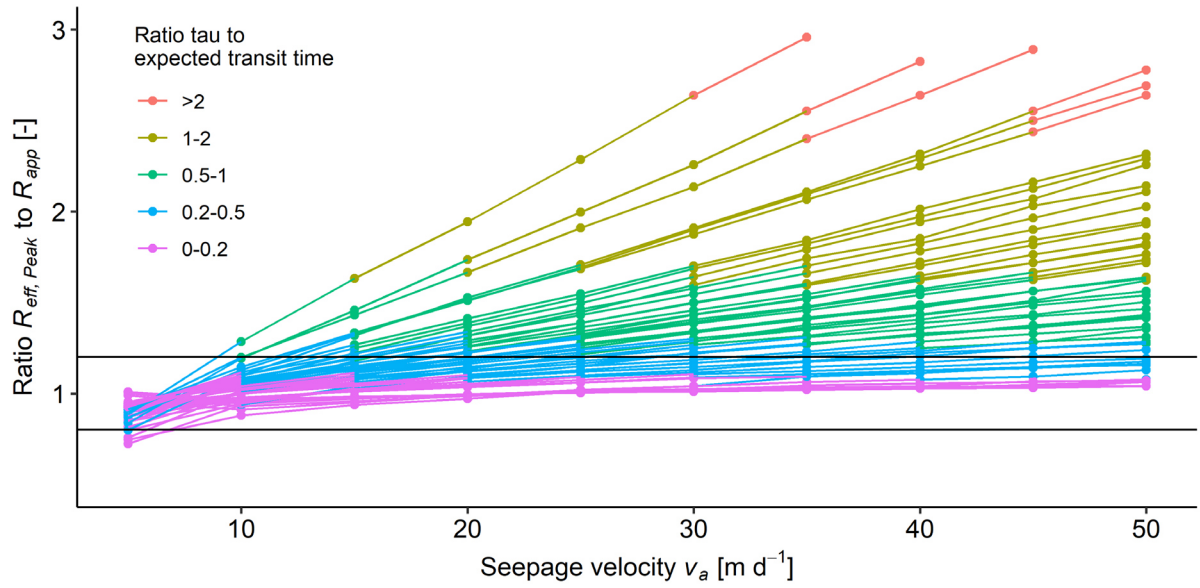
Fig. 12: Influence of the injection time τ_{pulse} on the thermal retardation. The effective retardation of the peak velocity (see section 3.1.2.1 for a definition) is only significantly influenced if the ratio of τ_{pulse} to the expected mean transit time is higher than 0.5. The black horizontal lines indicate the scatter which was observed in the experiments.

When $t = \tau_{pulse}$ was reached, the injection temperature was changed back to $T_{0,Celsius}$. The experiments where conducted in a vertical and in a horizontal setup. The pulse input of finite duration was carried out by setting one of the thermostats to the injection temperature T_{inj}. The other thermostat was set to the initial temperature $T_{0,Celsius}$. When the temperature in the inflow tubes reached T_{inj}, the three-way valves were adjusted to start the injection into the column. Again, this was the experimental start time ($t = 0$). When t was equal to τ_{pulse}, the injection temperature was set back to the initial temperature by changing the inflow from the first thermostat (T_{inj}) to the other thermostat ($T_{0,Celsius}$). Due to varying ambient temperatures, and despite thermal insulation of the tubes from the thermostats to the column, the measured injection temperature after the pulse (T_{end}) did not always exactly match the initial temperature. This means that T_{end} varied slightly (maximally by 0.1 of normalized temperature) from $T_{0,Celsius}$ (Fig. 11b). To minimize the free convection in the horizontal setup, reduced temperature differences were used. The injection temperature T_{inj} was set to 25 °C and the initial and end temperature to 20 °C. The experiments were stopped when the center temperature sensor most distant from the inflow reached a constant value near T_{end}. The experiment duration varied depending on the volume flow between 3 h and >15 h. Altogether, 43 experiments were conducted, as summarized in Table 6.

In the coupled heat and solute tracer experiments, the three-way valve at each inflow tube was employed to inject 2 ml of a 10^{-5} kg L^{-1} uranine solution, resulting in a total injected mass of 0.16 mg uranine per experiment. In the step input experiments, the solute tracer was injected simultaneously with the start of the hot water injection ($t_{sol\ inj} = 0$). In the finite duration pulse experiments, the uranine was injected when 50 % of the heat pulse was reached ($t_{sol\ inj} = 0.5\ \tau_{pulse}$). The samples were taken at the outflow of the column in varying time intervals depending on the applied volume flow.

Table 6: Details of the conducted experiments. The experiment duration varied between 3 h and >15 h depending on the volume flow. The duration of the pulse τ was 30 minutes for all finite duration pulse experiments.

Experiments	Pulse input of finite duration		Step input
Seepage velocities	~6-34 m/d		~5-50 m/d
Setup	vertical	horizontal	vertical
Flow direction	top to bottom	left to right = bottom to top (but horizontal)	top to bottom
Initial temperature	~15-20 °C	~20 °C	~10 °C
Input temperature	~25 °C	~25 °C	~15°C / ~30°C
Number of heat experiments	8	11	14
Coupled heat and solute experiments	-	8	2

3.1.2 Evaluation of thermal and solute breakthrough curves

To evaluate possible LTNE effects, the measured, effective thermal retardation (eq. 24) which is potentially influenced by LTNE effects, is compared with the predicted, apparent thermal retardation (eq. 25) which assumes LTE:

$$R_{eff} = \frac{v_a}{v_t} \tag{24}$$

where v_t [m s^{-1}] is the advective thermal velocity. The effective fluid or seepage velocity v_a [m s^{-1}] is defined as $v_a = \frac{q}{n_{eff}}$, with the specific discharge q [m s^{-1}] and the effective porosity n_{eff} [-]. The specific discharge is defined as $q = \frac{Q}{A}$, with the volume flow Q [m³ s^{-1}] and the cross-sectional area A [m²]. The predicted, apparent thermal retardation factor is defined by:

$$R_{app} = \frac{\rho_b c_b}{n_{tot}\rho_f c_f} = 1 + \frac{(1-n_{tot})\rho_s c_s}{n_{tot}\rho_f c_f} \tag{25}$$

where $\rho_{f,s,b}$ is the specific density of the fluid, solid or bulk porous media, $c_{f,s,b}$ is the specific heat capacity of the fluid, solid or bulk porous media, and n_{tot} is the total porosity.

The relative contributions of convective to conductive heat flow can be expressed by the thermal Péclet number Pe [-] (De Marsily, 1986):

$$Pe = \frac{qL}{D_{l,eff}} \tag{26}$$

where $D_{l,eff}$ [m² s⁻¹] effective longitudinal thermal dispersion, and L [m] is the characteristic length, usually set to the mean particle diameter (Rau et al., 2014).

3.1.2.1   Thermal breakthrough curves

In the step input experiments, five thermal velocities were calculated for each sensor and experiment by:

$$v_{therm} = \frac{distance_{Pt100}}{t_{char}} \tag{27}$$

with $distance_{Pt100}$ [m] as the distance of the temperature sensor from the inflow. The characteristic time t_{char} [s] for $v_{therm\,T25}$, $v_{therm\,T50}$ and $v_{therm\,T75}$ [m s⁻¹] is defined as the time when the normalized temperature reached 25 %, 50 %, 75 %, respectively. The t_{char} for $v_{therm\,peak\,dT/dt}$ [m s⁻¹] is defined as the time, when the first time derivative of the thermal BTC reaches its maximum. The t_{char} for the peak velocity in the finite duration pulse experiments is the time when the maximum temperature of the thermal BTC for each sensor is reached. These or similar approaches are common to determine the thermal velocity from thermal BTCs (Table 4) and were therefore chosen in this study.

Moreover, an analytical model for each setup was used to determine the longitudinal effective thermal dispersion coefficient $D_{l,eff,fit}$ [m² s⁻¹] (De Marsily, 1986) and the thermal velocity $v_{t,fit}$ [m s⁻¹] as explained in the following sections.

3.1.2.2 Analytical solution – step input

An analytical solution is used to derive the thermal velocity and the longitudinal effective thermal dispersion from the thermal BTC. The solution of the 1D convective dispersive heat transport equation for a step input is given by eq. (28) (van Genuchten and Alves, 1982; Runkel, 1996) and eq. (29) with the boundary and initial conditions listed in eq. (30a) and (30b), respectively:

$$G_{x,t} = \left[\frac{1}{2} erfc \left(\frac{x - v_{t,fit}t}{2\sqrt{D_{l,eff,fit}t}} \right) + \sqrt{\frac{v_{t,fit}^2 t}{\pi D_{l,eff,fit}}} exp \left[-\frac{(x - v_{t,fit}t)^2}{4D_{l,eff,fit}t} \right] \right. $$
$$\left. - \frac{1}{2} \left(1 + \frac{v_{t,fit}x}{D_{l,eff,fit}} + \frac{v_{t,fit}^2 t}{D_{l,eff,fit}} \right) exp \left(\frac{v_{t,fit}x}{D_{l,eff,fit}} \right) erfc(\frac{x + v_{t,fit}t}{2\sqrt{D_{l,eff,fit}t}}) \right] \tag{28}$$

$$T_{(x,t)} = T_{0,\text{Celsius}} + (T_{inj} - T_{0,\text{Celsius}})G_{x,t} \tag{29}$$

$$T_{(x,0)} = T_{0,\text{Celsius}} \tag{30a}$$

$$T_{(0,t)} = T_{inj} \tag{30b}$$

where $D_{l,eff,fit}$ [m² s⁻¹] is the longitudinal effective thermal dispersion coefficient and $v_{t,fit}$ [m s⁻¹] is the thermal velocity, t [s] is the time, x [m] is the distance, T_{inj} is the injection temperature and $T_{0,Celsius}$ is the initial temperature.

3.1.2.3 Analytical solution – multiple pulse input

As described in 3.1.1.5, due to varying ambient temperatures and despite the thermal insulation of the tubes from the thermostats to the column, the initial temperature did not always exactly match after the end of the pulse duration. For this reason, the analytical solution for a multiple pulse input boundary condition was used instead of a solution for a pulse input of finite duration. The analytical solution for multiple pulse input conditions can be written as the sum of the solutions for the individual pulses (eq. 31) (van Genuchten and Alves, 1982; Toride et al., 1995). This results in eq. (32) for the multiple pulse input conditions (eq. 33a, b, c) applied in the present study:

$$T_{(x,t)} = \sum_{j=1}^{i} (T_{j,0} - T_{j-1,0}) \, G_{(x,t-\tau_{i,pulse-1})} \tag{31}$$

$$T_{(x,t)} = \begin{cases} t \leq \tau_{pulse}\colon \; T_0 + (T_{inj} - T_0)G_{(x,t)} \\ t > \tau_{pulse}; \; T_0 + (T_{inj} - T_0)G_{(x,t)} + (T_{end} - T_{inj})G_{(x,t-\tau_{pulse})} \end{cases} \tag{32}$$

$$T_{(x,0)} = T_{0,Celsius} \text{ for } x \geq 0 \tag{33a}$$

$$T_{(0,t)} = T_{inj} \text{ for } \tau_{pulse} \geq t \geq 0 \tag{33b}$$

$$T_{(0,\infty)} = T_{end} \text{ for } t > \tau_{pulse} \tag{33c}$$

where $\tau_{i,pulse}$ [s] represents the duration of the pulse i, x [m] is the distance, t [s] is the time, T_{inj} [°C] is the injection temperature, and T_0 [°C] is the initial temperature. The normalized versions of eq. (29) and eq. (32) were used to determine the longitudinal effective thermal dispersion, $D_{l,eff,fit}$, and to fit the thermal velocity, $v_{t,fit}$. This was done by minimizing the sum of squared differences between the normalized measured temperatures and the normalized modeled temperatures for each sensor with the corresponding distance, x.

3.1.2.4   Solute breakthrough curves – Dirac input

To determine the hydrodynamic flow conditions and parameters of the experiments, the recorded solute BTCs were examined. The analytical solution to the 1D advection dispersion model for an instantaneous injection is given by (Lenda and Zuber, 1970), eq. (34) based on eqs. (35) and (36), given the initial and boundary conditions listed as eqs. (37a, b, c):

$$C(t) = \frac{M}{Q t_0} \frac{1}{\sqrt{4\pi P_D (\frac{t}{t_0})^3}} \exp\left[-\frac{\left(1 - \frac{t}{t_0}\right)^2}{4 P_D \frac{t}{t_0}}\right] \tag{34}$$

$$n_{eff} = \frac{Q t_0}{\pi r^2 x} \tag{35}$$

$$\alpha_i^s = x P_D \tag{36}$$

$$C_{(x,0)} = \frac{M}{Q} \delta(t) \text{ for } x \geq 0 \tag{37a}$$

$$C_{(0,0)} = 0 \tag{37b}$$

$$\lim_{x \to \infty} C_{(x,\infty)} = 0 \tag{37c}$$

where α_i^s [m] is the solute longitudinal dispersivity, Q [m³ s⁻¹] is the volume flow, r [m] is the radius of the column, M [g] the injected tracer mass, t_0 [s] is the mean transit time and P_D [-] is the dispersion parameter. The values of t_0 and P_D were determined by least-square based fitting of eq. (34) to the measured solute BTC. The seepage velocity is determined via $v_a = \frac{x}{t_0}$, where x is the distance between injection and the sample point, which here is equal to the length of the column (1.5 m).

3.2 Mathematical modeling to quantify LTNE effects using numerical and analytical solutions

The following section lays out the setup of the numerical parameter study used to evaluate if LTNE effects are likely to occur in conditions expected in natural porous media such as aquifers and streambeds. This chapter is based on the methods section of Gossler et al. (2020) but has been extended and adapted.

3.2.1 Heat transfer coefficient

As shown in section 2.5 the existing heat transfer coefficients do not represent the conditions expected in natural porous media. Therefore, a new regression using only the experimental data representative for conditions in porous aquifers (Re < 50 and n_{tot}< 0.5) is carried out. We found only one study (Kunii and Smith, 1961) inspecting Nu values for very low Re (Re < 0.1), and their study was disregarded because the mathematical model was criticized by several authors (Littman et al., 1968; Gunn and De Souza, 1974; Wakao et al., 1979). Because the raw data of all of the published experiments were determined with a Pr [-] of 0.7-1 (gas), we corrected the Nu [-] values based on the correlations of Wakao et al. (1979) and Zhu et al. (2019) (Table 3) using the Pr value of 9 (water, 10°C) for each Nu of the respective Re value z:

$$Nu_{cor,Re=z} = \left(Nu_{\mathrm{Pr}=9,Re=z} - Nu_{\mathrm{Pr}=0.7,Re=z}\right) + Nu_{orig,Re=z} \tag{38}$$

$Nu_{orig,Re=z}$ [-] gives the originally measured Nu [-] value at a Re [-] of z. To correct for the higher Pr of water, the amount of increase of the Nu due to the higher Pr is added. This amount is calculated as $\left(Nu_{\mathrm{Pr}=9,Re=z} - Nu_{\mathrm{Pr}=0.7,Re=z}\right)$. To limit the influence of this adaption, the data of Achenbach (1995) and Wakao et al. (1979) were adapted using the correlation of Wakao et al. (1979) as their correlations cover approximately the same Re range. The data of Sun et al. (2015), Tavassoli et al. (2015), Singhal et al. (2017b), and Chen and Müller (2019) were adapted by using the correlation of Zhu et al. (2019) who used their data to build a new correlation.

Theoretical considerations for heat transfer between a sphere and a fluid flowing around it show that Nu must have a minimum value of 2 (Ranz and Marshall, 1952; Shent et al., 1981). As argued for example by Nelson & Galloway (1975), lower Nu numbers may occur in a packed bed of spheres. In our work, due to the low range of Pr expected in groundwater conditions ($Pr^{1/3} \approx 2.08$ at 10°C and $Pr^{1/3} \approx 1.94$ at 20 °C), the common dependency of Nu on $Pr^{1/3}$ is not

resolved. Therefore, following the common dependency of *Nu* on *Re* with a lower limit (see e.g. Table 3) a correlation of

$$Nu = 1 + aRe^b \qquad (39)$$

is fitted to all available data using *a* and *b* as free parameters.

In addition to the parameter study of the new correlation, a parameter study is conducted for five (Wakao et al., 1979; Achenbach, 1995; Singhal et al., 2017b; Zanoni et al., 2017; Zhu et al., 2019) other *Nu* correlations, to evaluate the influence of the *Nu* correlation choice.

3.2.2   Numerical solution of the LTE and LTNE model

In the simulations conducted as part of our work, the LTE (eq. 2) and LTNE (eqs. 10 & 11) models with the following initial (eq. 40a) and boundary conditions (eq. 40b) were used.

$$T_{f(x,0)} = 0; T_{s(x,0)} = 0 \text{ at } t = 0 \qquad (40a)$$

$$T_{f(0,t)} = 1; \frac{\partial T_s}{\partial x} = 0 \text{ at } t > 0, x = 0 \qquad (40b)$$

The LTE and LTNE models explained above (section 2.2 & 2.4) were solved using the MATLAB function "pdepe" which utilizes a finite-element, piecewise nonlinear Galerkin/Petrov-Galerkin method with second-order accuracy in space (Skeel and Berzins, 1990). The time discretization is automatically adapted. A Linux Cluster (at the Leibniz Supercomputing Centre of the Bavarian Academy of Science and Humanities) was utilized to run the simulations in parallel. The MATLAB and R scripts used to run the simulations are available as stated in Gossler et al. (2020) at the mediaTum data repository (https://media- tum.ub.tum.de/1543886; 10.14459/2020md1543886).

3.2.3   Grid / mesh independency

To avoid boundary effects, the model domain was setup with 15 m length. The spatial discretization was 0.0025 m for distances less than 4.5 m (1.5 · maximum distance of interest = 3 m) and increased along the remaining distance. The fine numerical discretization and the chosen

input parameter range leads to simulations in which the nodal distance was smaller than the used grain size. While the representative elementary volume is usually larger than the mean grain size in the volume averaging approach (Rau et al., 2014), we do not consider this problematic, as we consider homogenous parameter conditions within the whole model domain (see also Appendix A for a further discussion). This computationally demanding configuration was chosen as conservative setup to assure mesh independency, but a sensitivity analysis revealed that the results are still acceptable at spatial discretization up to 0.01 m and when reducing the model domain length to 5 m. See Appendix A for the results of the mesh independency study.

3.2.4   Analytical solution for validation of numerical model

The breakthrough curves (BTCs) of the numerical LTE model are compared with the BTCs derived from the following analytical solution (eq. 41) (van Genuchten and Alves, 1982):

$$T_{x,t} = \frac{T_{degree,x,t} - T_0}{T_{inj} - T_0} = \frac{1}{2} erfc\left(\frac{x - v_{t,LTE,fit}}{2\sqrt{D_{l,eff,fit}t}}\right) + \frac{1}{2}\exp\left(\frac{v_{t,LTE,fit}x}{D_{l,eff,fit}}\right)erfc\left(\frac{x + v_{t,LTE,fit}t}{2\sqrt{D_{l,eff,fit}t}}\right) \qquad (41)$$

with $T_{x,t}$ [-] as the normalized temperature, T_0 [K] as the initial temperature, T_{inj} [K] as the injection temperature, $T_{degree,x,t}$ [K] as the temperature at distance x [m] at time t [s], $v_{t,LTE,fit}$ [m s^{-1}] as the advective thermal velocity and $D_{l,eff,fit}$ [m^{-2} s^{-1}] as the effective thermal dispersion.

The BTCs of the numerical LTNE model are compared with the BTCs of the analytical solution (eqs. 42-48) (Wakao and Kaguei, 1982):

$$T_{x,t} = \frac{1}{2} + \frac{2}{\pi}\sum_{n=1}^{\infty}\frac{1}{2n_{tot} - 1}Imag[(F(w))e^{wt}] \qquad (42)$$

With w and $F(w)$ defined as:

$$w = i(2n_{tot} - 1)\pi/\tau \qquad (43)$$

$$F(w) = \sum_{i=1}^{4} P_i e^{m_i} \tag{44}$$

i is the unit imaginary number and τ [s] as a time period long enough to reach $T = T_{inj}$

m_i is the i-th root of the following equation:

$$m_i^4 - \frac{v_a x}{\left(\frac{\lambda_f}{\rho_f c_f} + D_l\right)} m_i^3 - \left[\frac{n_{tot}\rho_f c_f w + h_{sf} a_{sf}}{n_{tot}\rho_f c_f \left(\frac{\lambda_f}{\rho_f c_f} + D_l\right)} + \frac{(1 - n_{tot})\rho_s c_s w + h_{sf} a_{sf}}{(1 - n_{tot})\lambda_s} \right] x^2 m_i^2$$

$$+ \frac{v_a x^3}{\left(\frac{\lambda_f}{\rho_f c_f} + D_l\right)(1 - n_{tot})\lambda_s} [(1 - n)\rho_s c_s w + h_{sf} a_{sf}] m_i \tag{45}$$

$$+ \left[\frac{\rho_s c_s}{\left(\frac{\lambda_f}{\rho_f c_f} + D_l\right)\lambda_s} w^2 + \frac{n_{tot}\rho_f c_f + (1 - n_{tot})\rho_s c_s}{n_{tot}\rho_f c_f \left(\frac{\lambda_f}{\rho_f c_f} + D_l\right)(1 - n_{tot})\lambda_s} h_{sf} a_{sf} w \right] x^4 = 0$$

P_i is an i-th root of

$$\sum_{i=1}^{4} \left(1 - \frac{n\rho_f c_f \left(\frac{\lambda_f}{\rho_f c_f} + D_l\right)}{n\rho_f c_f v_a x} m_i \right) P_i = 1 \tag{46a}$$

$$\sum_{i=1}^{4} \left(v_i + \frac{h_{sf} a_{sf} x^2}{1 - w_i} \right) P_i = 0 \tag{46b}$$

$$\sum_{i=1}^{4} m_i e^{m_i} P_i = 0 \tag{46c}$$

$$\sum_{i=1}^{4} \left(v_i + \frac{h_{sf} a_{sf} x^2}{1 + w_i} \right) e^{m_i} P_i = 0 \tag{46d}$$

and

$$v_i = n_{tot}\rho_f c_f \left(\frac{\lambda_f}{\rho_f c_f} + D_l\right) m_i^2 - n_{tot}\rho_f c_f v_a x \left[m_i + \left(w + \frac{h_{sf} a_{sf}}{n_{tot}\rho_f c_f} \right) \frac{x}{v_a} \right] \tag{47}$$

$$w_i = \frac{(1 - n_{tot})\lambda_s m_i}{(1 - n_{tot})h_{sf}a_{sf}x} \tag{48}$$

3.2.5 Parameter study

Table 7 shows the range of values used in our investigation. The parameters are independent of each other, e.g. the porosity does not constrain the seepage velocity etc. Dependent fluid properties, such as the thermal conductivity λ_f [W m^{-1} K^{-1}], the density ρ_f [kg m^{-3}] and the specific heat capacity c_f [J kg^{-1} K^{-1}], were calculated from the fluid temperature T_f (Furbo, 2015). *Nu* was computed through the new correlation given by eq. (39) (Fig. 25b). The resulting *Re* [-] ranges between 0.015 and 70 with 95 % of the simulations within the range of 1 to 50.

Table 7: Range of modeling parameter values as used in the parameter study representing typical porous aquifer ranges (Banks, 2012) . The thermal dispersivity is based on the power law relationship with the specific discharge q (Rau et al., 2012b).

Parameter	Range
Thermal conductivity solid λ_s:	1.5 – 8 W m^{-1} K^{-1}
Fluid temperature T_f :	2°C – 40°C
Seepage velocity v_a:	1 – 30 m d^{-1}
Porosity n_{tot}:	0.1 – 0.45
Particle size d_p:	1 mm – 15 cm
Thermal dispersivity β:	0.1 – 10 s^{-1}
Vol. heat capacity solid $\rho_s c_s$:	1.5*10^6 – 3.5*10^6 J m^{-3} K^{-1}

To investigate the entire parameter space, first a uniformly distributed random sample for each independent parameter (Table 7) was created. To decrease the computational cost of the sensitivity analysis the random parameter sets were extended using Saltelli's scheme (Saltelli, 2002). Then, the dependent fluid parameters were calculated. The number of parameter sets was varied from 48 to 32,000 resulting in 50,608 different parameter sets for each *Nu* correlation. Each parameter set was used in a model run where a unit step boundary condition was applied to create thermal BTCs for the LTE and LTNE models. The thermal BTCs were analyzed for the distances of 0.5 m, 1 m, 2 m, and 3 m.

3.2.6 Quantification of local thermal non-equilibrium

Three methods were used to quantify the magnitude of the effect of LTNE. Method 1 was newly developed in this study and compared to the two existing methods (Method 2 & 3), as explained in section 2.6. To enhance the comprehensibility and distinguishability of the methods, the terms introduced in the state of the art have been adapted from $LTNE_{LTE-LTNE}$ to $LTNE_{method2}$ and from $LTNE_{fluid,solid}$ to $LTNE_{method3}$.

Method 1: Comparison of the difference of effective thermal dispersion and advective thermal velocity between the LTE and LTNE model via the following approach:

1. Simulation of fluid temperature BTC with the LTNE model;

2. Estimation of the effective thermal dispersion coefficient $D_{l,eff,fit}$ and the advective thermal velocity $v_{t,fit}$ from the LTNE calculation (previous step) by fitting the analytical LTE model (van Genuchten and Alves, 1982) (eq. 41) using a standard non-linear least square fitting procedure;

3. Comparison of the estimated $D_{l,eff,fit}$ and $v_{t,fit}$ from the LTE model with the used $D_{l,eff}$ (eq. 3) and $v_{t,LTE}$ (eq. 7) in step 1.

$$LTNE_{method1,D_l} = \frac{D_{l,eff,fit}}{D_{l,eff}} \tag{49}$$

$$LTNE_{method1,v} = \frac{v_{t,fit}}{v_{t,LTE}} \tag{50}$$

Method 2: Maximum and average temperature difference between the normalized temperature obtained using the LTE model $T_{LTE,x}$ [-] and the fluid temperature obtained using the LTNE model (Lu and Xiang, 2012; Hamidi et al., 2019) $T_{LTNE,f,x}$ [-] for each evaluated distance x (N= number of timesteps).

$$LTNE_{method2,max,x} = max_N \left| T_{LTE,x} - T_{LTNE,f,x} \right| \tag{51}$$

and

$$LTNE_{method2,mean,x} = \frac{\sum_1^N \left| T_{LTE,x} - T_{LTNE,f,x} \right|}{N} \tag{52}$$

Method 3: Maximum and average normalized temperature difference between fluid and solid (Khashan and Al-Nimr, 2005; Khashan et al., 2006; Al-Sumaily et al., 2013; Abdedou and Bouhadef, 2015) obtained using the LTNE model for each distance *x*:

$$LTNE_{method3,max,x} = max_N|T_{LTNE,f,x} - T_{LTNE,s,x}| \tag{53}$$

and

$$LTNE_{method3,mean,x} = \frac{\sum_1^N|T_{LTNE,f,x} - T_{LTNE,s,x}|}{N} \tag{54}$$

3.2.7 Global parameter sensitivity analysis

To identify the dominant LTNE parameters a global parameter sensitivity was calculated using the function "sobolSalt" as part of the R package "sensitivity" (Iooss et al., 2019). This implements the Monte Carlo estimation of the variance-based sensitivity indices (Sobol indices) of the first and total order for each independent parameter.

Chapter 4   Results and discussion

4.1   Investigation of thermal retardation and local thermal non-equilibrium effects using one-dimensional column experiments

In the following part, the results and discussion of the laboratory experiments are described. This chapter is based on the results and discussion section of Gossler et al. (2019) but has been extended and adapted.

4.1.1   Solute transport experiments

The solute tracer experiments were carried out to examine the correlation between the seepage velocity (mean solute velocity) v_a [m s^{-1}], the volume flow Q [m³ s^{-1}] and the effective porosity n_{eff} [-] of the porous media (Table 8). The tracer mass recovery was calculated as given in Klotz et al. (1988). The calculated high tracer mass recoveries indicate that most of the tracer mass was successfully injected into the column, and sorption or degradation did not take place at a significant amount. The loss in tracer mass could be due to stopping the measurements too early, photolytic degradation or trapping of small amounts of the tracer in the injection valve. The difference between the effective porosity n_{eff} (0.35) and the measured total porosity n_{tot} (0.36) (see section 3.1.1.3) is very small and in line with known values for well sorted materials (Davis and De Wiest, 1966). Similar estimates of effective porosity values derived from solute tracer experiments for gravel aquifers are reported in the literature ranging from 0.36 – 0.42 (Perlmutter and Lieber, 1970) and 0.35 - 0.39 (Garabedian et al., 1991).

Table 8: Measured and calculated parameters derived from the solute tracer experiments.

Parameter	n_{eff}	Tracer mass recovery	Longitudinal solute dispersivity
	[-]	[-]	[mm]
Mean	0.35	0.92	38
Standard deviation	0.02	0.08	5

The analytical model in eq. (34) successfully reproduces the solute BTCs from the laboratory measurements at all volume flows (Fig. 13). As expected, the determined values of v_a showed a linear dependency on Q. A linear regression (through origin) was applied (Fig. 14) to predict the values of v_a based on the applied volume flow for the "heat only" experiments . The regression curve based on the analytical modeling results matches well with the corresponding

v_a calculated by the specific discharge. The regression from the velocities determined with the analytical model from the solute BTCs shows nearly the same slope as the expected value from the specific discharge (Fig. 14). This indicates that the flow through the column was nearly uniform with negligible effects of increased fluid flow along the column wall or preferential flow paths within the porous system.
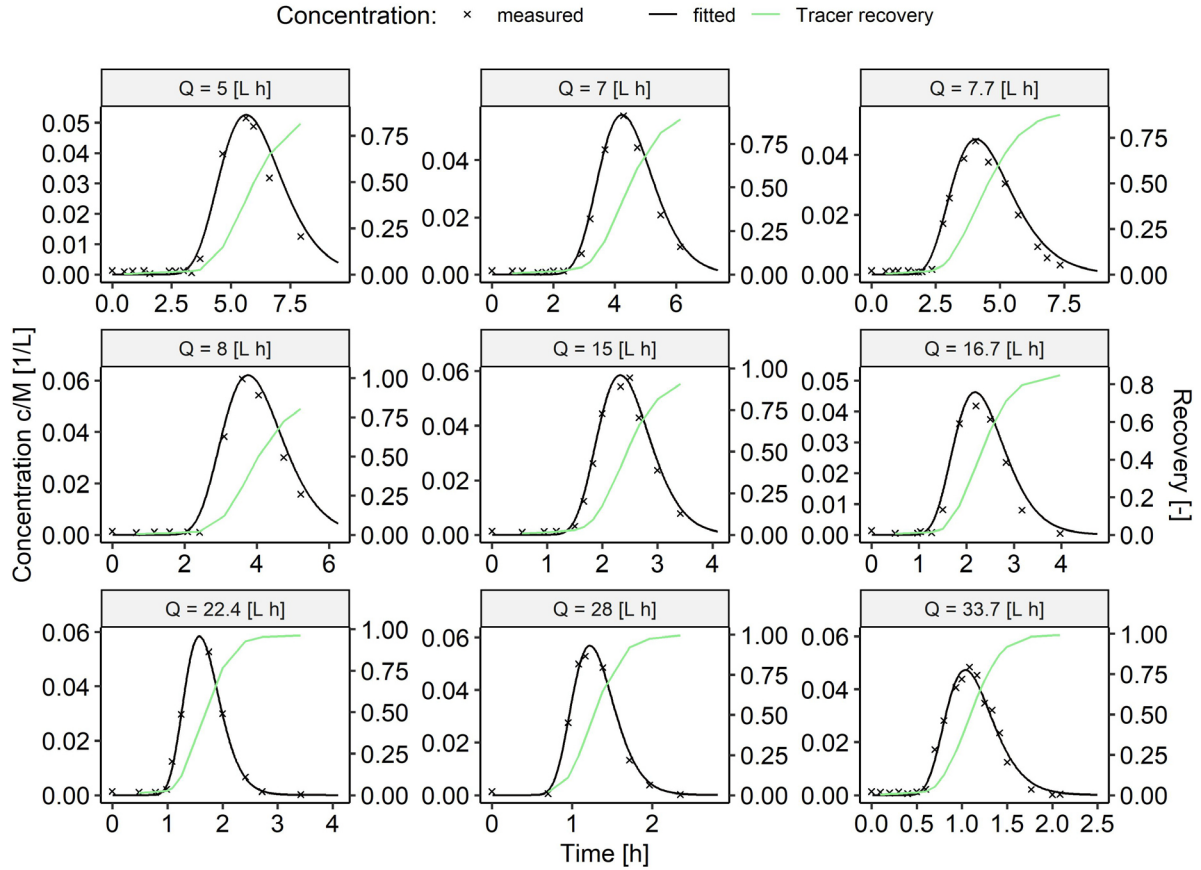
Fig. 13: Solute BTCs for 9 experiments with different volume flows. In each experiment 0.16 mg of uranine was injected. The black continuous line shows the fitted model and the black crosses are the measured uranine concentrations from the laboratory experiments.The mass recovery (continous green lines) varies between 0.79 and 1 with a mean value of 0.92.
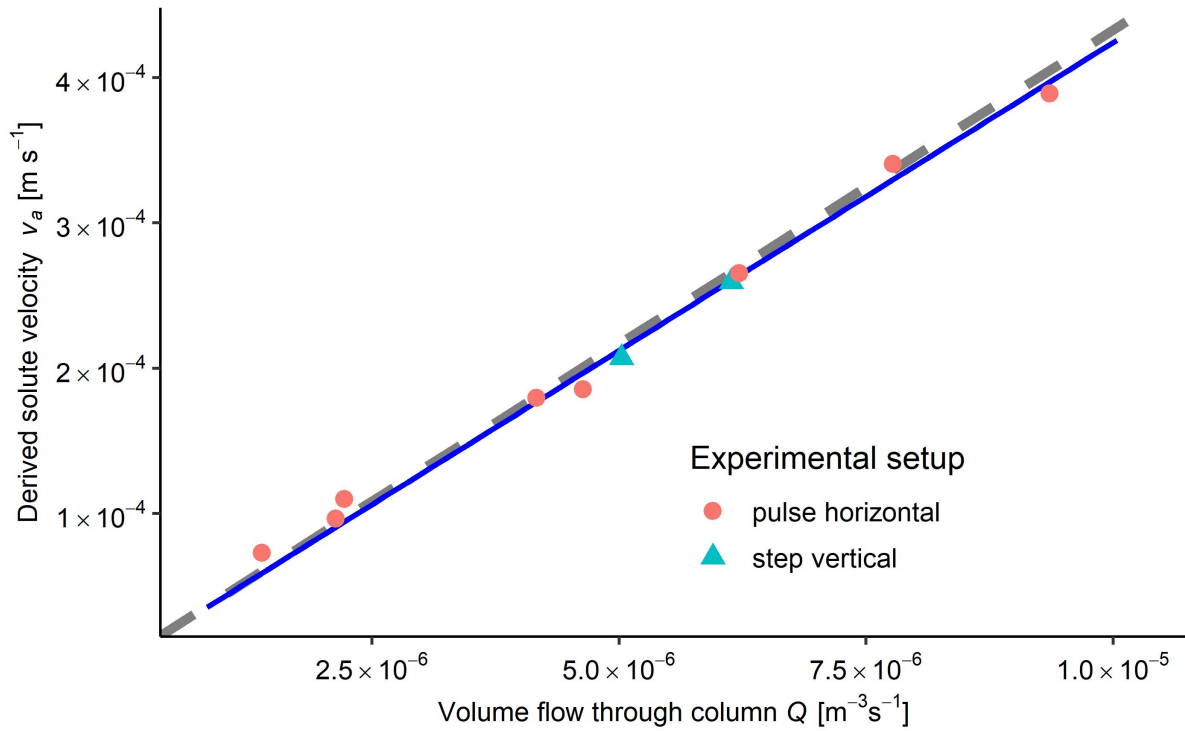
Fig. 14: The fitted solute velocities v_a derived from the uranine BTCs show a linear dependency (blue continuous line) on the volume flow Q (R² > 0.99). The black dashed line shows the expected linear dependency of the seepage velocity on the volume flow through the column, if the velocity is calculated with the effective porosity, the cross-sectional area of the column and the volume flow.

4.1.2 Heat transport experiments

4.1.2.1   Comparison of thermal velocities for step input scenarios

The effective thermal retardation in the step input experiments demonstrates good agreement with the apparent thermal retardation for $v_{therm\,fit}$ and $v_{therm\,T50}$ indicating that LTNE effects do not significantly influence the derived thermal velocity. An example of the thermal BTCs of the center temperature sensors from a step input experiment are shown in Fig. 15. The black lines indicate the modeled temperatures for each sensor, whereas the colored lines show the measured temperatures. The modeled temperatures from the analytical solution fit well with the measured temperatures for all step input experiments. With rising distance from the inflow, the differences between measured and modeled temperatures increase at the end of the BTCs (max. 0.08 of normalized temperature as highest deviation of all experiments). We interpret this as being due to slight heat loss from the column due to lower room temperatures.

The thermal BTCs of the off-center temperature sensors were used to check for uniform flow through the column. Fig. 16 shows the thermal BTCs of different vertical profiles, at ± 8 cm from the center (see Fig. 7 for sensor location), at 10 cm and 30 cm (top-to-bottom experiment (a)) and 110 cm and 130 cm (bottom-to-top experiment (b)). The bottom-to-top experiment was carried out to check for uniform flow in close proximity to the inflow area. The off-center temperature sensors delineate a nearly simultaneous increase with the temperature of the center locations. The + 8 cm sensors show a slightly faster increase. The mostly simultaneous rise of the temperature indicates that a uniform flow through the column was achieved.
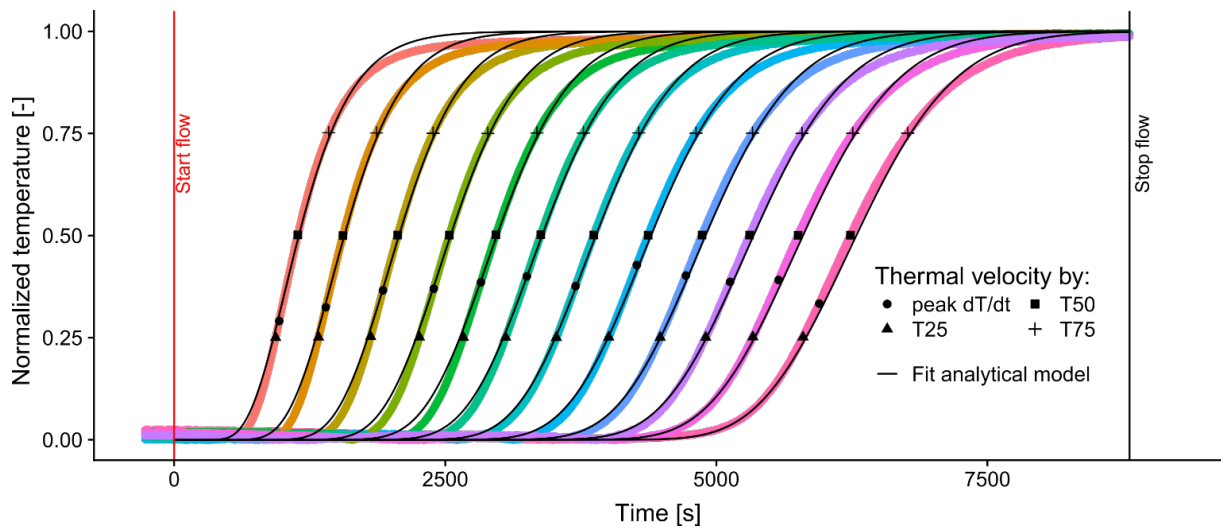
Fig. 15: Example of the thermal BTCs of a step input experiment with a seepage velocity of 37 m d^{-1}. The colored lines show the measured temperatures with each color indicating a different distance from the inflow. The black lines are derived by the fitted model for each sensor.
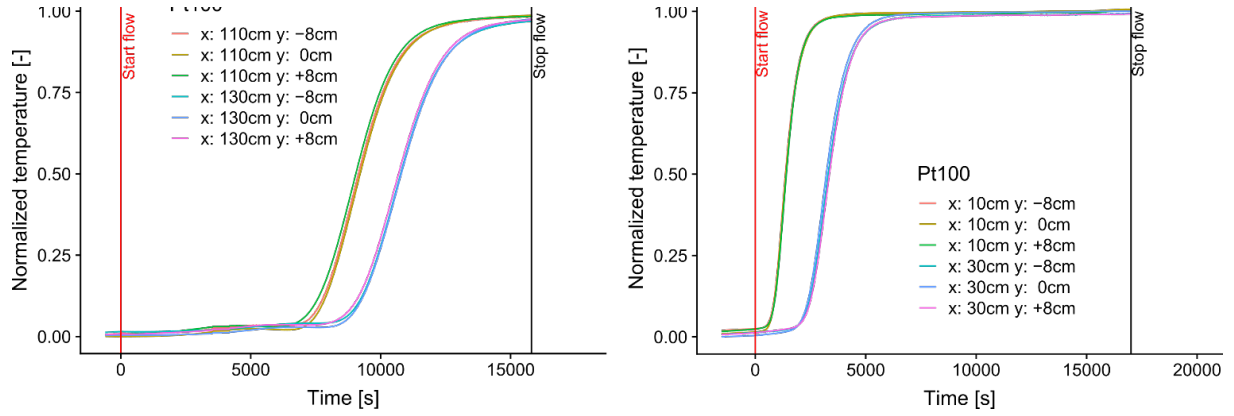
Fig. 16: Thermal BTCs for the lateral positions ± 8 cm from the center and center sensors showing similar behavior and indicating mostly uniform flow through the column; a) illustrates the BTCs in a top-to-bottom setup, with the sensors at + 8 cm showing a slightly faster increase; b) depicts the thermal BTCs for a bottom-to-top experiment.

The effective thermal retardation factors, R_{eff} obtained by eq. (24) for the different experiments are shown in Fig. 17a. The corresponding apparent retardation factor, R_{app} (eq. 25) determined for the different thermal velocities in relation to the seepage velocity is 1.88. The normalized deviation of R_{eff} from R_{app} is shown in Fig. 17b. While $v_{therm\ T25}$ and $v_{therm\ peak\ dT/dt}$ generally deliver lower values of R_{eff} than of R_{app}, $v_{therm\ T75}$ yields higher values. The deviations increase at seepage velocities lower than around 10 m d^{-1}. However, the discrepancy between R_{eff} and R_{app} were small for $v_{therm\ fit}$ and $v_{therm\ T50}$ for all investigated velocities. These systematic deviations between R_{eff} and R_{app} for the different calculation procedures result in systematic deviations in the derived seepage velocities or heat capacities (Table 9), if the thermal velocities are used with R_{app} (eq. 25).
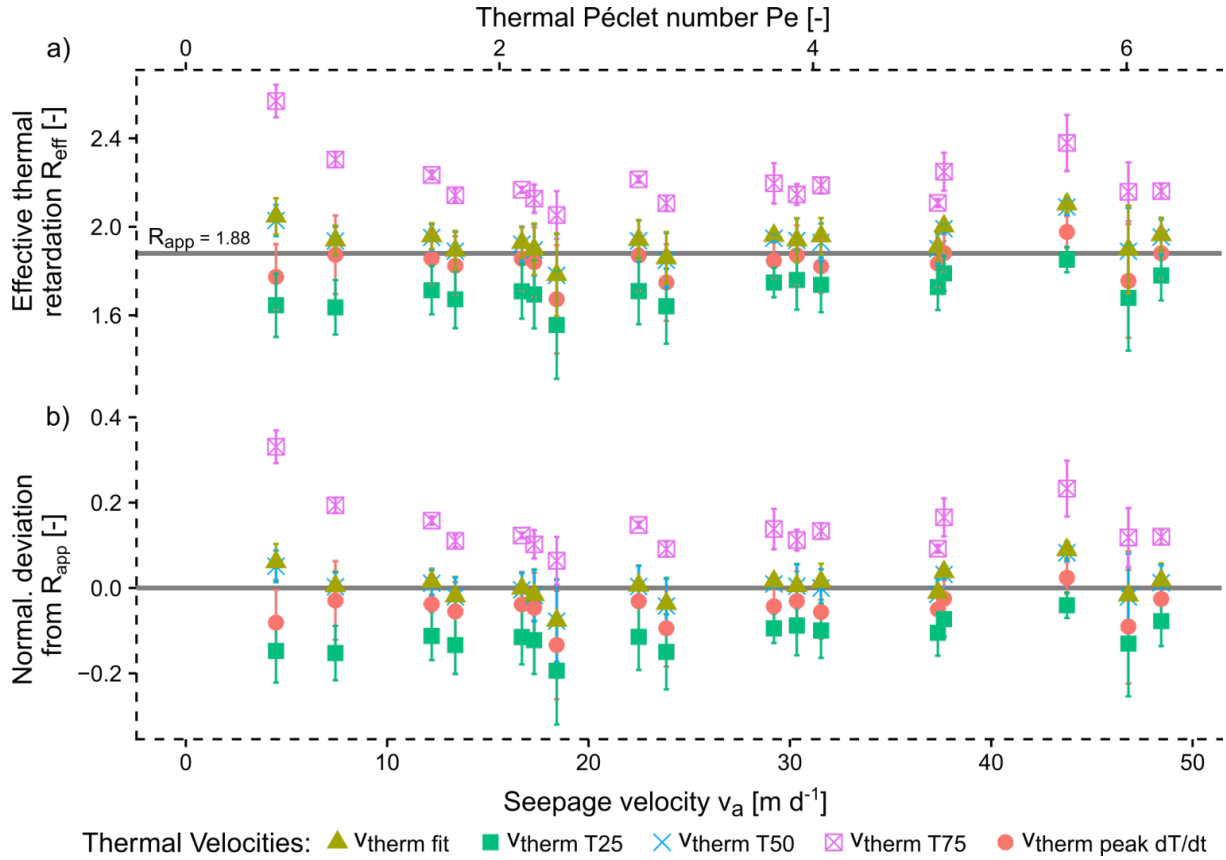
Fig. 17: a) Determined effective thermal retardation calculated by eq. (24) from the measured thermal velocities and seepage velocities for all step input experiments. The apparent thermal retardation of 1.88 calculated by eq. (25) from the heat capacities and total porosity is shown as the gray line. Fig. 17b): shows the normalized deviation from R_{app}. The error bars indicate the standard deviation when all distances are compared in one experiment.

Table 9: Overview of the deviations between the apparent thermal retardation R_{app} and the effective thermal retardation R_{eff} for the step input experiments and the resulting consequences if these thermal velocities are used to infer seepage velocities or heat capacities.

Thermal velocity	R_{eff} vs. R_{app}	Mean deviation [%]	Impact on evaluation if v_{therm} is used to infer seepage velocities / heat capacities.
$v_{therm\ T25}$	$R_{eff} < R_{app}$	-11.1	Overestimation of seepage velocities / underestimation of heat capacity of porous media; deviation increases with lower seepage velocities (<10 m/d).
$v_{therm\ T75}$	$R_{eff} > R_{app}$	14.1	Underestimation of seepage velocities / overestimation of heat capacity of porous media; deviation increases with lower seepage velocities (<10 m/d).
$v_{therm\ peak\ dT/dt}$	$R_{eff} \sim< R_{app}$	-4.3	Overestimation of seepage velocities / underestimation of heat capacity of porous media.
$v_{therm\ fit}$	$R_{eff} \sim R_{app}$	-0.7	Can be used to infer seepage velocities and heat capacity.
$v_{therm\ T50}$	$R_{eff} \sim R_{app}$	-0.2	

The absolute values of R_{eff} and deviations from R_{app} for the different thermal velocities vary among the experiments and show scatter (Fig. 17). These variations cannot be explained by non-ideal input conditions, as the influence of non-uniform boundary conditions in laboratory soil columns should dissipate at 3/2 of the radius of the column (Barry, 2009), meaning for this setup at distances higher than 21.75 cm. The relative differences between the thermal velocities are quite constant. Fig. 18 shows the normalized deviation from $v_{therm\,fit}$ for each thermal velocity and in relation to the seepage velocity. The value of $v_{therm\,fit}$ is chosen as the reference velocity. Obviously, these fitted values can be seen as the most reliable to estimate the thermal velocity as the analytical model accounts for both advective and dispersive conductive heat transport. For seepage velocities > ~10 m d^{-1} the deviations from $v_{therm\,fit}$ are quite constant, with around 10 % overestimation of the seepage velocity for $v_{therm\,T25}$ and 10-15 % underestimation for $v_{therm\,T75}$. At lower seepage velocities, the differences from $v_{therm\,fit}$ rise, especially for $v_{therm\,T25}$ and $v_{therm\,T75}$. The $v_{therm\,peak\,dT/dt}$ vary between $v_{therm\,fit}$ and $v_{therm\,T25}$, and exhibit the highest variability among one (Fig. 17) and also all experiments (Fig. 18).
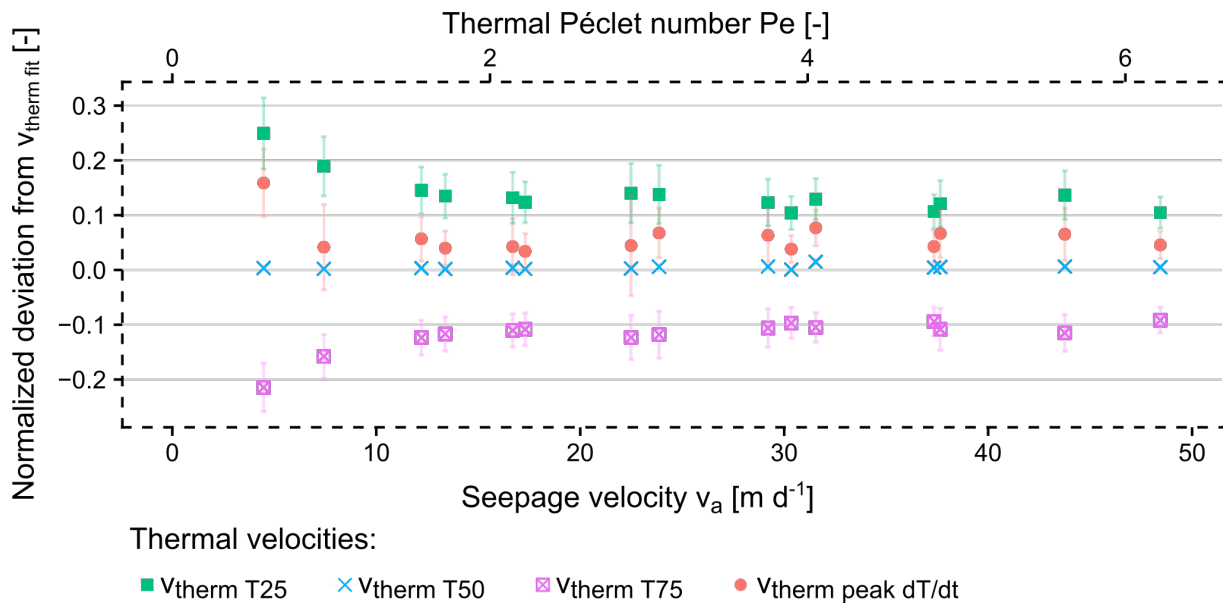
Fig. 18: Normalized deviation from the thermal velocity determined by the analytical model ($v_{therm\,fit}$) of the different v_{therm} for the step input experiments. The error bars indicate the standard deviation for the velocity of all distances.

The constant relative differences of the determined thermal velocities from $v_{therm\,fit}$ (Fig. 18) indicate that the scatter in R_{eff} (see Fig. 17a) could also be caused by the experimental setup. A possible explanation could be the occurrence of wall flow in some of the experiments. Wall

flow could lead to an overestimation of the seepage velocity in the center of the column. Other studies (such as Bandai et al., 2017), using a column with saturated porous media to investigate heat and solute dispersivities experienced the occurrence of wall flow, but it was considered negligible. Another explanation could be non-uniform heat flow due to the large grain sizes. Rau et al. (2012b) observed non-uniform heat flow due to preferential flow paths in 1D tank experiments with grain sizes of 2 mm and hypothesized that these effects could be considerably more significant in sediments with larger grain sizes. However, as these variations are relatively small compared to the total deviations of R_{eff} from R_{app}, this is not considered as a relevant bias for the results here.

In this study, the thermal velocity determined with the analytical model results in a good agreement between R_{eff} and R_{app} for all investigated seepage velocities. As a comparison, in the experiments of Rau et al. (2012b), the seepage velocities derived from the thermal BTCs with an analytical model demonstrated a systematic overestimation of the solute derived velocities by approximately 20 %, which was explained by spatial heterogeneities. Another reason for their systematic overestimation could be the occurrence of LTNE effects. As discussed in Rau et al. (2014), the LTE assumption might be flawed in natural materials in the Darcy range. Our results showed a reasonably good agreement between the expected and effective thermal retardation. Hence, if LTNE effects occur within the investigated porous medium of our experiment, they are masked by the scatter in the effective thermal retardation possibly caused by non-uniform flow induced by the large grain sizes or the laboratory setup. This means that LTNE effects, if they occur within the examined experimental conditions, do not significantly influence the resulting thermal velocity determined by fitting the analytical solution to the thermal BTCs of the step input experiments. But LTNE effects could influence thermal mechanical thermal dispersion, as Bandai et al. (2017) showed that effective thermal dispersion is particle-size dependent, while solute dispersion is not. Fig. 19 depicts the summary of the effective thermal dispersion coefficients of the step input experiments of our study compared with the data from Bandai et al. (2017). This comparison confirms the dependency of the normalized thermal dispersion coefficient on the grain size. Smaller grain sizes appear to lead to higher normalized dispersion coefficients for the same Péclet number.
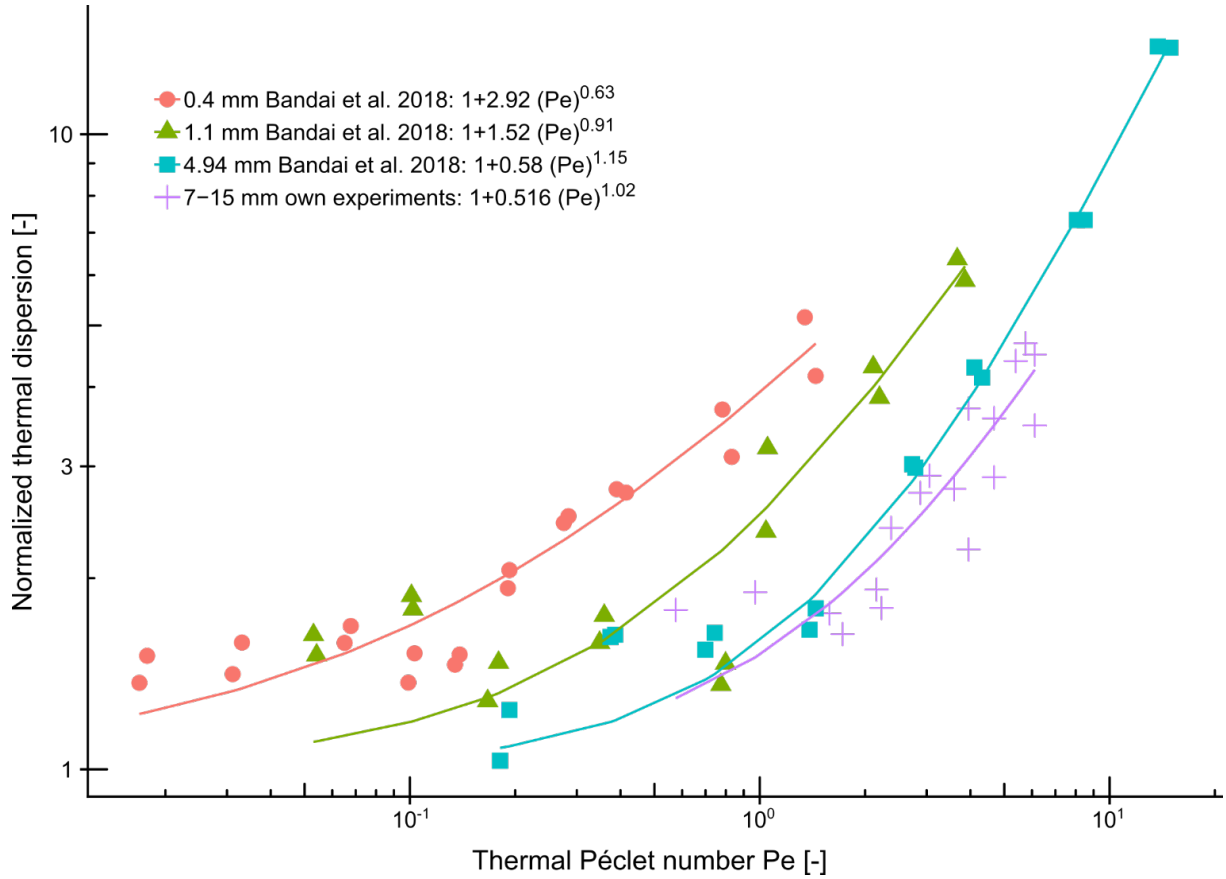
Fig. 19: Comparison of the normalized thermal dispersion coefficient D_l / κ_b for different grain sizes with data from Bandai et al. (2017). The values for the best fit for the power law equation between normalized thermal dispersion and thermal Péclet number (eq. 26) as suggested by Metzger et al. (2004) & Bandai et al. (2017) is shown in the legend.

As argued by Rau et al. (2012b), non-uniform flow could introduce lateral heat fluxes, which are violating the 1D assumption of the analytical model. This could also cause different longitudinal thermal dispersion values derived from the 1D analytical model.

The effective thermal retardation factor R_{eff} for the thermal velocity $v_{therm\ T50}$ matches the expected R_{app}. This is in agreement with the results of the numerical study of Irvine et al. (2013), where solute and heat derived velocities from the mean value between injection and initial temperature/concentration showed little deviation. This demonstrates that the thermal velocity determined by the mean between the injection and initial temperature is mainly influenced by advection. The difference between thermal conduction and solute diffusion and the differences in solute and heat mechanical dispersion obviously have no relevant effect on this thermal velocity ($v_{therm\ T50}$) for the range of seepage velocities investigated in the present experiment.

The thermal velocities from $v_{therm\ T25}$, $v_{therm\ T75}$ and $v_{therm\ peak\ dT/dt}$ show systematical deviations between R_{eff} and R_{app}. These velocities are therefore influenced by thermal dispersion. Using these velocities with R_{app} to derive the seepage velocity or heat capacities (eqs. 24 and 25) results in erroneous values. However, as the measured deviations were nearly constant at seepage velocities higher than 10 m d^{-1}, these deviations could be compensated by applying a correction factor (here around 0.86 for $v_{therm\ T75}$ and 1.11 for $v_{therm\ T25}$, see Fig. 18) if the deviations are known or determined by prior experiments. Such an approach was used by Somogyvári & Bayer (2017) to reduce the measurement time of thermal BTCs in a field experiment to reconstruct aquifer heterogeneity with a thermal tracer experiments in a tomographic setup.

4.1.2.2   Comparison of thermal velocities for finite duration pulse scenarios

The experiments with a pulse input of finite duration were conducted to evaluate if the peak velocity in a finite duration pulse heat tracer setup can be used to infer the seepage velocity and involved bulk heat capacity. At seepage velocities higher than 10 m d^{-1}, the effective thermal retardation for the peak velocity and the fitted velocity demonstrates good agreement with the apparent thermal retardation. At seepage velocities lower than 10 m d^{-1}, the effective thermal retardation is lower than expected for the peak velocity (Fig. 23).

In the vertical setup of the pulse input of finite duration experiments, the BTCs depict unexpected tailing and multiple peaks (Fig. 20). This behavior is interpreted as an influence of free convection. These effects were observed even at temperature differences between T_{inj} and T_0 smaller than 5 K. The finite duration pulse setup leads to situations where water with higher temperature (T_{inj}) and therefore lower density was located beneath the colder and denser water (T_{end}).
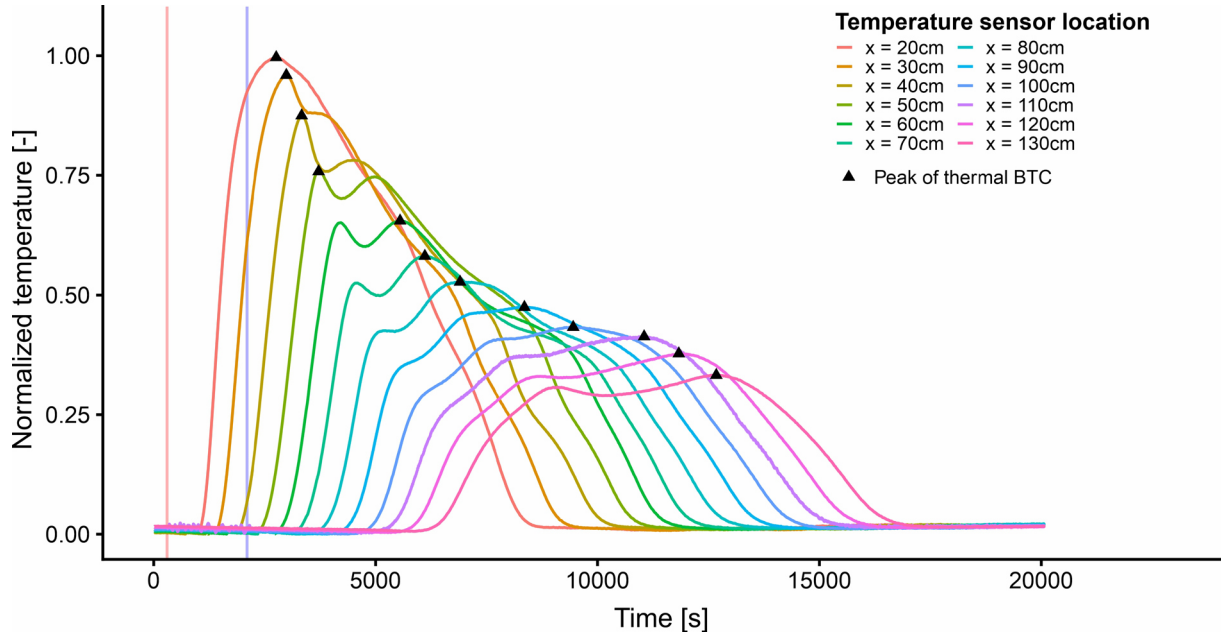
Fig. 20: Measured thermal BTCs of the center temperature sensors in an experiment with a pulse input of finite duration in vertical setup with water flow from the top of the column with an expected seepage velocity of 32 m d^{-1}, $T_{inj.}$ = 23.5 °C, T_0 =18 °C, T_{end} = 18 °C. The red vertical line indicates the start of the pulse and the blue vertical line the end of the hot water injection. The thermal BTCs showed unexpected behavior like multiple peaks. This was interpreted as influence of free convection. The experiments with a pulse input of finite duration in the vertical setup where not included in further analysis.

Free convection can occur due to thermally induced density differences of the water. Some studies concluded that density effects can be neglected, if the temperature difference is lower than 15 °C (Ma and Zheng, 2010; Russo and Taddia, 2010). Nagano et al. (2002) investigated the influence of natural convection on forced horizontal flow experimentally. They developed a criterion based on the *Reynolds number* and the modified Rayleigh number under which natural convection exerts an obvious influence for a system of forced flow. According to this criterion, which depends among other parameters on the permeability, the kinematic viscosity, particle diameter and temperature difference, the experiments should not be influenced by free convection. Schincariol & Schwartz (1990) concluded in an experimental study that buoyancy effects occur at density difference higher than 0.8 kg m^{-3}. Due to the nonlinear dependency of the water density on temperature, density effects can occur at lower temperature differences if the absolute temperature is higher. The used temperatures of 20 °C initial temperature and 25 °C injection temperature lead to density differences of 1.16 kg m^{-3} which would explain the observed effects according to the findings of Schincariol & Schwartz (1990). Density driven free convection has also been observed in a field experiment with temperature

62

differences of 8 °C (ambient temperature 17 °C injection temperature 9 °C) and advection dominated conditions (Ma et al., 2012). Therefore, density effects should be accounted for if heat is used as a tracer, keeping in mind the nonlinear dependency of the water density on temperature.

As these effects generate biased BTCs where the 1D modelling approach assumed in this study is flawed, only the experiments in the horizontal setup are used in the further investigation. In the horizontal setup, the free convection is not acting in the same direction as the forced convection.

Fig. 21 shows the thermal BTCs for an experiment with a pulse input of finite duration. The highest pulse temperature is reached at the first temperature sensor at a distance of 10 cm from the inflow. With increasing distance, the pulse temperature decreases and the BTCs spread. The modeled values show the best fitted temperatures from the analytical model (eq. 32). While in the step input scenario, the fit of the analytical model is very good, the analytical model in the scenarios with a pulse input of finite duration is not able to match the observed temperatures at all distances and experiments. This could be caused by the temperature differences in vertical direction, which developed in the experiment shortly after the inflow (Fig. 22). With increasing distance from the inflow, the differences in temperatures increased. Nevertheless, the peak velocities are similar and as the solute tracer experiments showed homogenous flow, we consider the peak velocities as unbiased. As normalization of the temperature was done with the injection temperature and initial temperature, negative normalized temperatures can occur (Fig. 22) when the end temperature T_{end} differed from the initial temperature T_0. As explained in 3.1.1.5 this did occur to a lesser extent in some of the experiments due to varying room temperatures.
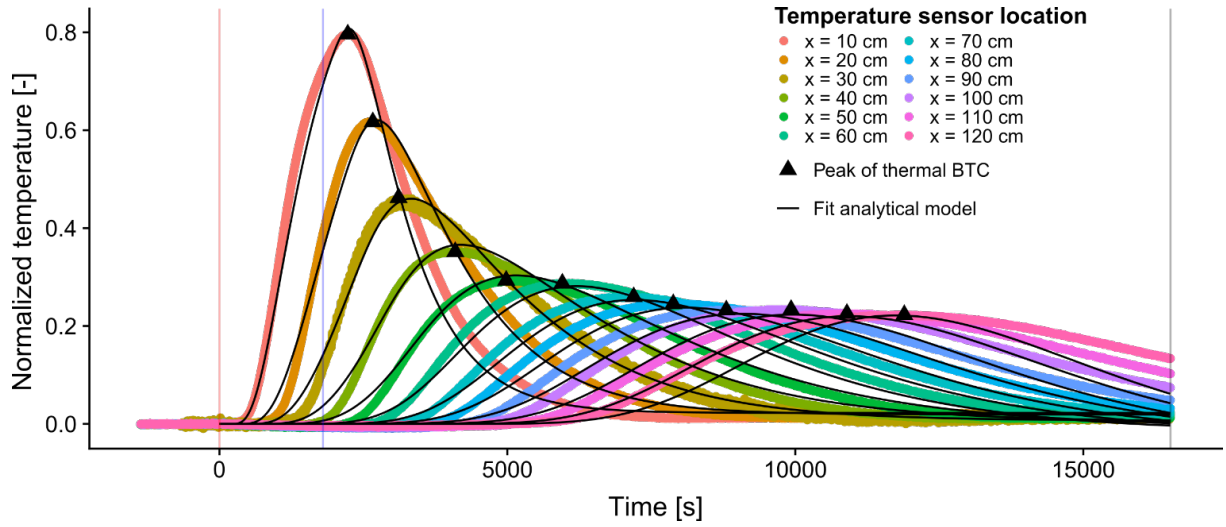
Fig. 21: Thermal BTCs and fit of the analytical model of a finite duration pulse experiment with a seepage velocity of 20.2 m d^{-1}. The colored lines are the measured temperatures for the center temperature sensors in different distances to the inflow. The vertical red, blue and gray line indicate the start of the pulse, the end of the pulse and the stop of the volume flow, respectively.
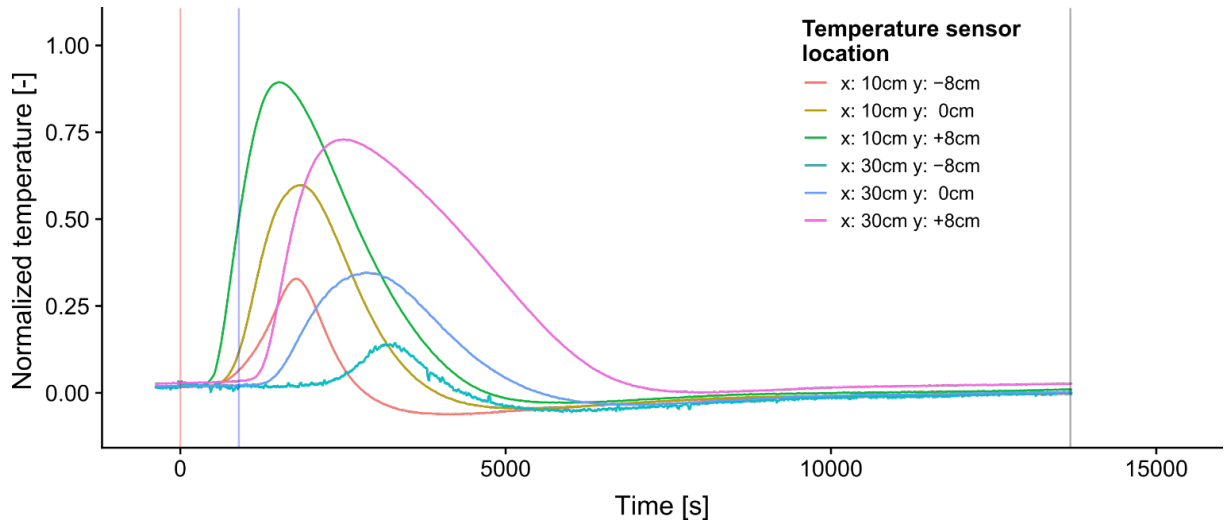
Fig. 22: Thermal BTCs for the lateral positions ± 8 cm from the center at 10 cm and 30 cm after inflow for an experiment with a pulse inpute of finite duration with a seepage velocity of 22 m d^{-1}. The temperature sensors at the top position (+ 8cm) show the highest temperatures, and the bottom sensors (-8 cm) show the lowest temperature during the pulse. The vertical red and blue line indicate the start and stop of the temperature pulse.

Fig. 23 shows the effective thermal retardation R_{eff} for all experiments with a pulse input of finite duration, if the thermal velocity is determined by either the peak velocity or an analytical model (eq. 32). For higher seepage velocities, values of R_{eff} determined with the peak and

analytical model are in the range of the apparent retardation R_{app}. At seepage velocities lower than 10 m d^{-1}, R_{eff} referring to the thermal peak velocities generally decreases, reaching values of less than 30 % lower than $R_{app.}$ This demonstrates that the peak velocity does not represent a purely advective velocity. As heat losses would lead to a delayed peak arrival time (Pan et al., 2019), the peak velocity is influenced by conduction at seepage velocities lower than 10 m d^{-1} for the investigated porous medium. One experiment with a seepage velocity of around 6.3 m d^{-1} deviates from this behavior (gray triangle in Fig. 23). This experiment is considered as an outlier, and a possible explanation could be an error in the determination of the volume flow. The measured R_{eff} for the thermal velocity determined by the analytical model showed lower deviations from R_{app}. Nevertheless, the overall deviation of R_{eff} is clearly higher than in the step input experiments (Fig. 23). A possible reason for this is the influence of the free convection in the horizontal experiments. The boundary conditions of the analytical solution would be violated by the temperature differences induced by free convection.

Similar results, that the peak velocity was overestimating the thermal velocity compared to the velocity derived from an analytical model in slow flow conditions (~8.1 m d^{-1}), were found by Becker et al. (2013). They used fiber optic distributed temperature sensing to measure infiltration rates in a recharge basin. A good agreement between thermal peak transit times and solute tracer transit times was reported by Becker et al. (2015), who employed peaks of diurnal temperature signals and bromide and B^{10}-enriched boric acid in a managed aquifer recharge system to determine mean transit times. However, seepage velocities were not determined. The deviations of R_{eff} for the peak velocity from R_{app} at lower seepage velocities can most likely be explained by the influence of thermal conduction on the thermal peak velocity. With decreasing seepage velocities, the influence of thermal conductivity increases as expressed by the thermal Péclet number (eq. 26).
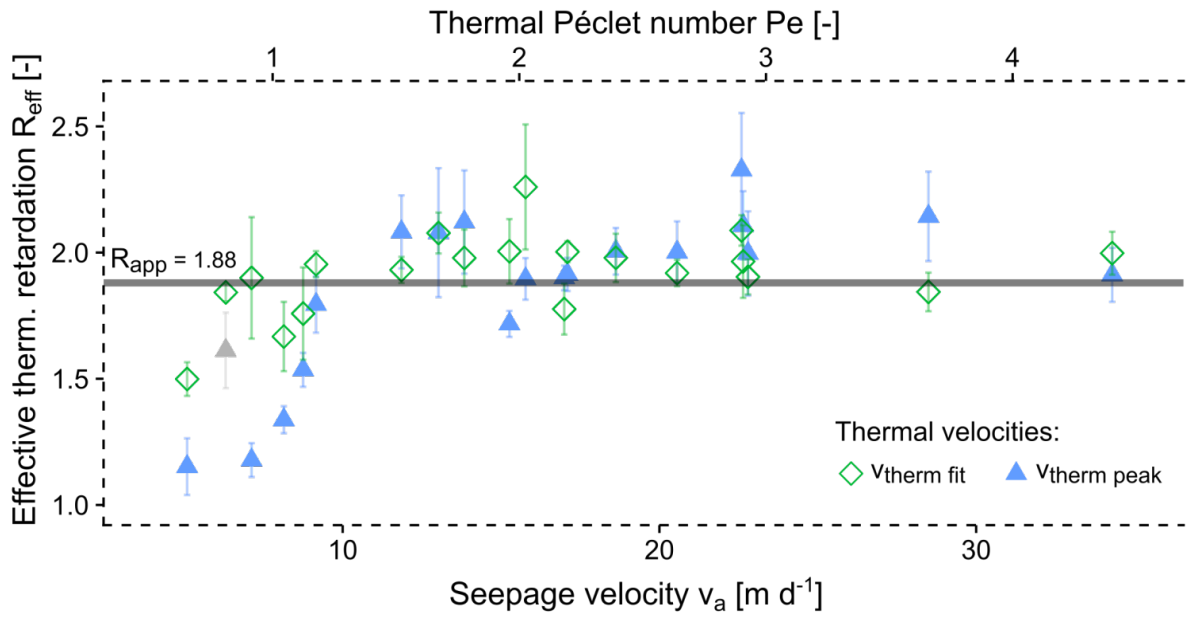
Fig. 23: Influence of the seepage velocity on effective thermal retardation (v_a / v_{therm}) for the horizontal experiments with a pulse input of finite duration. The thermal velocity is either determined as fitting parameter of an analytical model (eq. 32) or as the peak velocity. The apparent thermal retardation of 1.88 calculated by eq. (25) from the heat capacities and total porosity is shown as the gray line. The error bars represent the standard deviation for the velocity of all distances. The gray triangle is considered as an outlier. With lower seepage velocities, the effective thermal retardation for the peak velocities starts to differ from the apparent retardation.

4.2   Short summary conclusion paper 1

The experimental part of this thesis systematically compared the apparent thermal retardation R_{app} with the effective thermal retardation R_{eff} to evaluate possible influences of LTNE effects on the heat transport in conditions of a highly permeable porous aquifer. Furthermore, different methods to determine the advective thermal velocity were evaluated. Overall, 43 one-dimensional heat and coupled heat and solute tracer experiments with a step input scenario and a scenario with a pulse input of finite duration were conducted in laboratory experiments, using a gravel filled column.

The results show that when a step input signal is interpreted, the thermal velocities determined by an analytical model or the mean between the injection and the initial temperature can be used with R_{app} to predict the seepage velocities or bulk heat capacity of the porous medium in one-dimensional settings. These findings also reveal that LTNE effects do not remarkable influence the resulting thermal velocities from these two methods. However, the normalized thermal dispersion coefficient seems to be dependent on particle size, which could be governed by LTNE.

In the step input experiments, the effective thermal retardation of thermal velocities derived by the peak of the first time derivative or self-defined values between injection and initial temperatures (e.g. $v_{therm\,T25}$ / $v_{therm\,T75}$) deviate from R_{app} because these velocities are not strictly advective and influenced by the thermal dispersion coefficient. The effective thermal retardation by these methods shows a systematical deviation of 10-15 % from R_{app}. However, the results suggest that these deviations are nearly constant at seepage velocities higher than 10 m d^{-1}, and that these deviations could be compensated by applying a correction factor (here ca. 0.86 for $v_{therm\,T75}$ and 1.11 for $v_{therm\,T25}$) if the deviations are known or determined by prior experiments. This would allow reduction of the measurement time in future thermal tracer experiments, since the complete thermal BTC is not needed for evaluation.

The peak velocity appears to be significantly faster than predicted by R_{app} in cases with seepage velocities lower than 10 m d^{-1} leading to higher thermal velocities and an overestimation of the seepage velocity if R_{app} is applied. This is most likely due to the influence of thermal conduction on the thermal peak velocity. This has implications when heat is used as a tracer, for example in managed aquifer recharge systems, which could lead to an overestimation of the seepage velocity and therefore an underestimation of the mean transit time.

4.3 Mathematical modeling of local thermal non-equilibrium effects using numerical and analytical solutions

In the following part, the results and discussion of the numerical parameter study are presented. This chapter is based on the results and discussion section of Gossler et al. (2020) but has been extended and adapted.

4.3.1 Adapted Nusselt correlation

The available Nu values found in literature with conditions expected in natural porous aquifers ($Re < 50$, $n < 0.5$) are shown in Fig. 24. As all available data on Nu values are determined with gas or air as fluid ($Pr = 0.7$), the original Nu values were adapted for water as fluid ($Pr = 9$) using the Nu correlations and eq. (38). To limit the influence of this adaption, the data of Achenbach (1995) and Wakao et al. (1979) were adapted using the correlation of Wakao et al. (1979) as their correlations cover approximately the same Re range. The data of Sun et al. (2015), Tavassoli et al. (2015), Singhal et al. (2017b), and Chen and Müller (2019) were adapted by using the correlation of Zhu et al. (2019) who used their data to build a new correlation.
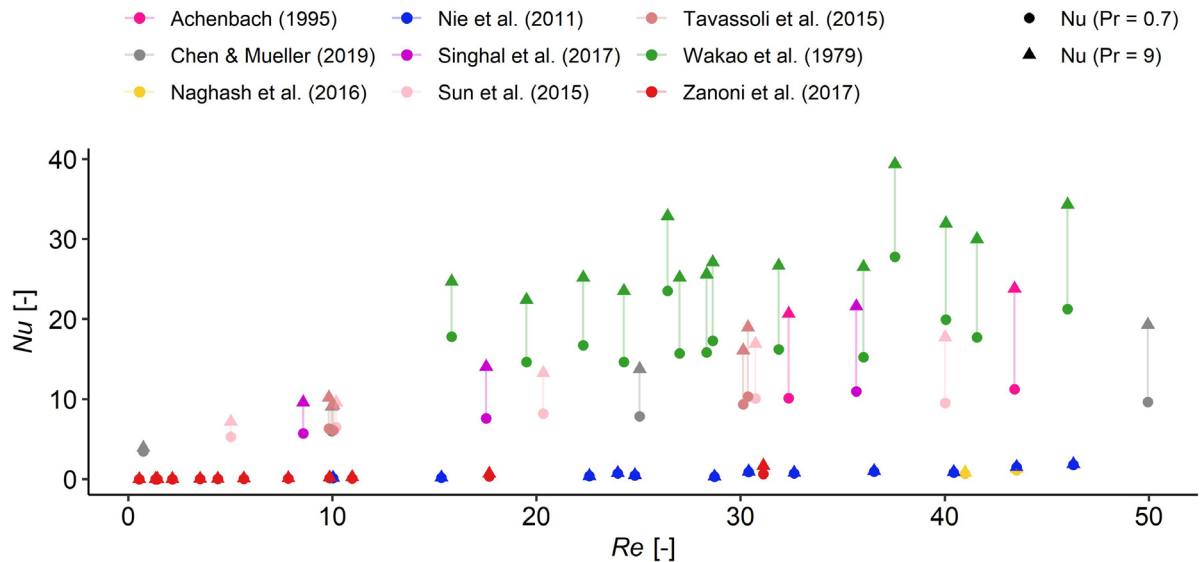
Fig. 24: Summary of literature based Nusselt values for the Reynolds ($Re < 50$) and porosity ($n < 0.5$) range expected in natural porous aquifers. As most studies were conducted with gas as a fluid, the Nusselt numbers were corrected for the Prandtl number of water using eq. (38).

Some correlations and data (Nie et al., 2011; Naghash et al., 2016; Zanoni et al., 2017) result in very low Nu numbers for the investigated Re range (Fig. 25a). A reason for the discrepancy

in *Nu* values between some publications (Nelson and Galloway, 1975; Nie et al., 2011; Naghash et al., 2016; Zanoni et al., 2017) (first group) and other studies (Wakao et al., 1979; Achenbach, 1995; Sun et al., 2015; Singhal et al., 2017b; Zhu et al., 2019) (second group) is not obvious and, therefore, the unrealistic data for porous aquifers from the first group was not included in our regression. The new regression based on the available data and eq. (39) is shown in Fig. 25. This correlation with best fit values *a* = 3.1 and *b* = 0.57 is used in all of the presented analysis.
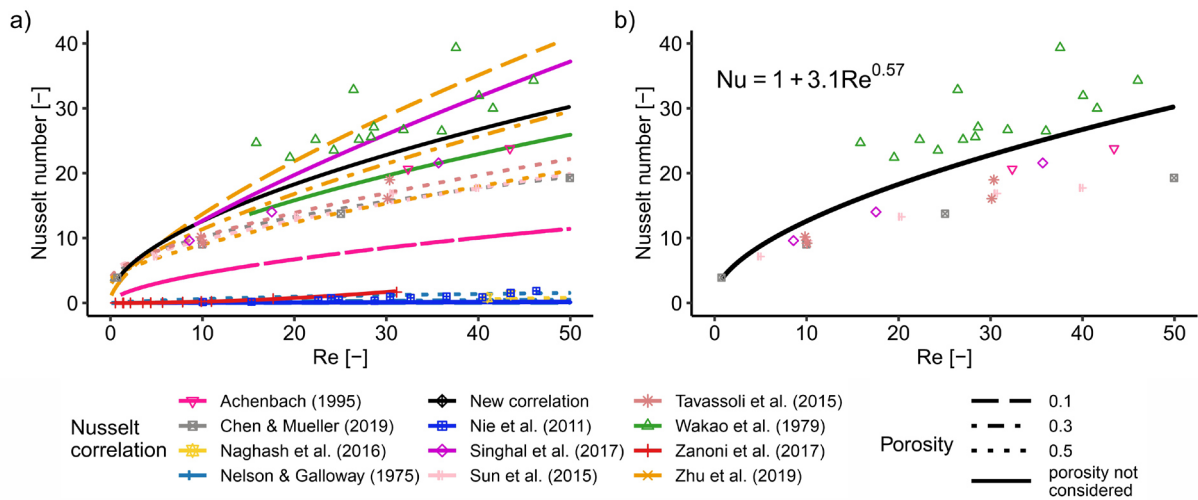
Fig. 25: a) Comparison of different Nusselt correlations with the respective data points. b) Used data for the new correlation based on the Prandtl corrected Nusselt values of published experimental data.

4.3.2 Validation of numerical model with analytical solution

The numerical LTE model demonstrates an excellent match to the analytical LTE model under all conditions (Fig. 26 & Fig. 27). Further, the numerical LTNE model matches the analytical LTNE model very well under most conditions (Fig. 26 & Fig. 27). Results from the analytical and numerical LTNE model deviate only for low flow conditions and small particle sizes. We assume that this deviation arises from a failure to compute the analytical solution for which we identified two possible reasons: (1) The function used to find the 4 complex roots of the analytical solution (eq. 45) sometimes fails to find all four roots under these conditions; (2) some roots can have values that are higher than 600 which leads to infinite values in the next step of the analytical solution and requires solving of the system of equations (eqs. 46a-d) including exp(root) (eq. 46c). To continue the computations in the latter case, values exceeding 600 were capped. A further indication of the failure to calculate LTNE fluid temperatures

using the analytical solution was a deviation of the results from that calculated using the analytical and numerical LTE solution. The numerically derived LTNE fluid temperature and solid matched the LTE solution as expected (Fig. 28).

Nu = 9.63, n = 0.322 d_p = 0.0316, v_a = 13, β = 7.89
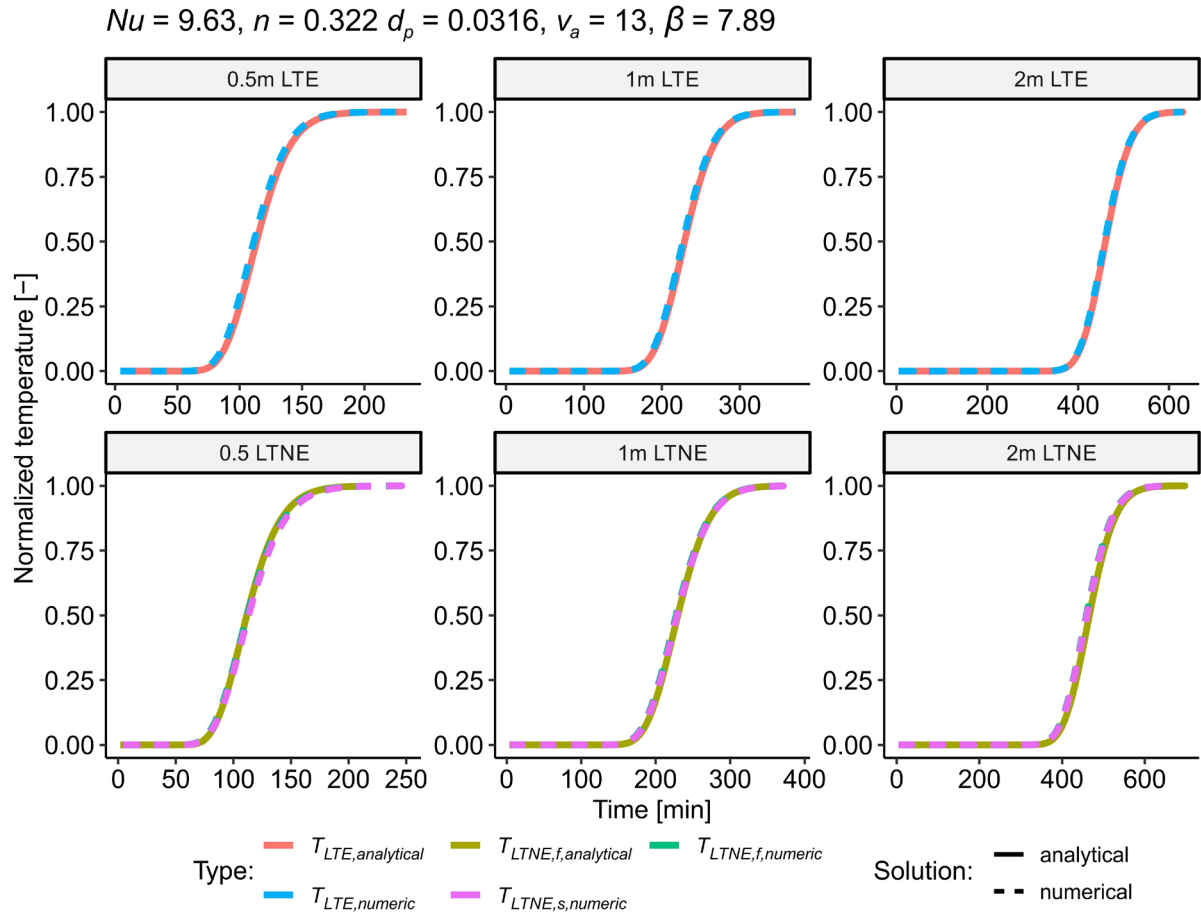
Fig. 26: Comparison of thermal BTCs calculated by the numerical and analytical LTE and LTNE models for 0.5 m, 1 m and 2 m distances. The numerical model fits the analytical solution very well. Here, we used a grain size and velocity that lie in the center of the total range considered. The Nusselt number is based on the correlation developed in this work (eq. 39 & Fig. 25b).
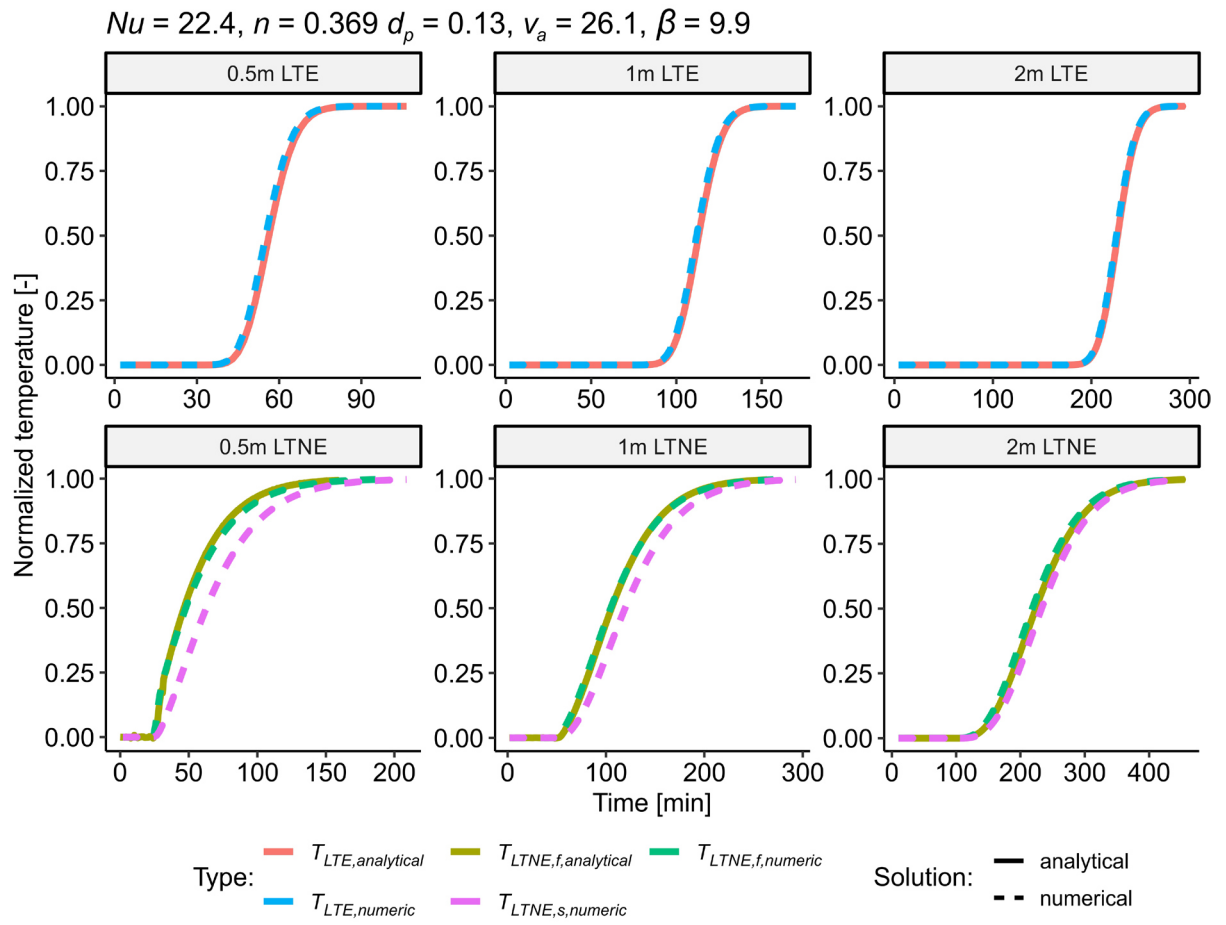
Fig. 27: Comparison of thermal BTCs derived from the numerical and analytical LTE and LTNE models for 0.5 m, 1 m and 2 m distances. The numerical and analytical models match very well. Here, we use LTNE favorable conditions with a grain size and velocity at the upper end of the range considered. The Nusselt number is based on the correlation developed in this work (eq. 39 & Fig. 25b).
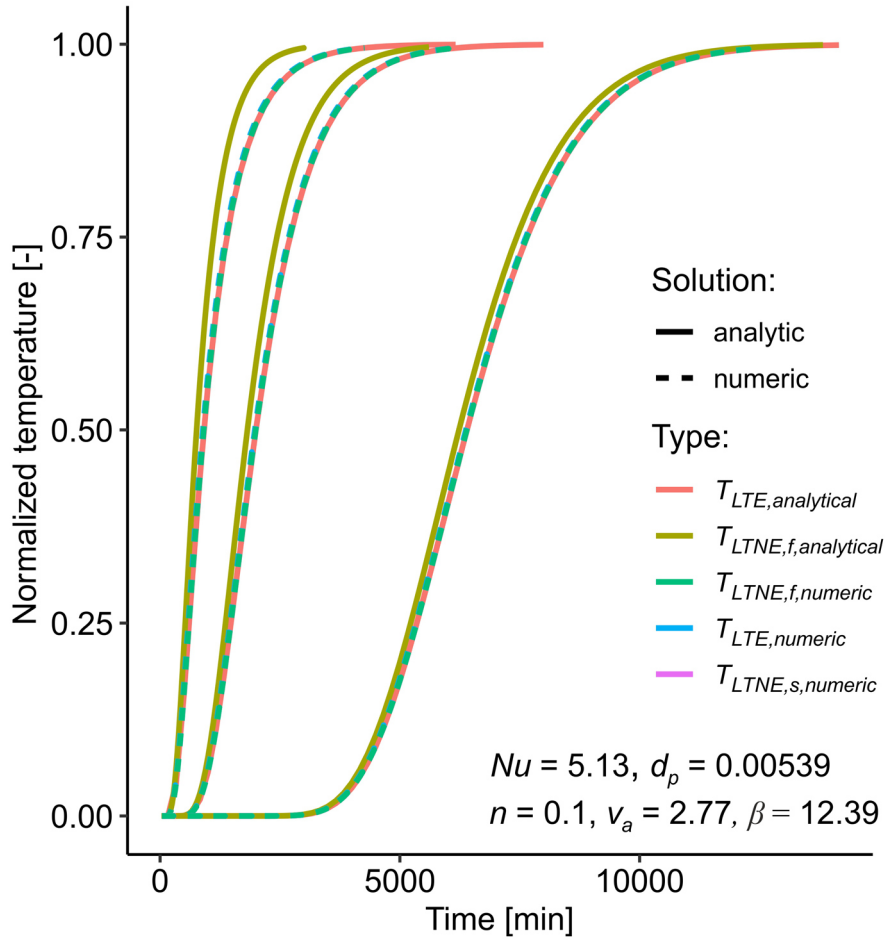
Fig. 28: For conditions of seepage velocity and particle sizes on the lower end of the range considered in this work, the numerical LTNE fluid temperature is identical to the analytical and numerical LTE model. The deviation of the analytically calculated LTNE fluid likely originates from problems associated with the calculation (see section 4.3.2 for an explanation).

4.3.3 Comparison of thermal breakthrough curves obtained from the LTE model and LTNE models

Significant differences between the modelled thermal BTCs calculated using the LTE and LTNE models can be found within the assumed parameter ranges representative of the conditions in natural porous aquifers. As an example, Fig. 29 highlights the thermal BTCs obtained from the LTE and LTNE models for particle sizes (< 0.5 cm) with slow seepage velocities (< 2 m d^{-1}) at the lower end of the investigated parameter range (Fig. 29a, b & c) and for large particles sizes (> 7.5 cm) with high seepage velocities (> 20 m d^{-1}) (Fig. 29d, e & f). Furthermore, the three different methods used to evaluate the degree of LTNE are illustrated. For low seepage velocities and small particle sizes, the LTE and LTNE models result in similar (visually the same) thermal BTCs regarding effective dispersion and advective thermal velocity (method 1). The computed normalized temperature differences between the LTE and LTNE fluid temperature (method 2) and LTNE fluid and solid temperature (method 3) are very low (< 0.005). In contrast, in the simulations for large particle sizes and high seepage velocities, the thermal BTCs from the two models differ significantly. The solid and fluid temperature of the LTNE model is noticeably more dispersed (method 1) and significant temperature differences between the LTE temperature and LTNE fluid temperature (method 2) as well as solid and fluid temperature (method 3) can be observed.
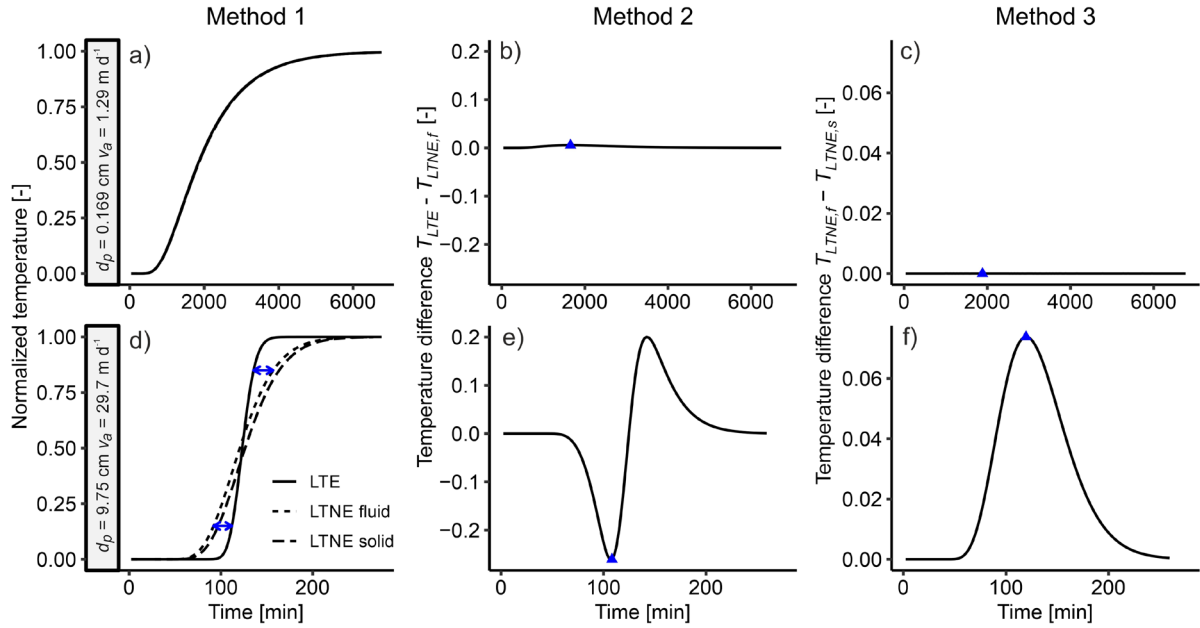
Fig. 29: Example of thermal BTCs illustrating the three different methods used to quantify LTNE. The plots a), b) and c) summarize conditions with small particles sizes d_p and low seepage velocities v_a. The plots d), e) and f) display large particle sizes and high seepage velocity conditions. Method 1 uses a normalized temperature BTC. The degree of LTNE is measured as the difference in thermal dispersion (blue arrows) and advective thermal velocity between the LTNE fluid temperature and the LTE model. Method 2 uses the temperature difference between the normalized LTE temperature and normalized LTNE fluid temperature. Method 3 measures the maximum and average temperature difference between the normalized solid and fluid temperatures. The blue triangles indicate the position of the maximum absolute values.

4.3.4   Influence of the Nusselt correlation on LTNE effects

To investigate the influence of the *Nu* correlation choice, the parameter study was extended to the *Nu* correlations suggested by Zanoni et al. (2017) as well as four others (Wakao et al., 1979; Achenbach, 1995; Singhal et al., 2017b; Zhu et al., 2019). For the *Nu* correlation by Zanoni et al. (2017) (very low *Nu* values), nearly all tested conditions lead to strong LTNE effects (Fig. 30 & Fig. 31).
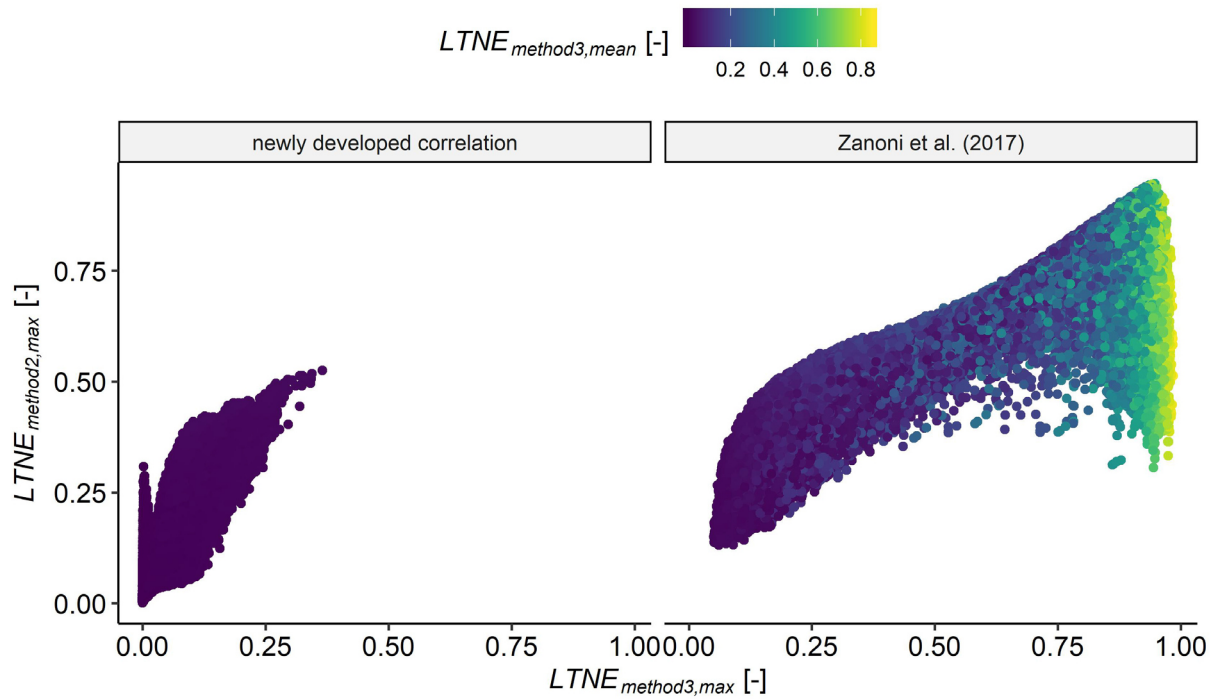
Fig. 30: Comparison of the LTNE effects for the newly developed Nusselt correlation and the Nusselt correlation of Zanoni et al. (2017) as an example of the group of correlations leading to very low Nusselt values. All simulations with the Zanoni et al. correlation lead to significant LTNE effects (e.g. $LTNE_{method2,max}$ always larger than 0.1).
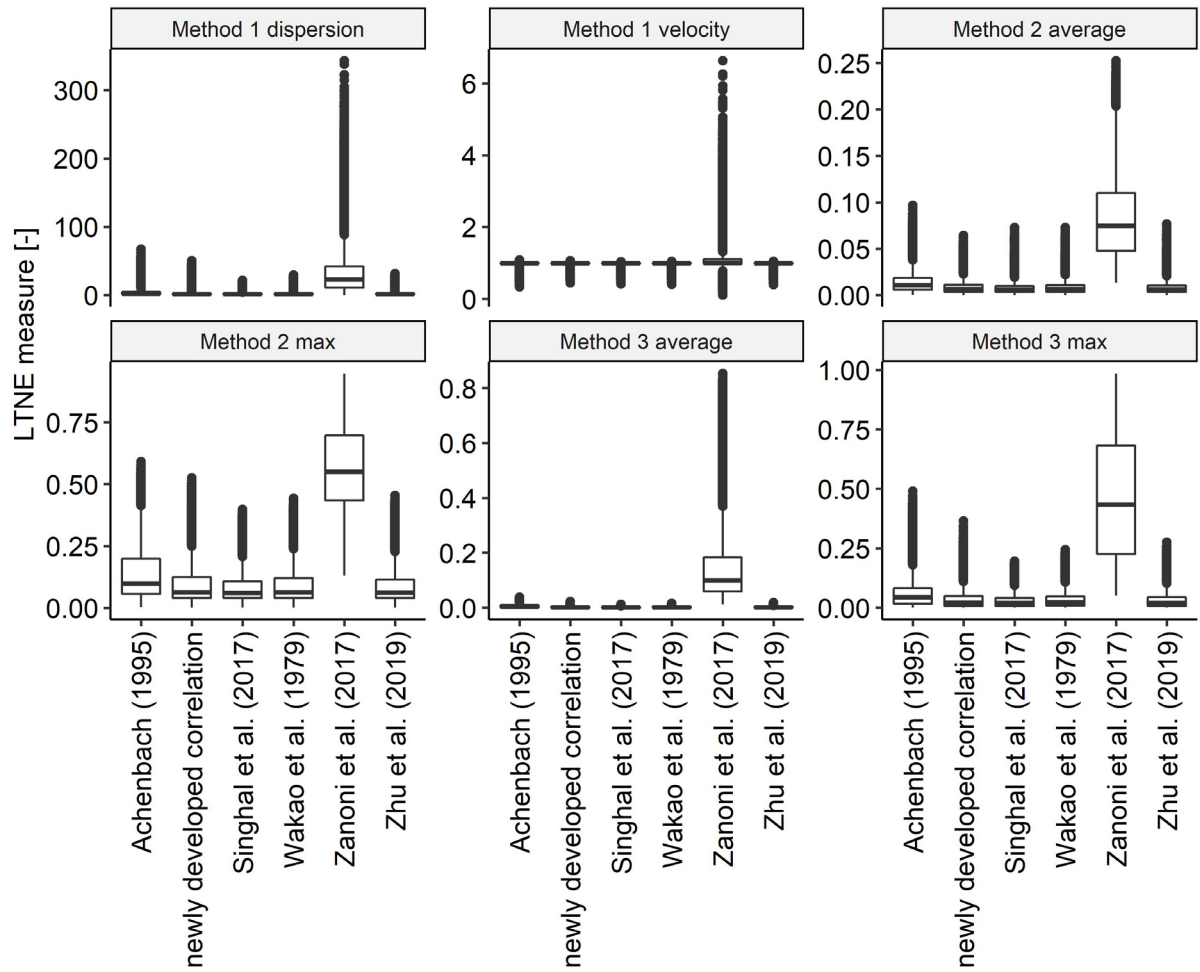
Fig. 31: Comparison of the LTNE effects for all investigated Nusselt correlations. All simulations with the Zanoni et al. (2017) correlation lead to significant LTNE effects and deviate highly from the other correlations.

As an example, Fig. 32 a & b show the thermal BTCs using different *Nu* correlations for the identical conditions as in Fig. 29 a, b & c. It is clear that the fluid temperature front calculated using the LTNE model with the *Nu* correlation of Zanoni et al. (2017) shows no significant retardation compared to the fluid front. By contrast, the solid phase temperature increases much slower due to the very low heat exchange between the fluid and solid phases as caused by the low *Nu* values from this correlation (Table 10 for values of *Nu*). Both fluid and solid BTCs obtained from the LTNE model for the *Nu* correlation of Zanoni et al. (2017) differ significantly from the temperature calculated using the LTE model. In fact, fitting the analytical LTE model to the fluid temperature BTC obtained from the LTNE model fails to achieve a satisfactory result (Fig. 33). All other *Nu* correlations lead to similar BTCs. This shows that *Nu* correlations

leading to very low *Nu* numbers are not suitable for natural conditions when simply adjusting the *Pr* to a value appropriate for water.

In conditions with large particle sizes and high seepage velocities (Fig. 32 c & d), all breakthrough curves of the different *Nu* correlations differ from the LTE model showing higher dispersion, while slightly differing from each other. Therefore, the general outcome that LTNE conditions lead to higher thermal dispersion is nearly independent of the choice of the *Nu* correlation.
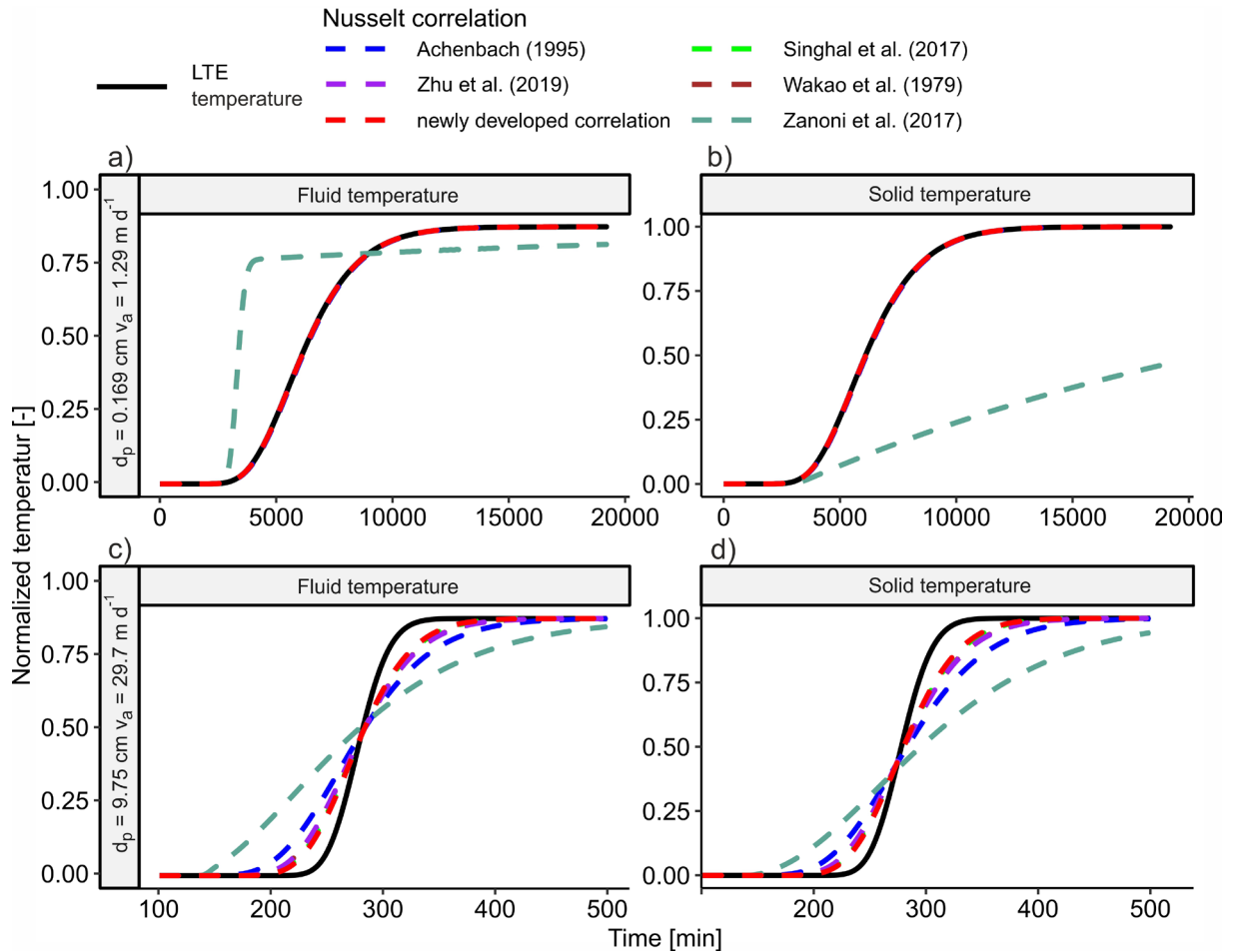
Fig. 32: Comparison of the thermal breakthrough curves for different *Nu* correlations for identical parameter sets as in Fig. 29. In conditions with small particles sizes d_p and low seepage velocities v_a (a & b), the breakthrough curves for the second group of *Nu* correlations are identical and also match the LTE temperature. For conditions with large particle sizes and high seepage velocity conditions (c & d), the breakthrough curves for all *Nu* correlations differ significantly from the LTE model.

Table 10: Overview of the different resulting *Nu* values for the parameters of Fig. 32.

Parameter Setting	Lower row Nusselt [-]	Upper row Nusselt [-]
Wakao et al. (1979)	2.23	20.50
Achenbach (1995)	0.145	10.80
Singhal et al. (2017)	2.76	25.90
Zanoni et al. (2017)	1.49e-06	3.15
Zhu et al. (2019)	3.35	19.90
newly developed correlation	1.39	28.40
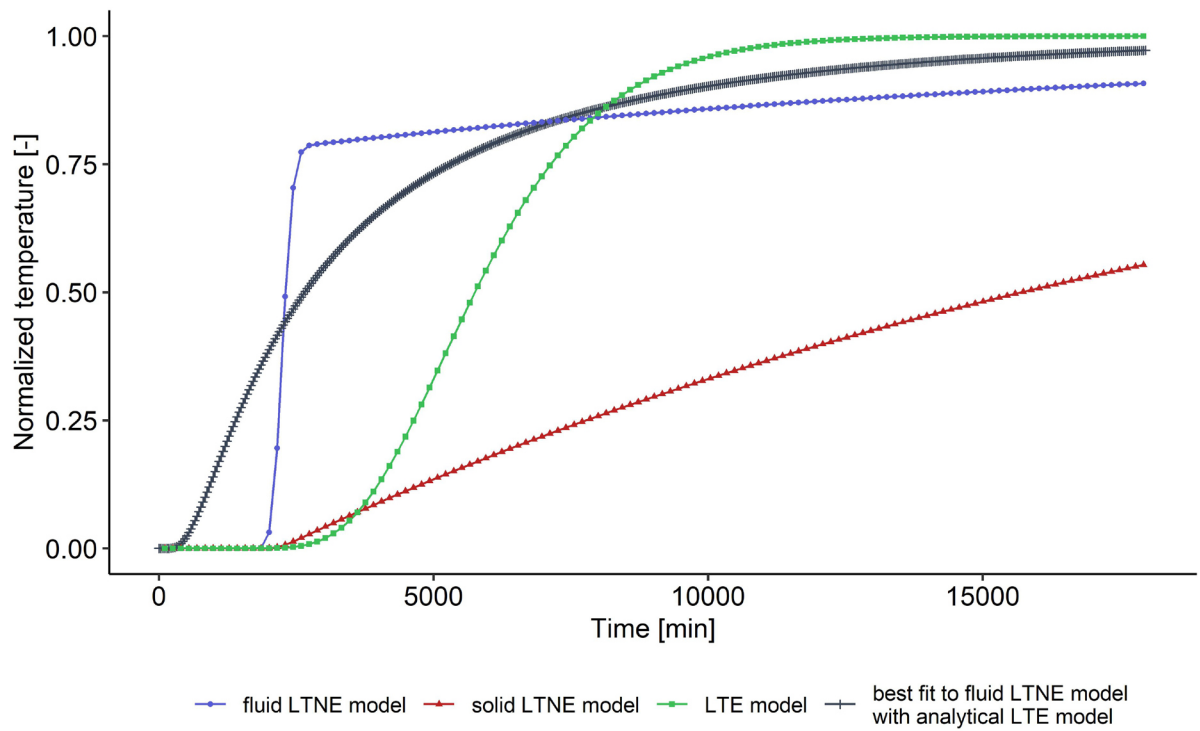
Fig. 33: Example thermal BTCs with the *Nu* number determined by the correlation of Zanoni et al. (2017) with identical parameters (d_p = 0.016 m, v_a = 1.91 m d^{-1}) for the LTE and LTNE model. The fluid temperature front calculated by the LTNE model is significantly faster compared to the fluid temperature front of the LTE model. The analytical LTE model fails to properly fit the thermal BTC of the LTNE fluid.

4.3.5 Analysis of the parameter sensitivity

The parameter sensitivity analysis converged within the investigated number of parameter settings (Fig. 34). It reveals that when evaluating all three methods the most sensitive parameters are the seepage velocity, the particle size and the porosity (Fig. 35). The least sensitive parameters are found to be the fluid temperature, the volumetric heat capacity of the solid and the thermal dispersivity (Fig. 35).
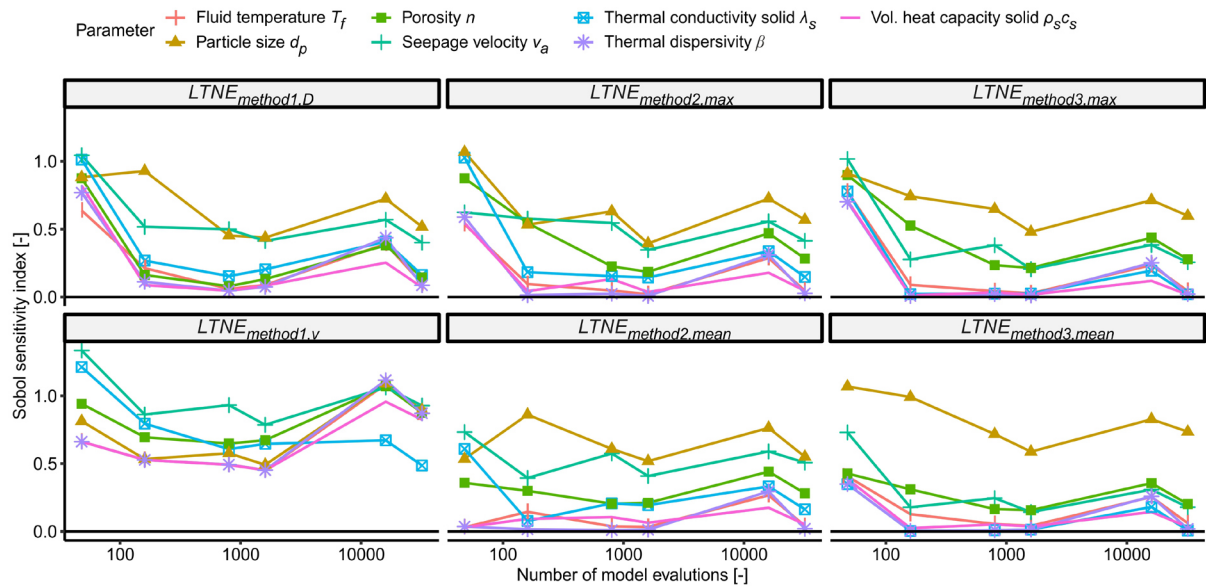
Fig. 34: Convergence plot of the sensitivity analysis for the newly derived *Nu* correlation. The sensitivity analysis converged for all methods except for the velocity of method 1. This shows a high variation of the sensitive parameters which is likely due to the very small influence of LTNE effects on the advective thermal velocity. Different methods illustrate little deviation of the sobol indices when the number of model runs is increased.
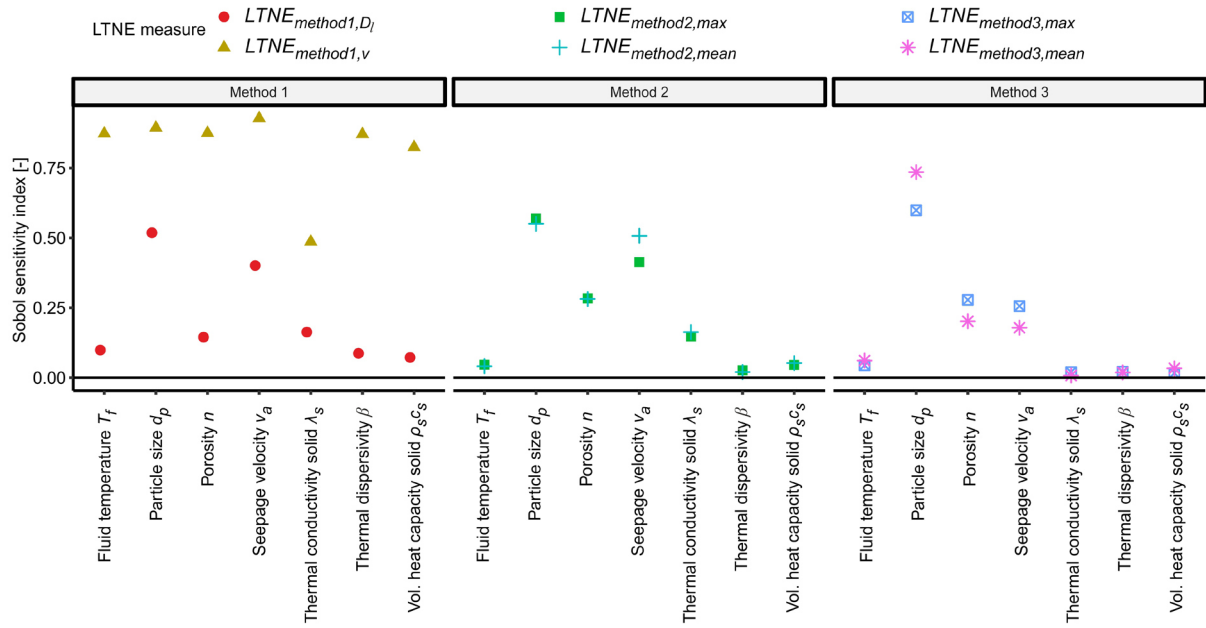
Fig. 35: Sensitivity of the many parameters in the different methods required to quantify LTNE effects. Note that we use our newly developed Nusselt correlation. Particle size and seepage velocity have a high influence on the results calculated by all methods.

In many engineering applications the ratio of fluid to solid phases thermal conductivities is reported as an important LTE criterion (Lee and Vafai, 1998; Minkowycz et al., 1999; Dehghan et al., 2014b). The ratio between the thermal conductivity of water (Huber et al., 2012) and common aquifer materials (Côté and Konrad, 2005) is usually in the range 0.1 - 0.5. The differences between the thermal conductivities in engineering applications with air as fluid and metals as a solid phase span a much broader range. We believe that our analysis did not find this to cause sensitivity because of the limited range of thermal conductivities expected in aquifer settings, as was the focus in our study.

4.3.6 Influence of LTNE effects on the advective thermal velocity

The modeled against the fitted thermal velocity is shown in Fig. 36a, highlighting an excellent fit ($R^2 > 0.99$) with generally very small differences (for 95 % of the simulations the deviation is smaller than 5 %). A small number of simulations at low Peclet numbers and large particle sizes deviate from the expected thermal advective velocity (Fig. 36b). Aside from these conditions the influence of LTNE effects on the advective velocity is generally very low. The fitted advective thermal velocities exceed the modeled velocities slightly (< 5%) at very high velocities. The results also illustrate that this is not flow distance dependent, as the correlations are similar for all investigated distances (Fig. 37).

a)

b)
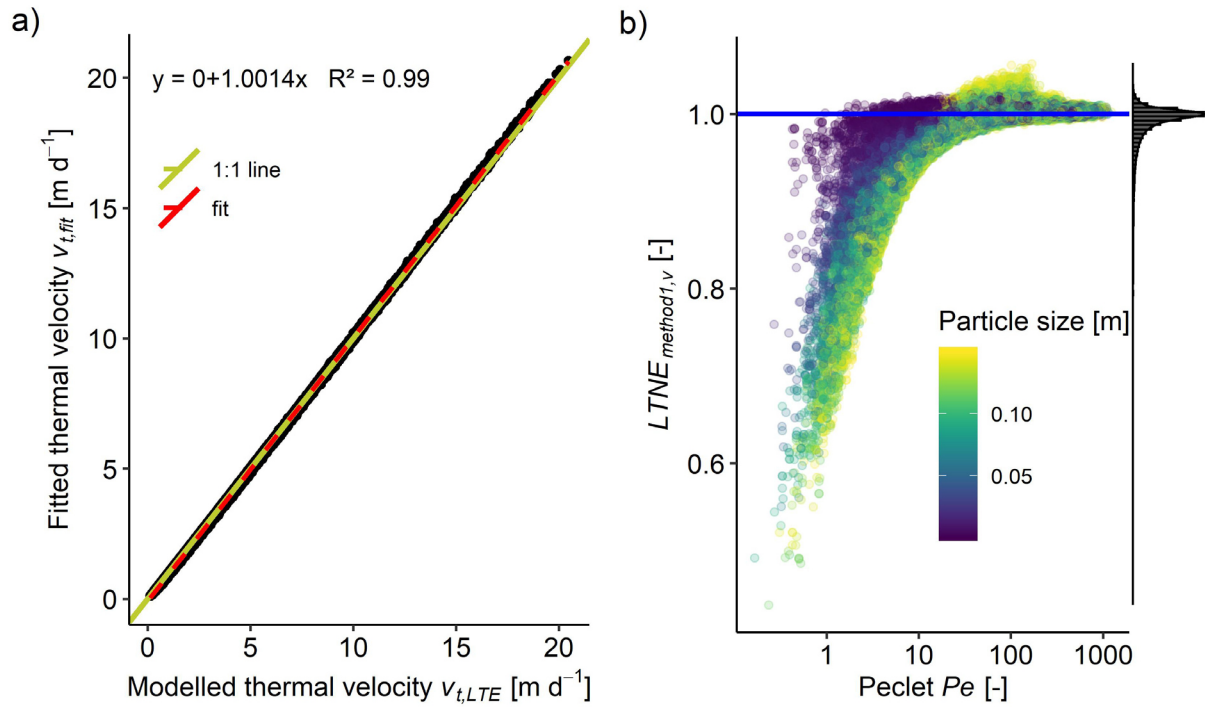
Fig. 36: (a) The differences between the fitted advective thermal velocity and the modeled advective thermal velocity are very small for most simulations. For 95 % of the simulations the deviation is smaller than 5 %. The fitted velocity deviates at very high velocities by a small amount (< 5 %) from the modeled advective thermal velocity. This shows that the influence of LTNE effects on the advective thermal velocity is generally very small. b) For a small part of the simulations at low Peclet numbers in combination with large particle sizes, the fitted velocity is smaller than the modeled thermal velocity. This deviation at low Peclet numbers, representing conduction dominated situations at small flow distances, is contributed to the differences in the boundary conditions immanent in the chosen LTE and LTNE models.
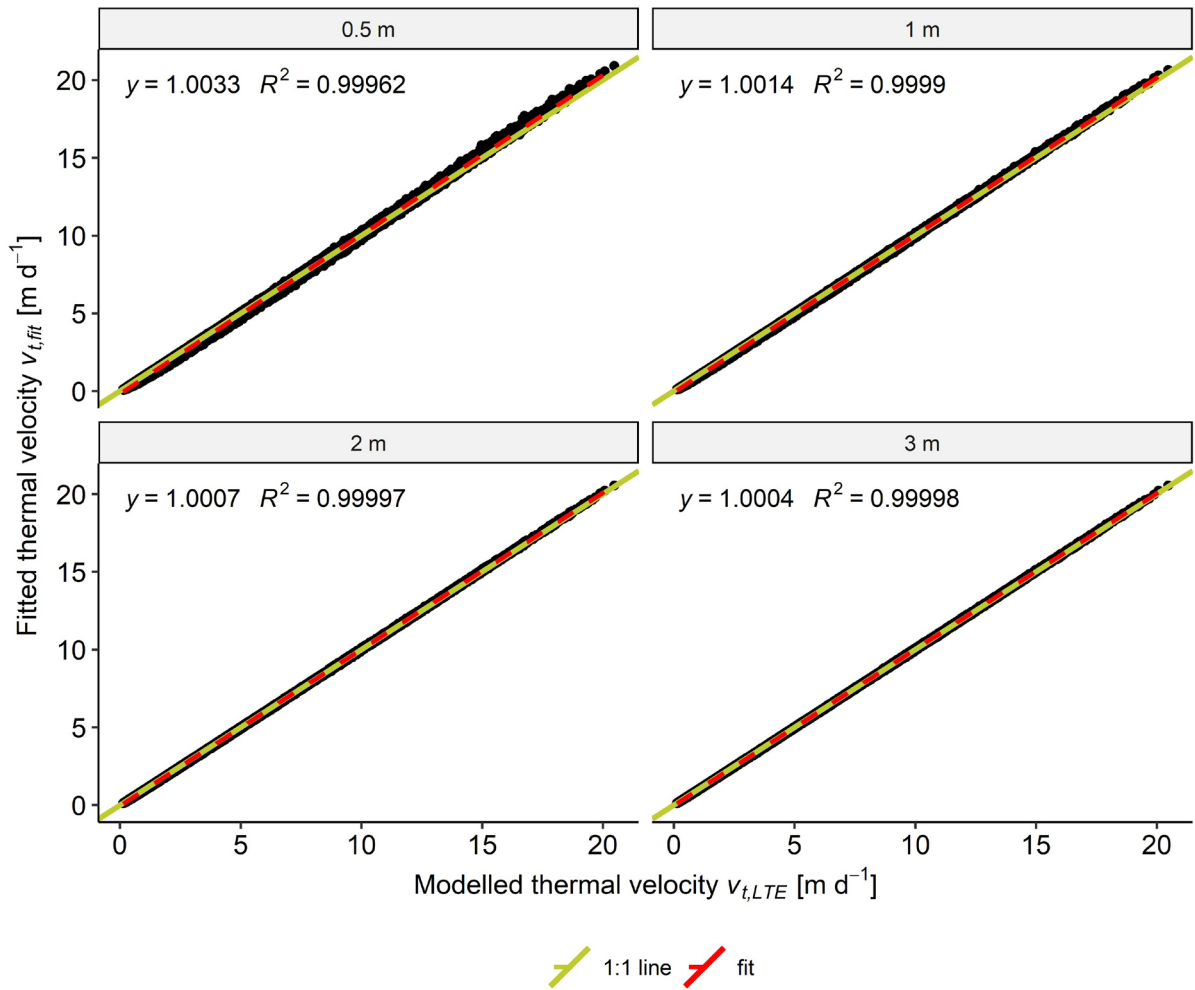
Fig. 37: The differences between the fitted advective thermal velocity and the modeled advective thermal velocity are very small for all investigated distances. This shows that the influence of LTNE effects on the advective thermal velocity is very limited.

These observations are in agreement with the experimental results of section 4.1. No significant influence on the advective thermal velocity could be observed within the analyzed range of seepage velocities expected in gravel aquifers (5-50 m d^{-1}). In a numerical study, Roshan et al. (2014) investigated the influence of LTNE effects on velocity estimates from the damping and phase shifting of the diel temperature signal with depth in a streambed for flux conditions leading to $0.001 < Re < 0.01$. They come to an opposite conclusion, stating that LTNE effects are limited to very slow seepage velocities but can lead to velocity deviations up to a factor of 150. A possible explanation of these findings is their choice of the Nu correlation which leads to very low Nu numbers at low seepage velocities but increases significantly at higher velocities. Furthermore, the mathematical model used to derive the Nu values (Kunii and Smith,

1961) on which the correlation of Roshan et al. (2014) is based, was criticized by several authors (Littman et al., 1968; Gunn and De Souza, 1974; Wakao et al., 1979).

4.3.7 Influence of LTNE effects on the thermal dispersion

In contrast to the advective thermal velocity, the effective thermal dispersion can be significantly influenced by LTNE effects. We evaluate that an increase by a factor of over 30 ($LTNE_{method1,D_l}$) is possible within the range of parameters investigated in this study (Fig. 38). Increasing flow velocities and particle sizes also lead to increasing LTNE effects and consequently, to a higher effective thermal dispersion. Similar results are obtained for all investigated distances (Fig. 39).
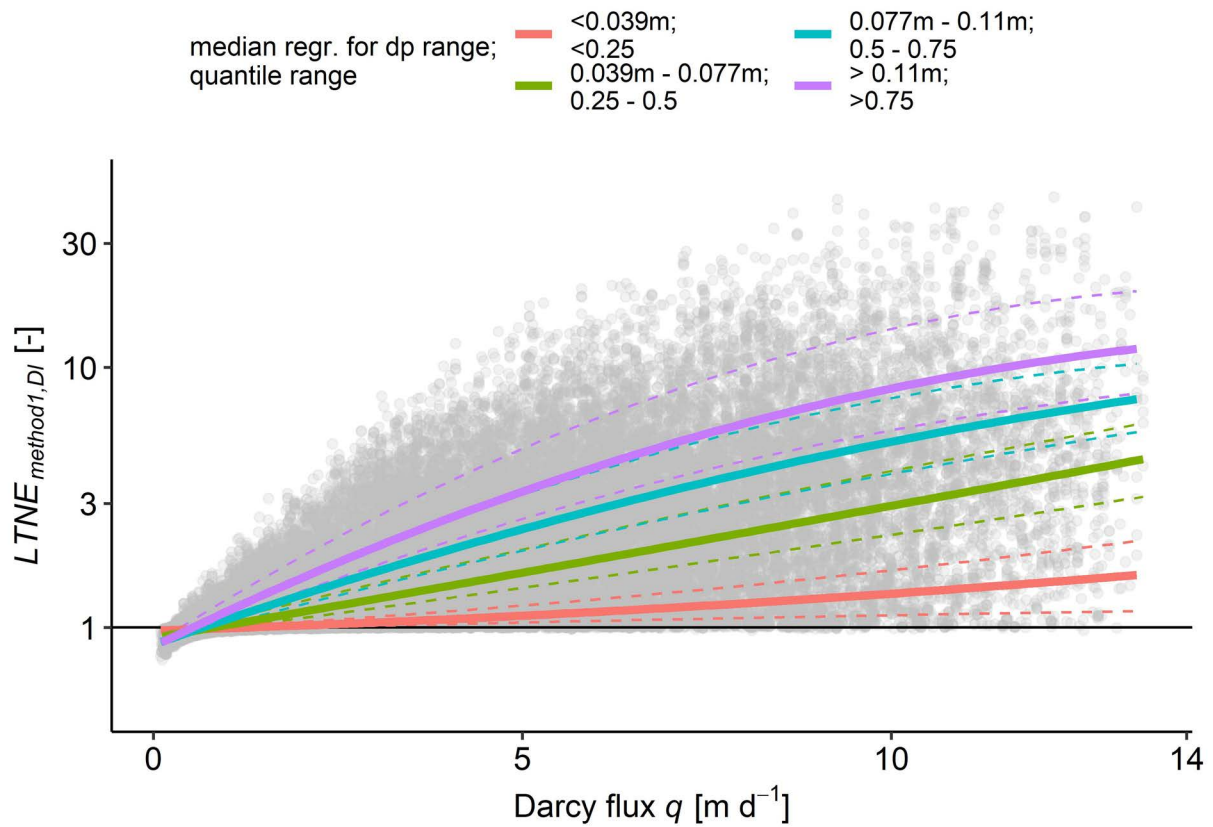
Fig. 38: The influence of Darcy flux on the normalized deviation of the thermal dispersion difference ($LTNE_{method1,D_l}$) caused by LTNE effects. Each grey dot is the result of one simulation. The solid colored lines show the smoothed median values (dashed lines 0.25/0.75 quantile) of the normalized dispersion deviations for groups of simulations with different particle size ranges. Larger particle sizes and higher Darcy fluxes lead to higher LTNE effects resulting in a significant increase in the thermal dispersion.
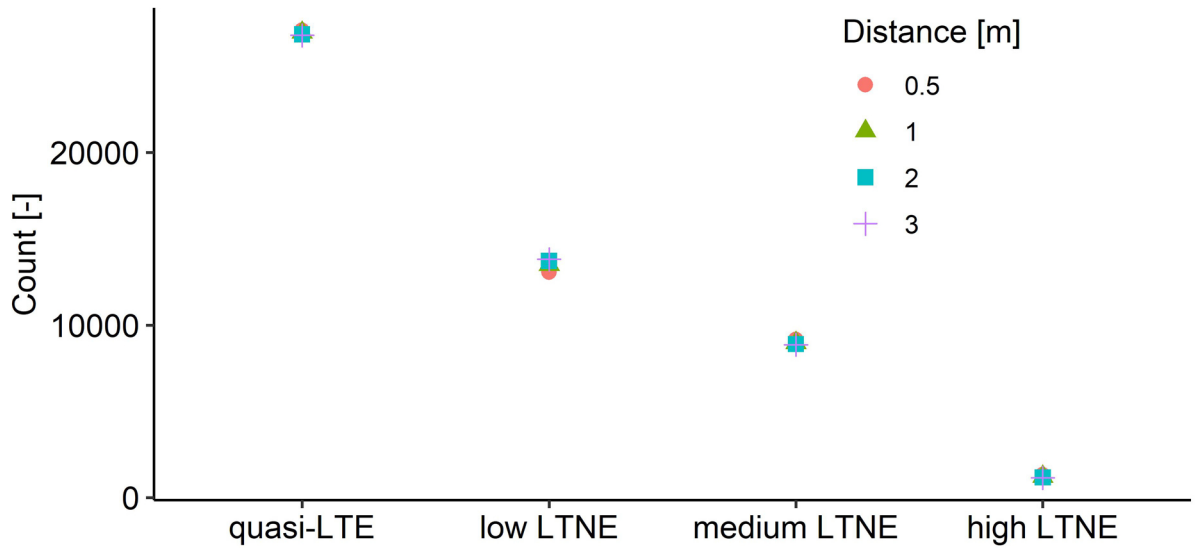
Fig. 39: Influence of the distance on the LTNE measure based on the deviation of thermal dispersion ($LTNE_{method1,D_l}$). The count for each category is very similar which means that the observation distance does not significantly influence the degree of LTNE.

To elucidate the conditions under which this increase in thermal dispersion can be expected, the LTNE effects on thermal dispersion have been categorized in Table 11. As the thermal dispersion is generally an uncertain parameter in modeling, we considered an increase up to 50 % as within the usual uncertainty range. An increase above a factor of 10 is considered as highly influenced by LTNE effects. Following this categorization and the grain size-based aquifer types according to Table 11, we reveal that LTNE effects can be expected in gravel aquifers with high Darcy fluxes (Fig. 40). This tendency can be observed for all *Nu* correlations of the second group (see section 4.3.1) of *Nu* correlations (Fig. 41).

Furthermore, we identify the following threshold values considering all combinations of parameters for which no significant LTNE effects ($LTNE_{method1,D_l}$ < 1.5) could be observed: If either the particle size is < 7 mm or the seepage velocity is < 1.6 m d^{-1} no significant LTNE effects ($LTNE_{method1,D_l}$ < 1.5) should be expected. A previous laboratory study (Bandai et al., 2017) observed increasing thermal dispersion values with increasing particle sizes and suspected LTNE effects as the cause for this. The presented results confirm the assumption that LTNE effects can significantly enhance the effective thermal dispersion coefficient which is also in accordance with the results of the laboratory experiments (section 4.1.2).

Table 11: Categorization of the LTNE effects and typical aquifer types

Aquifer type	Seepage velocity [m d^{-1}]	Particle size [mm]	Porosity [-]	LTNE categorization	Quasi-LTE	Low LTNE	Medium LTNE	High LTNE
sand	1-3	1-2	0.1-0.2					
sand – gravel	2-10	1.5-30	0.15-0.3	$LTNE_{method1,Dl}$ $= \dfrac{D_{l,eff,fit}}{D_{l,eff}}$	<1.5	1.5-3	3-10	>10
gravel	5-30	20-150	0.25-0.45					
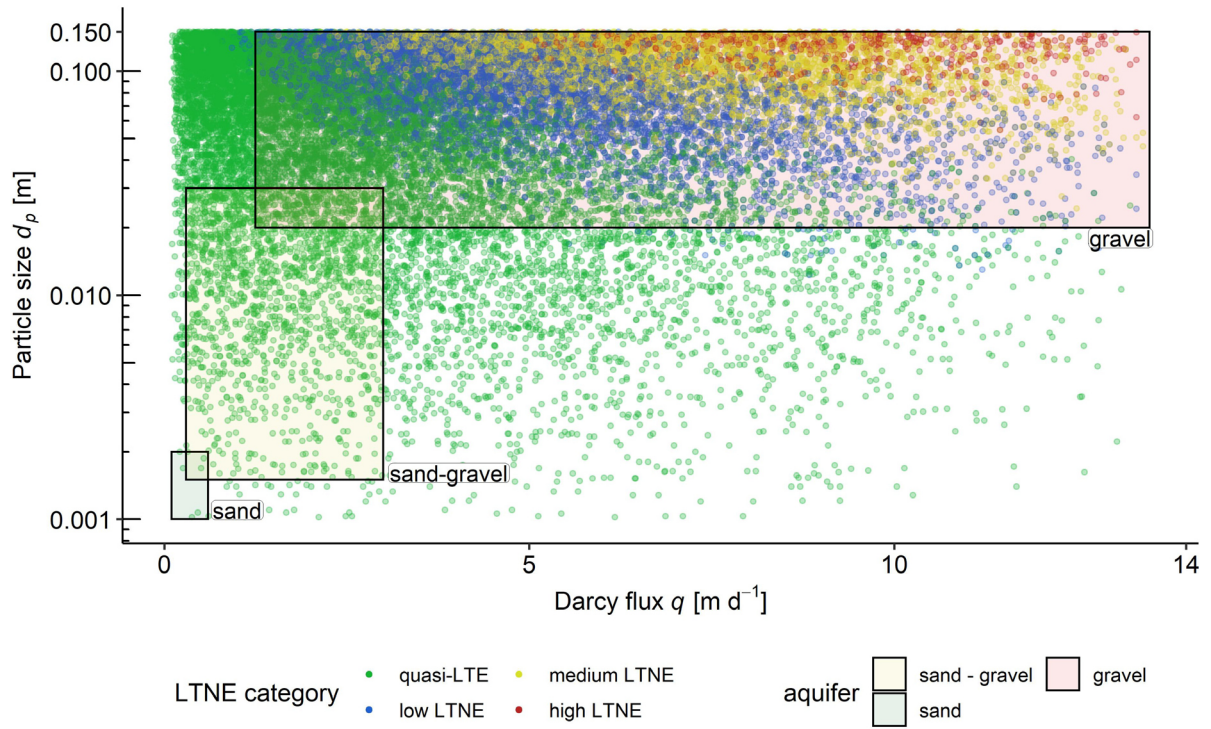
Fig. 40: Categorized LTNE effects based on Darcy flux and particle size. Increased thermal dispersion due to LTNE effects is mainly expected for conditions with high flow velocities and large grain sizes like gravel aquifers.
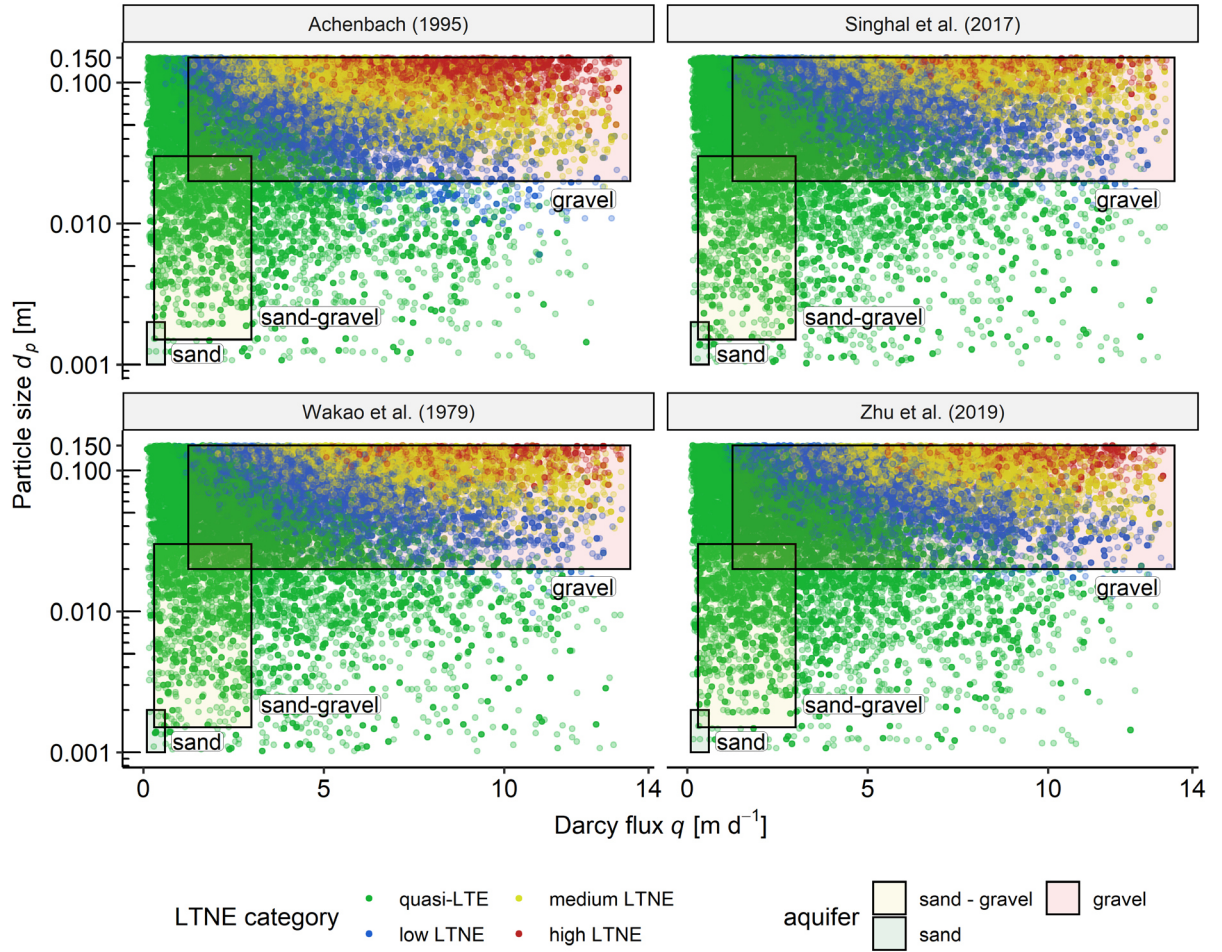
Fig. 41: LTNE effects categorized by Darcy flux q and particle size d_p for different Nusselt correlations. These plots show that LTNE effects become significant in gravel aquifers for all Nusselt correlations. The results are very similar to the ones derived using our newly developed Nu correlation.

4.3.8 Comparison of methods to quantify LTNE effects

The comparison of the results of the three methods for all simulations shows a significant relationship between them (Fig. 42). Yet, for some parameter settings (low Pe and large d_p) the differences between the LTE and fluid LTNE temperatures ($LTNE_{method2}$) are large while the differences between solid and fluid temperature ($LTNE_{method3}$) are close to zero. These findings are in accordance with the results of some other studies (Rees et al., 2008; Hamidi et al., 2019) which showed, that LTE and LTNE models can differ even if the temperature differences between the fluid and solid phase are nearly equal. Interestingly, while $LTNE_{method1,Dl}$ does not capture these LTNE effects, $LTNE_{method1,v}$ shows a strong correlation with $LTNE_{method2,max}$ (Fig. 42b). These deviations are limited to conditions of low Pe numbers (Fig. 36b & Fig. 42b).

A possible explanation for these discrepancies at low Pe are the differences in the boundary conditions between the LTE and LTNE models. When trying to model a scenario in which a hot or cold fluid is injected into a porous medium, the boundary condition necessary for the LTE model and the assumption inherent to the LTE model induce that under conduction-dominated conditions (low Pe), the thermal conductivity of the solid phase also contributes significantly to heat transport at the boundary. The LTNE model allows to set more appropriate boundary conditions, allowing to only affect the fluid phase at the boundary.
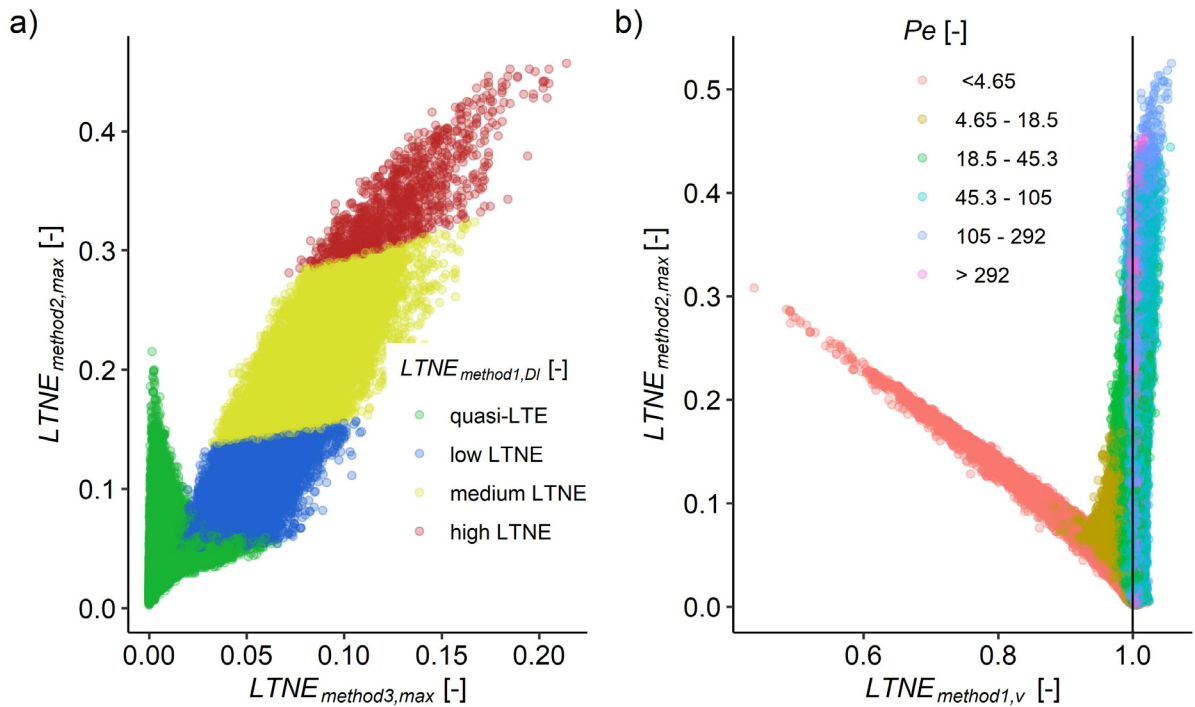
Fig. 42: Relationship between the different LTNE quantification methods. a) While the methods show a significant correlation between them, $LTNE_{method2,max}$ detects increased differences between the LTE and LTNE fluid temperature for low Péclet conditions in which the difference between fluid and solid temperature ($LTNE_{method3,max}$) is negligible and the dispersion is not significantly increased ($LTNE_{method1,Dl}$). b) $LTNE_{method1,v}$ shows an overestimation of the advective velocity of the LTE model for these low Péclet conditions and a correlation with $LTNE_{method2,max}$.

4.3.9 Criterion to estimate LTNE conditions

To estimate if LTNE effects are likely to occur in porous aquifers, we use the four most sensitive parameters, particle size d_p, porosity n, seepage velocity v_a and thermal conductivity of the solid phase λ_s, as explanatory variables to derive a new equation in a two-step regression procedure. First, to find the best model formula, an exhaustive screening approach with the

R package "glmulti" (Calcagno and de Mazancourt, 2010) was applied on the normalized (ordered quantile normalization (Peterson and Cavanaugh, 2019)) $LTNE_{method1,D_l}$ value and the scaled explanatory variables (min-max normalization). In other words, the above-mentioned explanatory variables are used to predict the value of $LTNE_{method1,D_l}$. The value of $LTNE_{method1,D_l}$, predicted by the regression is called $LTNE_{cat}$. All possible models including pairwise interactions were considered up to a maximum number of seven terms. The selection was based on the Bayesian information criterion which penalizes models with higher number of parameters to prevent overfitting (Schwarz, 1978). The regression analysis was conducted with the results for the flow distance of 1 m as the influence of the distance on $LTNE_{method1,D_l}$ is very limited. Note that using all distances would introduce ties in the dataset. These ties cause problems in the ordered quantile normalization (Peterson and Cavanaugh, 2019) which was applied to achieve a normal distribution for the $LTNE_{method1,D_l}$ value. The model formula in eq. (55) with six terms shows the best results concerning limited complexity and adequate accuracy (adjusted R² = 0.89). In order to enable a practical application, the regression coefficients were determined by applying this model to the original data (not normalized and scaled) (adjusted R² = 0.64) resulting in:

$$LTNE_{cat} = 0.42 - 0.04v_a - 1.45n + 0.21\lambda_s + 2.15d_pv_a + 118.11d_pn - 8.38\lambda_sd_p \qquad (55)$$

The predicted value $LTNE_{cat}$ (eq. 55) was compared with the associated LTNE category (Table 11) for each simulation in a cumulative distribution plot (Fig. 43). The boundaries of the categories (Table 3, Fig. 43) are based on the 5% and 95% quantiles of this cumulative distribution. This can be viewed as a probability measure, e.g. if $LTNE_{cat}$ is < 1.4 it is likely that no LTNE effects occur. 95 % of the simulations which show low LTNE effects are above this value. No simulation with medium or high LTNE effects results in an $LTNE_{cat}$ < 1.4. If $LTNE_{cat}$ is in the low LTNE – medium LTNE range (3.3-4.6) both categories are equally possible, as simulation with parameter sets resulting in this range can be within both categories (Fig. 43). The accuracy of this approach is reasonable, as $LTNE_{cat}$ gives only a qualitative assessment of the LTNE conditions.

Table 12: Categories of the LTNE effects and the corresponding values of $LTNE_{cat}$.

LTNE category	$LTNE_{cat}$	Boundaries based on quantiles
quasi-LTE	< 1.4	< 5% quantile low LTNE
quasi-LTE – low LTNE	1.4-2.2	5% quantile low LTNE – 95 % quantile quasi LTE
low LTNE	2.2-3.3	95 % quantile quasi LTE – 5% quantile medium LTNE
low LTNE – medium LTNE	3.3-4.6	5% quantile medium LTNE – 95 % quantile low LTNE
medium LTNE	4.6-6.5	95 % quantile low LTNE – 5% quantile high LTNE
medium LTNE – high LTNE	6.5-7.8	5% quantile high LTNE – 95 % quantile medium LTNE
high LTNE	> 7.8	>95 % quantile medium LTNE
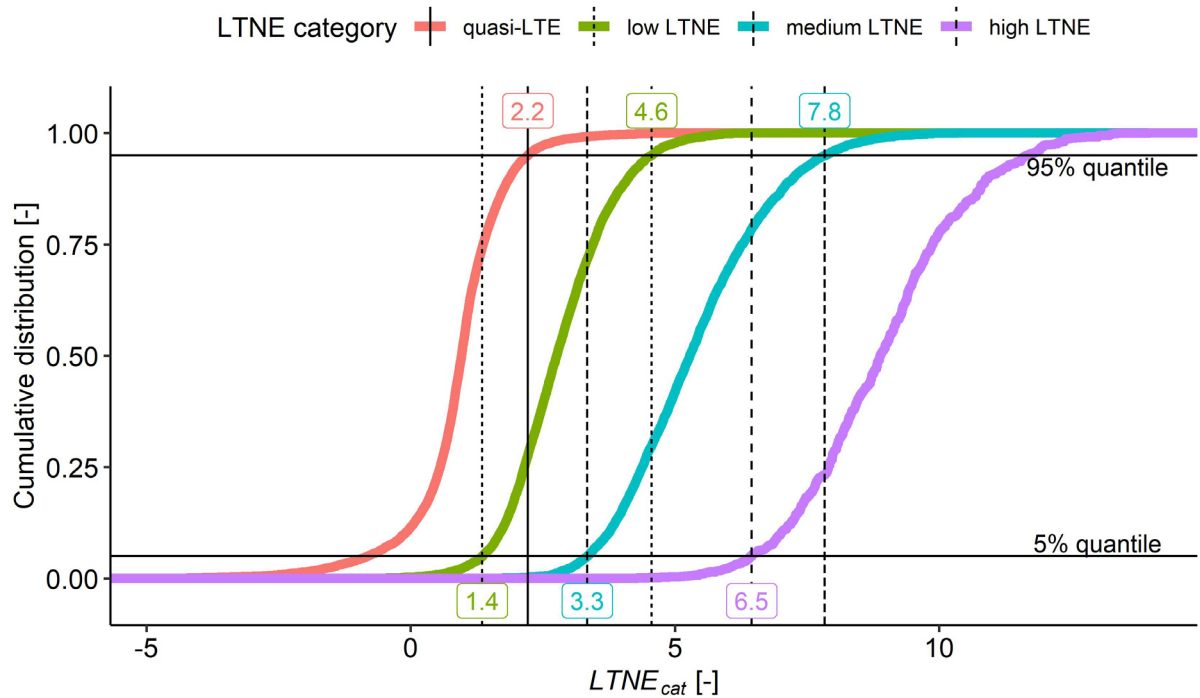
Fig. 43: Cumulative distribution of the LTNE categories based on Table 11 and the predicted values by eq. (55). The 5% and 95% quantile values of $LTNE_{cat}$ of the different LTNE categories are used to determine the boundary values of the LTNE categories Table 12.

To verify the assumption of the limited influence of the distance, the regression analysis was performed for all four distances. The resulting parameters (a_1-a_6) of the formula provided by this screening approach (eq. 56) causes the mean of all four models to vary less than 6 % with the quantile boundaries remaining similar (Fig. 44).

$$LTNE_{cat} = intercept + a_1 v_a + a_2 n + a_3 \lambda_s + a_4 d_p v_a + a_5 d_p n + a_6 \lambda_s d_p \qquad (56)$$
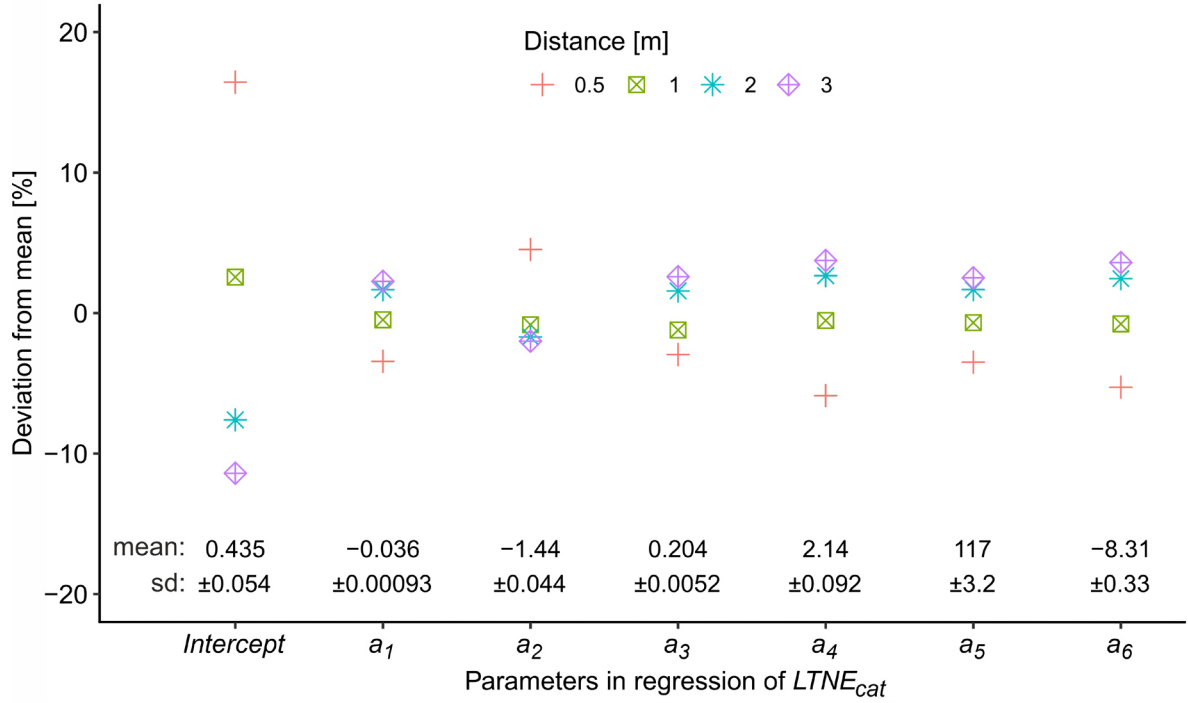
Fig. 44: Influence of flow distance on the regression parameters. The percental variation of the fitting parameters a_{1-6} and the standard deviation (sd) of the absolute values is very small.

4.3.10 Evaluation of laboratory experiments with the LTNE criterion

To check if LTNE effects are likely to occur in the laboratory experiments of the first part according to the results of the numerical parameter study, the properties and conditions of the step input laboratory experiments are used in the derived LTNE criterion (eq. 56). Using the parameters and uncertainties of the laboratory experiments (Table 5 and Table 6) with a simple Monte-Carlo estimate (10^6 runs), the resulting $LTNE_{cat}$ is around 0.75 (Fig. 45) and therefore quasi-LTE conditions are expected. To evaluate if LTNE effects influenced the effective thermal dispersion of the laboratory experiments, the newly developed $LTNE_{method1,Dl}$ (eq. 49) was calculated for the step input scenarios. Fig. 46 shows the fitted effective thermal dispersion $D_{l,eff,fit}$ (eq. 28) values of the step input experiments which were used to calculate the thermal dispersivity β (Fig. 47a) with eq. (3). This is based on the power law relationship with the specific discharge (eq. 4) as suggested in Rau et al. (2012b). The resulting thermal dispersivity values vary significantly and decrease with increasing seepage velocities. As the thermal dispersivity is considered a material property this behavior is unexpected. Using the

median of the calculated thermal dispersivity ($\sim 88\ \mathrm{s^{-1}}$) the resulting $LTNE_{method1,Dl}$ are within the range of 0.75-1.5 (Fig. 47b) and, therefore quasi-LTE conditions. Whether the relationship between the thermal dispersivity and the specific discharge is based on a power law or a linear relationship is not fully clear (see section 2.2) (e.g. Afshari et al., 2019; Anderson, 2005; Metzger et al., 2004; Rau et al., 2012b; Vandenbohede et al., 2009). Hence, using eq. (57) which describes the thermal mechanical dispersion based on a linear relationship with the specific discharge (e.g. Anderson, 2005) the resulting values of $\beta_{q\ not\ squared}$ are shown in Fig. 47c displaying a lower variance and no significant correlation of the thermal dispersivity with the specific discharge. The $LTNE_{method1,Dl}$ using the median value of $\beta_{q\ not\ squared}$ ($\sim$0.015 m) are again within the quasi-LTE range (0.75-1.5) (Fig. 47d).

$$D_l = \beta_{q\ not\ squared} \left| \frac{\rho_f c_f}{\rho_b c_b} q \right| \tag{57}$$

Collectively, this indicates that the thermal dispersion of the laboratory experiments in this study can be better described by a linear relationship of the thermal dispersivity with the specific discharge as β based on a power law shows a significant correlation with the seepage velocity. Furthermore, the predicted quasi LTE conditions of the developed LTNE criterion for the laboratory experiments are confirmed as neither the advective thermal velocity nor the effective thermal dispersion are significantly influenced by LTNE effects.
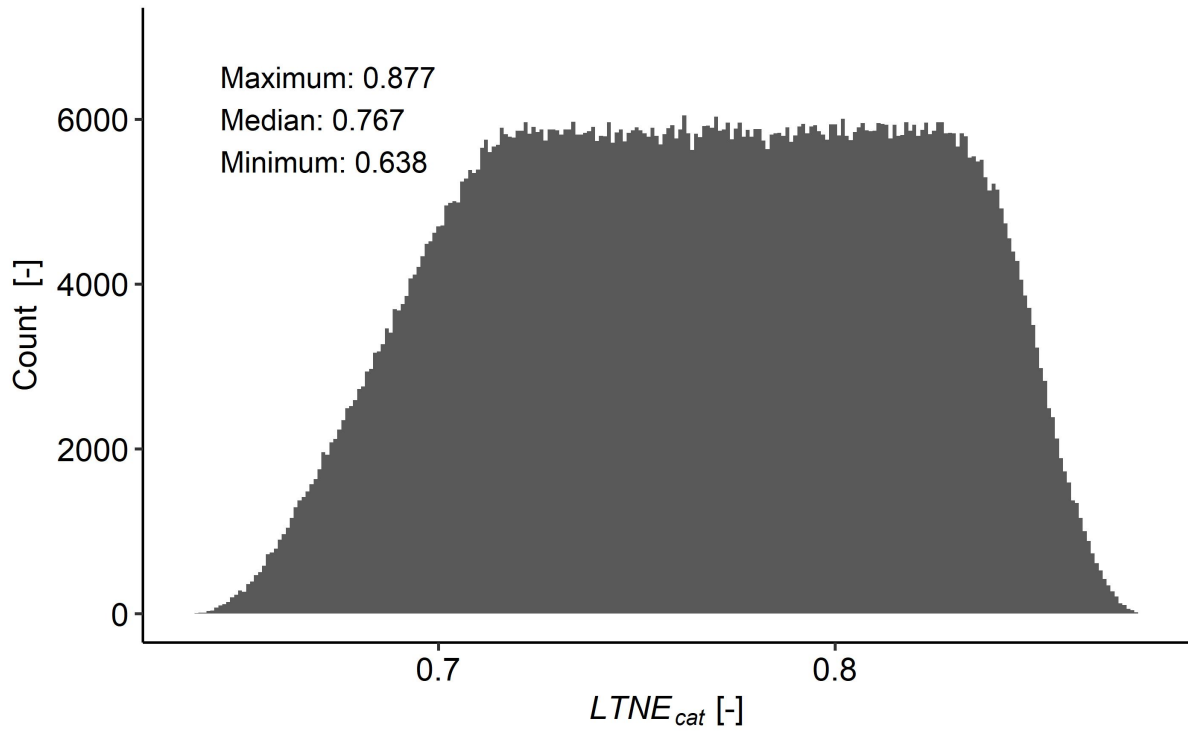
Fig. 45: Distribution of $LTNE_{cat}$ for the laboratory experiments (see Table 5 and Table 6 for parameters and uncertainties) based on a simple monte carlo estimate (10^6 runs). The $LTNE_{cat}$ value indicates that LTNE effects are unlikely to occur in these settings.
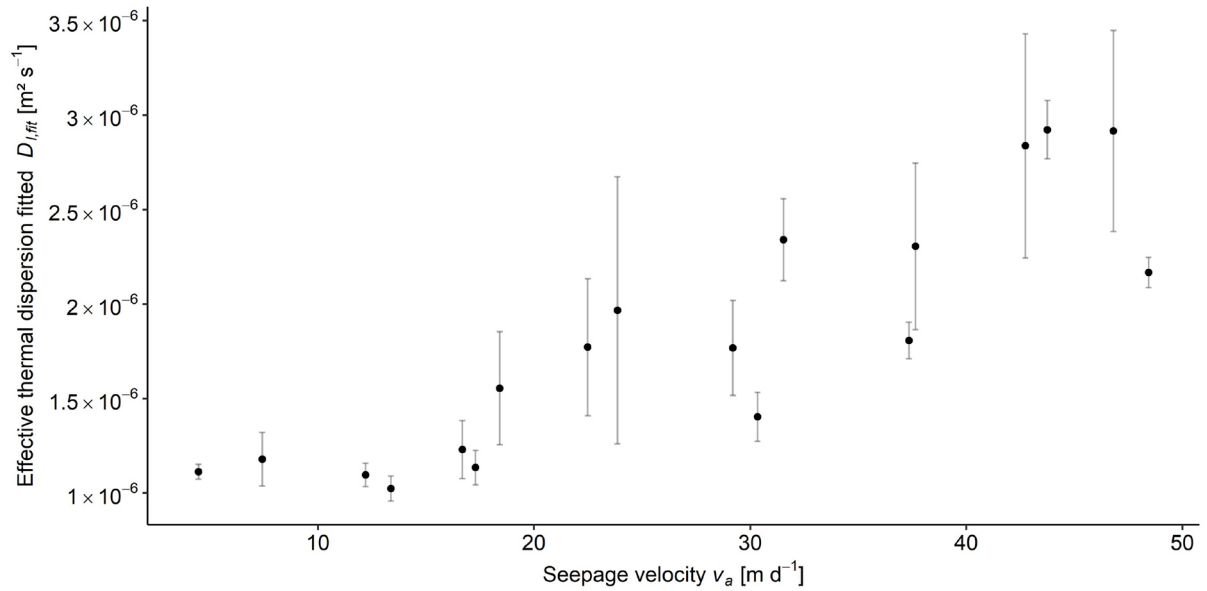
Fig. 46: Fitted effective thermal dispersion $D_{l,eff,fit}$ from the laboratory experiments. As expected, the effective thermal dispersion increases with increasing seepage velocities. The error bars indicate the standard deviation when all distances are compared in one experiment.
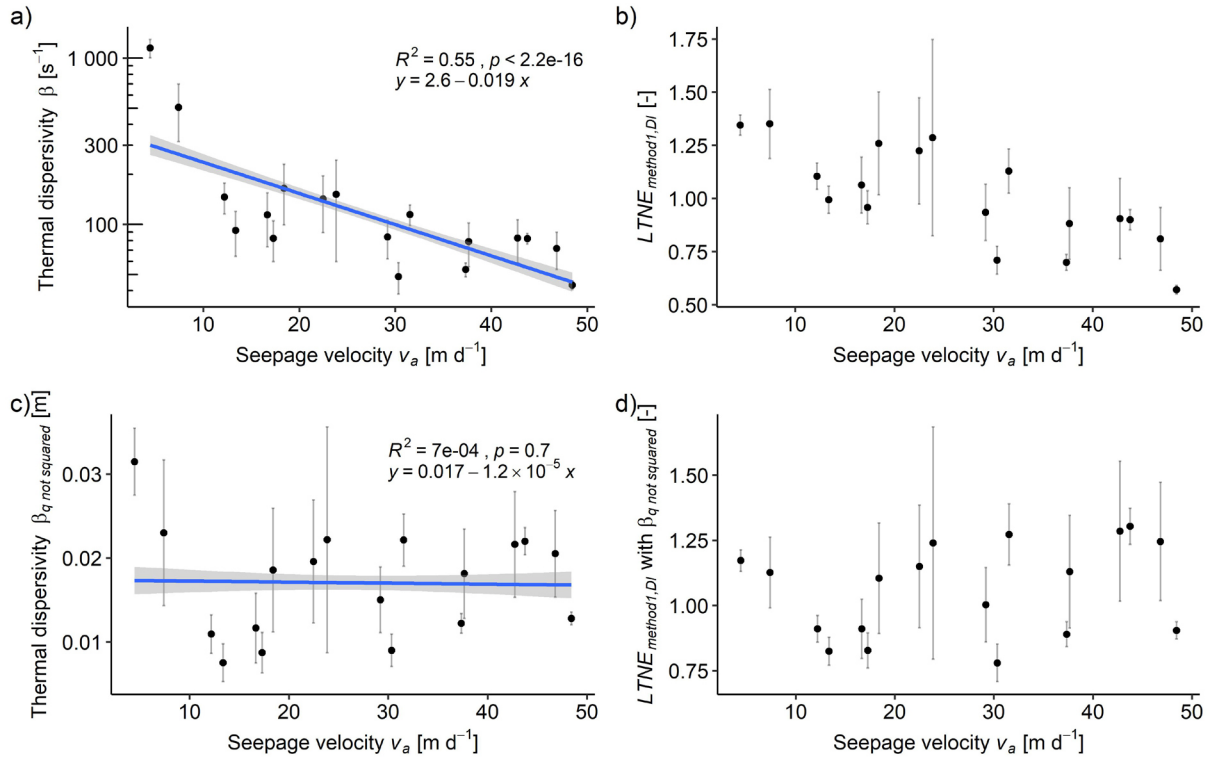
Fig. 47: a) Thermal dispersivity of the step input laboratory experiments values based on the fitted effective thermal dispersion $D_{l,eff,fit}$ and eq. (4). b) Calculated $LTNE_{method1,Dl}$ values for the step input laboratory experiments. The median of the thermal dispersivity β of all experiments (~88) is used in the calculation. c) and d) are the equivalent plots of a) and b) but with the thermal mechanical dispersion D_l not based on a squared relationship with the specifc discharge q (eq. (57)). The median value of $\beta_{q\,not\,squared}$ used to calculate $LTNE_{method1,Dl}$ is ~0.015 m. The error bars indicate the standard deviation when all distances are compared in one experiment.

4.3.11 Limitations of the used approach

Our study focuses on a 1D setup with homogenous parameter settings in each simulation to investigate LTNE effects. Even though most of the parameter settings expected in porous aquifers are covered, the influence of macroscopic heterogeneity on LTNE effects remains unclear. A recent publication investigated LTE and LTNE approaches for fractured porous media (Hamidi et al., 2019). They showed that high permeability and porosity contrasts can lead to significant LTNE effects resulting in a difference of up to 7 % in local fluid temperatures. This indicates that macroscopic heterogeneity could additionally increase LTNE effects.

Furthermore, we used the arithmetic mean particle size as a referential particle size in our simulations. The sensitivity analysis showed that the particle size is a highly influential parameter for LTNE effects. Similarly, Heinze and Blöcher (2019) revealed that the particle size is a crucial parameter for LTNE effects during infiltration processes. For transferring the results to aquifers with unsorted grain size distributions, further research is necessary to reveal if for instance a representative grain size would be suitable. Candidates are statistical grain size values such as the geometric or harmonic means as common for calculation of thermal or hydraulic conductivity.

Another assumption of our study is that we consider most parameters independent of each other (see section 3.2.5). Certainly, some parameters such as particle size and porosity can be correlated (e.g. Urumović & Urumović, 2014), but these correlations depend on many influences such as grain size distribution, shape of the grains, and compaction. Therefore, we have not elaborated further on which conditions are more or less frequent in natural aquifers, and rather provide the full range of parameter combinations.

4.4 Short summary paper 2

The limitations of the LTE assumption in heat transport modeling for natural porous aquifers have been investigated by an extensive 1D parameter study comparing thermal BTCs of local thermal equilibrium (LTE) and local thermal non-equilibrium (LTNE) models. A new correlation to determine the Nusselt number based on available literature data tailored to porous aquifers was derived. As all available data on Nu are determined with air as fluid, more laboratory studies measuring the heat transfer with water as a fluid are required.

While LTNE effects do not occur for grain sizes smaller than 7 mm or for seepage velocities that are slower than 1.6 m d^{-1}, LTNE effects can occur within the conditions expected in porous aquifers such as gravel aquifers with high seepage velocities and large grain sizes. The effective thermal dispersion can be increased by a factor of over 30 caused by LTNE effects. The advective thermal velocity is not significantly influenced even in conditions with strong LTNE effects. Only at low Pe conditions in combination with large particle sizes, the LTE model can lead to an overestimation of the advective thermal velocity. A criterion to predict if LTNE conditions will occur is developed based on the most influential properties, the porous media particle size, seepage velocity, porosity, and thermal conductivity of the solid phase. Our results can be used as a guide towards more accurate modeling of heat transport in natural porous media.

Chapter 5   Conclusion

A fundamental understanding of heat transport in natural porous media is crucial in many areas of research and applied fields. Using laboratory experiments and numerical modeling, it is shown that the commonly used assumption of local thermal equilibrium can lead to a significant underestimation of the effective thermal dispersion in conditions expected in natural porous media such as gravel aquifers with large grain sizes and high seepage velocities. This can cause a substantial deviation between the modeled and the actual temperature development, for example in the prediction of the spreading of thermal plumes in groundwater heat pump systems. The effects of local thermal non-equilibrium on the advective thermal velocity are minor (< 10 % deviation) even in conditions in which the thermal dispersion is significantly influenced. Only at low *Pe* conditions in combination with large particle sizes, the LTE model can lead to an overestimation of the advective thermal velocity. Using the thermal retardation factor to estimate water fluxes, mean transit times or the bulk heat capacity of the aquifer from thermal tracer experiments requires the determination of the advective thermal velocity from the thermal breakthrough curve. Using thermal velocities which can be influences by the thermal dispersion such as the peak velocity, can lead to deviations over 30 % resulting in erroneous flux estimates and mean transit times.

5.1   Implications for heat transport modeling in natural porous media

The increased thermal dispersion caused by LTNE under certain conditions such as high seepage velocities and large grain sizes can have significant consequences for the modeling and management of geothermal groundwater use, such as groundwater-based heat pump systems, which cycle groundwater by operating extraction and injection well doublets. With a steady increase of such systems leading to densely used aquifers (Pophillat et al., 2020), there is a growing need for reliable prediction of the induced thermal plumes (Ferguson, 2009; Hähnlein et al., 2013; Herbert et al., 2013; Epting et al., 2017; Böttcher et al., 2019). To delineate a thermal range or a thermally affected zone in an aquifer, the value for thermal dispersion is of crucial importance (Molina-Giraldo et al., 2011; Park et al., 2015, 2018; Pophillat et al., 2020). The relative difference of the length, width and stabilization time of a 1 K thermal plume can vary over 100 % due to different transversal and longitudinal thermal dispersivity values when compared to a reference scenario (Pophillat et al., 2020). This also affects the

overall potential of thermal groundwater use in aquifers, as it is a spatially limited resource, inter alia constraint by a minimum distance of adjacent systems to prevent a thermal break-through between them (Böttcher et al., 2019). Consequently, the processes, such as the heat transfer between the fluid and solid phases, that determine the magnitude of LTNE effects must be well understood. For example, we expect that LTNE effects can occur even in aquifers with low natural seepage velocities as the flow velocity increases significantly towards injection and extraction wells (Park et al., 2015). Using a commonly applied formula (e.g. Houben, 2015) (Fig. 48) to estimate the induced seepage velocities shows that the influence of extraction and injection can easily reach more than 10 m distance for frequently found extraction or injection rates (Fig. 48). This demonstrates that seepage velocities which can induce LTNE effects can be easily reached in the vicinity of such wells.

$$v_a = \frac{Q_{extr}}{2\,\pi\,x_{well}\,n_{eff}M}$$
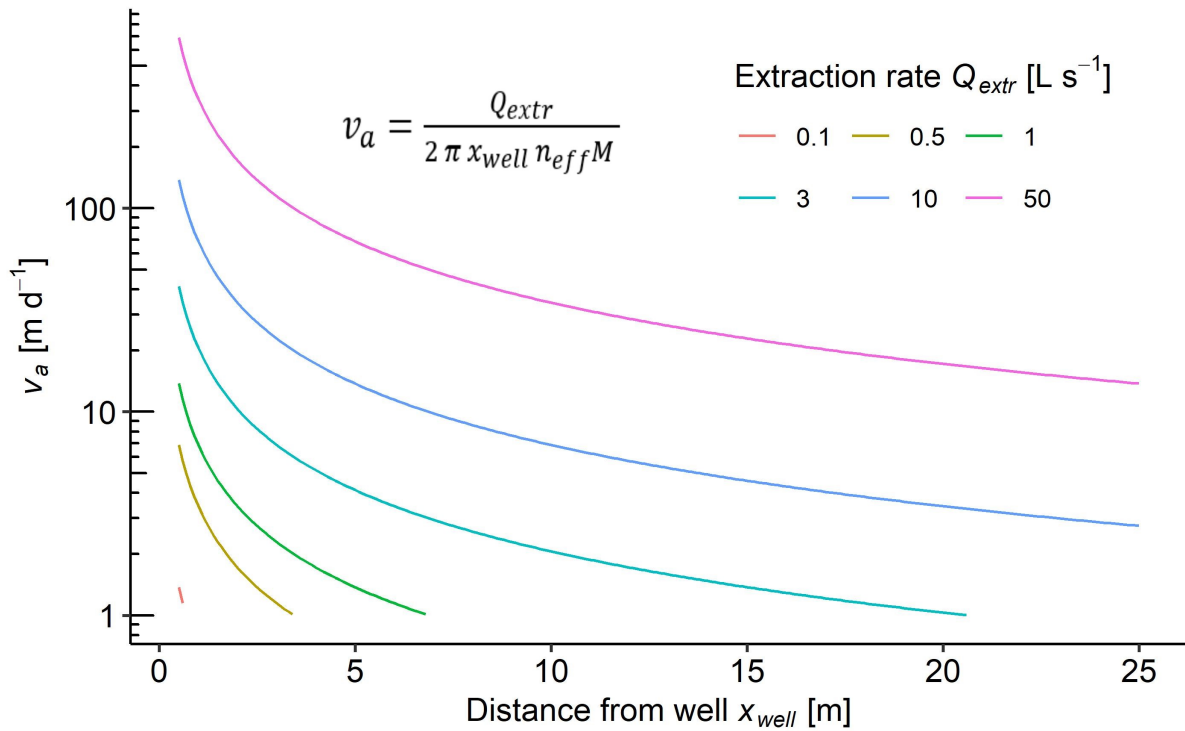
Fig. 48: Influence of water injection or extraction on the seepage velocity and distance for an aquifer of $M = 10$ m saturated height with an effective porosity of $n_{eff} = 0.2$ for different extraction rates. Seepage velocities in which LTNE effects can be expected are easily reached in the vicinity of pumped bores and LTNE effects should therefore be taken into consideration.

Additionally, the highly transient operation typical for groundwater-based heat pump systems (Muela Maya et al., 2018) can enhance the effects of LTNE (Minkowycz et al., 1999). Therefore, an increase in effective thermal dispersion due to LTNE effects should be carefully considered

under the conditions depicted in Fig. 40. Thermal non-equilibrium potentially also affects the storage of thermal energy in aquifers composed of large particle sizes. The increased spreading of the thermal front in the fluid phase due to an incomplete storage in the solid phase leads to an initially lower energy density in the area of interest than is expected when an LTE model is used.

In dynamic interfaces with surface-water bodies, such as when aquifers interact with rivers, groundwater can reach velocities higher than 10 m d^{-1} (e.g. Angermann et al., 2012; Cremeans et al., 2018; Rau et al., 2014). These systems are potentially influenced by LTNE effects. While several studies investigated the influence of heterogeneity (Irvine et al., 2015a) or the deviation from the assumptions of the analytical model (Reeves and Hatch, 2016) on the flux estimates, it remains unclear, how an increase of effective thermal dispersion due to LTNE conditions affects flux estimates from phase shift or amplitude ratios from diurnal temperature time series (e.g. Irvine et al., 2015b). As the groundwater velocities for interactions with lakes are usually well below 1 m d^{-1} (Rosenberry et al., 2015), the LTE assumption is mostly applicable for these conditions. Only at low Pe numbers in combination with large particle sizes an LTE model can overestimate the advective thermal velocity.

When using thermal breakthrough curves to estimate the mean transit time for example in managed aquifer recharge applications (Becker et al., 2013, 2015; Bekele et al., 2014) care should be taken regarding the thermal peak velocity. The thermal peak velocity can differ significantly from the advective thermal velocity in conditions with slow seepage velocities leading to an underestimation of the mean transit time.

Even in conditions with strong LTNE effects, for some of these cases, i.e. when the advective component is of interest, the LTE model is appropriate (Fig. 40) because the LTNE effects do not significantly influence the advective thermal velocity in advection dominated conditions.

Recommendations for practical use:

When heat transport in natural porous media such as porous aquifers is modeled, one should consider if LTNE effects are likely to occur in the expected conditions in the area of interest. This can be done using Fig. 40 and the LTNE criterion (eq. 55 and Table 12) developed in section 4.3.9 by roughly estimating the relevant parameters particle size, seepage velocity, po-

rosity, and the thermal conductivity of the solid phase. Besides considering the natural conditions, anthropogenic influences on the seepage velocity such as extraction and injection wells should be taken into account (Fig. 48). If only the advective part of the heat transport is of interest, an LTE model can be appropriate even in LTNE favorable conditions as the advective thermal velocity is not significantly influenced. If all heat transport processes are relevant, for example in estimating the thermal plume of a thermal groundwater application, the usage of an LTNE model is in order. Using an LTE model in LTNE favorable conditions can lead to a significant underestimation of the thermal dispersion. Vice versa, using an LTNE model in LTE favorable conditions does not influence the results as both model outcomes are identical. Consequently, using an LTNE model can be considered as being on the safe side if one is unsure if LTNE effects could occur. The heat transfer coefficient, necessary when using an LTNE model, can be readily estimated by using the new correlation to determine Nusselt number given in Fig. 25 which is based on available literature data and tailored to porous aquifers.

5.2   Future developments and outlook

Detailed knowledge about heat transport processes in natural porous media is of high importance in multiple fields. The currently applied methods and models all rely on certain conditions and assumptions. These assumptions should be constantly checked and adapted if necessary. The steady increase of computational power and availability in recent decades enables to continuously increase the representable level of detail in numerical modeling, even allowing particle resolved direct numerical modeling approaches. Furthermore, developments like fiber optic distributed temperature sensing allow for continuous and spatially highly resolved in-situ temperature measurements in field applications enabling a comparison between modeling results and field measurements. These advances can be utilized to increase the understanding of heat transport in natural porous media.

Possible future research could address finding an appropriate Nusselt correlation with water as fluid and for conditions expected in natural porous media, either with laboratory experiments or with a particle resolved direct numerical modeling approach. Furthermore, an investigation of LTNE effects in the field is still lacking. This could be accomplished by monitoring thermal breakthrough curves in the vicinity of wells of geothermal applications in aquifers with large grain sizes. Additionally, this study investigated LTNE effects in a one-dimensional

approach in the laboratory experiments and in the numerical parameter study. The influence of heterogeneity and the transition from 1D to 3D regarding possible LTNE conditions is still unclear.

References

Abdedou, A., Bouhadef, K., 2015. Comparison between two local thermal non equilibrium criteria in forced convection through a porous channel. J. Appl. Fluid Mech. 8, 491–498. https://doi.org/10.18869/acadpub.jafm.67.222.22233

Abdulagatova, Z., Abdulagatov, I.M., Emirov, V.N., 2009. Effect of temperature and pressure on the thermal conductivity of sandstone. Int. J. Rock Mech. Min. Sci. 46, 1055–1071. https://doi.org/10.1016/j.ijrmms.2009.04.011

Achenbach, E., 1995. Heat and flow characteristics of packed beds. Exp. Therm. Fluid Sci. 10, 17–27. https://doi.org/10.1016/0894-1777(94)00077-L

Adams, M.C., Davis, J., 1991. Kinetics of fluorescein decay and its application as a geothermal tracer. Geothermics 20, 53–66. https://doi.org/10.1016/0375-6505(91)90005-G

Afshari, S., Hejazi, S.H., Kantzas, A., 2019. Pore-level modeling of effective longitudinal thermal dispersion in non-isothermal flows through granular porous media. Chem. Eng. Sci. 199, 451–462. https://doi.org/10.1016/j.ces.2019.01.028

Aguilar-Madera, C.G., Valdés-Parada, F.J., Goyeau, B., Alberto Ochoa-Tapia, J., 2011. One-domain approach for heat transfer between a porous medium and a fluid. Int. J. Heat Mass Transf. 54, 2089–2099. https://doi.org/10.1016/j.ijheatmasstransfer.2010.12.020

Ahmed, A.K.A., Marhaba, T.F., 2017. Review on river bank filtration as an in situ water treatment process. Clean Technol. Environ. Policy 19, 349–359. https://doi.org/10.1007/s10098-016-1266-0

Al-Nimr, M.A., Abu-Hijleh, B.A., 2002. Validation of thermal equilibrium assumption in transient forced convection flow in porous channel. Transp. Porous Media 49, 127–138. https://doi.org/10.1023/A:1016072713296

Al-Sumaily, G.F., Sheridan, J., Thompson, M.C., 2013. Validation of thermal equilibrium assumption in forced convection steady and pulsatile flows over a cylinder embedded in a porous channel. Int. Commun. Heat Mass Transf. 43, 30–38. https://doi.org/10.1016/j.icheatmasstransfer.2013.01.009

Alazmi, B., Vafai, K., 2004. Analysis of variable porosity, thermal dispersion, and local thermal nonequilibrium on free surface flows through porous media. J. Heat Transfer 126, 389–399. https://doi.org/10.1115/1.1723470

Amiri, A., Vafai, K., 1998. Transient analysis of incompressible flow through a packed bed. Int. J. Heat Mass Transf. 41, 4259–4279. https://doi.org/10.1016/S0017-9310(98)00120-3

Amiri, A., Vafai, K., 1994. Analysis of dispersion effects and non-thermal equilibrium, non-Darcian, variable porosity incompressible flow through porous media. Int. J. Heat Mass Transf. 37, 939–954. https://doi.org/10.1016/0017-9310(94)90219-4

Anderson, M.P., 2005. Heat as a ground water tracer. Ground Water 43, 951–968. https://doi.org/10.1111/j.1745-6584.2005.00052.x

Anderson, M.P., Woessner, W.W., Hunt, R.J., 2015. Applied Groundwater Modeling, Applied

References

Groundwater Modeling. https://doi.org/10.1016/b978-0-08-091638-5.00001-8

Angermann, L., Krause, S., Lewandowski, J., 2012. Application of heat pulse injections for investigating shallow hyporheic flow in a lowland river. Water Resour. Res. 48, 1–16. https://doi.org/10.1029/2012WR012564

Attard, G., Bayer, P., Rossier, Y., Blum, P., Eisenlohr, L., 2020. A novel concept for managing thermal interference between geothermal systems in cities. Renew. Energy 145, 914–924. https://doi.org/10.1016/j.renene.2019.06.095

Bakker, M., Caljé, R., Schaars, F., Van Der Made, K.J., De Haas, S., 2015. An active heat tracer experiment to determine groundwater velocities using fiber optic cables installed with direct push equipment. Water Resour. Res. 51, 2760–2772. https://doi.org/10.1002/2014WR016632

Bandai, T., Hamamoto, S., Rau, G.C., Komatsu, T., Nishimura, T., 2017. The effect of particle size on thermal and solute dispersion in saturated porous media. Int. J. Therm. Sci. 122, 74–84. https://doi.org/10.1016/j.ijthermalsci.2017.08.003

Banks, D., 2015. A review of the importance of regional groundwater advection for ground heat exchange. Environ. Earth Sci. 73, 2555–2565. https://doi.org/10.1007/s12665-014-3377-4

Banks, D., 2012. An introduction to thermogeology: Ground source heating and cooling: Second edition, 2. ed. ed, An Introduction to Thermogeology: Ground Source Heating and Cooling: Second Edition. Wiley-Blackwell, Oxford u.a. https://doi.org/10.1002/9781118447512

Barry, D.A., 2009. Effect of nonuniform boundary conditions on steady flow in saturated homogeneous cylindrical soil columns. Adv. Water Resour. 32, 522–531. https://doi.org/10.1016/j.advwatres.2009.01.003

Bear, J., 1972. Dynamics of Fluids in Porous Media, Dover Edit. ed, Soil Science. New York. https://doi.org/10.1097/00010694-197508000-00022

Becker, M.W., Bauer, B., Hutchinson, A., 2013. Measuring artificial recharge with fiber optic distributed temperature sensing. Groundwater 51, 670–678. https://doi.org/10.1111/j.1745-6584.2012.01006.x

Becker, T.E., Clark, J.F., Johnson, T.A., 2015. Heat, 10B-enriched boric acid, and bromide as recycled groundwater tracers for managed aquifer recharge: Case study. J. Hydrol. Eng. 20. https://doi.org/10.1061/(ASCE)HE.1943-5584.0001070

Bekele, E., Patterson, B., Toze, S., Furness, A., Higginson, S., Shackleton, M., 2014. Aquifer residence times for recycled water estimated using chemical tracers and the propagation of temperature signals at a managed aquifer recharge site in Australia. Hydrogeol. J. 22, 1383–1401. https://doi.org/10.1007/s10040-014-1142-0

Bodvarsson, G., 1972. Thermal problems in the siting of reinjection wells. Geothermics 1, 63–66. https://doi.org/10.1016/0375-6505(72)90013-2

Bonner, R., Aylward, L., Harley, C., Kappelmeyer, U., Sheridan, C.M., 2017. Heat as a hydraulic tracer for horizontal subsurface flow constructed wetlands. J. Water Process Eng. 16, 183–192. https://doi.org/10.1016/j.jwpe.2017.01.007

References

Bonte, M., Röling, W.F.M., Zaura, E., Van Der Wielen, P.W.J.J., Stuyfzand, P.J., Van Breukelen, B.M., 2013. Impacts of shallow geothermal energy production on redox processes and microbial communities. Environ. Sci. Technol. 47, 14476–14484. https://doi.org/10.1021/es4030244

Bortolozzi, R.A., Deiber, J.A., 2001. Comparison between two- and one-field models for natural convection in porous media. Chem. Eng. Sci. 56, 157–172. https://doi.org/10.1016/S0009-2509(00)00415-2

Böttcher, F., Casasso, A., Götzl, G., Zosseder, K., 2019. TAP - Thermal aquifer Potential: A quantitative method to assess the spatial potential for the thermal use of groundwater. Renew. Energy 142, 85–95. https://doi.org/10.1016/j.renene.2019.04.086

Boulton, A.J., Findlay, S., Marmonier, P., Stanley, E.H., Maurice Valett, H., 1998. The functional significance of the hyporheic zone in streams and rivers. Annu. Rev. Ecol. Syst. 29, 59–81. https://doi.org/10.1146/annurev.ecolsys.29.1.59

Brielmann, H., Griebler, C., Schmidt, S.I., Michel, R., Lueders, T., 2009. Effects of thermal energy discharge on shallow groundwater ecosystems. FEMS Microbiol. Ecol. 68, 273–286. https://doi.org/10.1111/j.1574-6941.2009.00674.x

Brunke, M., Gonser, T., 1997. The ecological significance of exchange processes between rivers and groundwater. Freshw. Biol. 37, 1–33. https://doi.org/10.1046/j.1365-2427.1997.00143.x

Buntebarth, G., Schopper, J.R., 1998. Experimental and theoretical investigations on the influence of fluids, solids and interactions between them on thermal properties of porous rocks. Phys. Chem. Earth 23, 1141–1146. https://doi.org/10.1016/S0079-1946(98)00142-6

Buonomo, B., Manca, O., Lauriat, G., 2014. Forced convection in micro-channels filled with porous media in local thermal non-equilibrium conditions. Int. J. Therm. Sci. 77, 206–222. https://doi.org/10.1016/j.ijthermalsci.2013.11.003

Byun, S.Y., Ro, S.T., Shin, J.Y., Son, Y.S., Lee, D.Y., 2006. Transient thermal behavior of porous media under oscillating flow condition. Int. J. Heat Mass Transf. 49, 5081–5085. https://doi.org/10.1016/j.ijheatmasstransfer.2006.05.036

Caissie, D., Luce, C.H., 2017. Quantifying streambed advection and conduction heat fluxes. Water Resour. Res. 53, 1595–1624. https://doi.org/10.1002/2016WR019813

Calcagno, V., de Mazancourt, C., 2010. glmulti: An R package for easy automated model selection with (generalized) linear models. J. Stat. Softw. 34, 29. https://doi.org/10.18637/jss.v034.i12

Carbonell, R.G., Whitaker, S., 1984. Heat and Masstransfer in Porous Media, in: Bear, J., Corapcioglu, M.Y. (Eds.), Fundamentals of Transport Phenomena in Porous Media. Springer Netherlands, Dordrecht, pp. 121–196. https://doi.org/10.1007/978-94-009-6175-3_3

Casasso, A., Sethi, R., 2019. Assessment and minimization of potential environmental impacts of ground source heat pump (GSHP) systems. Water (Switzerland) 11, 1–19. https://doi.org/10.3390/w11081573

Cesba wiki [WWW Document], n.d. URL http://wiki.cesba.eu/wiki/Shallow_Geothermal_Energy_Guidelines (accessed 12.10.20).

References

Chen, Y., Müller, C.R., 2019. Lattice Boltzmann simulation of gas-solid heat transfer in random assemblies of spheres: The effect of solids volume fraction on the average Nusselt number for Re ≤ 100. Chem. Eng. J. 361, 1392–1399. https://doi.org/10.1016/j.cej.2018.10.182

Collier, A.R., Hayhurst, A.N., Richardson, J.L., Scott, S.A., 2004. The heat transfer coefficient between a particle and a bed (packed or fluidised) of much larger particles. Chem. Eng. Sci. 59, 4613–4620. https://doi.org/10.1016/j.ces.2004.07.029

Colombani, N., Giambastiani, B.M.S., Mastrocicco, M., 2015. Combined use of heat and saline tracer to estimate aquifer properties in a forced gradient test. J. Hydrol. 525, 650–657. https://doi.org/10.1016/j.jhydrol.2015.04.026

Conant, B., 2004. Delineating and Quantifying Ground Water Discharge Zones Using Streambed Temperatures. Ground Water. https://doi.org/10.1111/j.1745-6584.2004.tb02671.x

Constantz, J., 2008. Heat as a tracer to determine streambed water exchanges. Water Resour. Res. 46, 1–20. https://doi.org/10.1029/2008WR006996

Constantz, J., Cox, M.H., Su, G.W., 2003. Comparison of Heat and Bromide as Ground Water Tracers Near Streams. Ground Water 41, 647–656. https://doi.org/10.1111/j.1745-6584.2003.tb02403.x

Côté, J., Konrad, J.M., 2005. A generalized thermal conductivity model for soils and construction materials. Can. Geotech. J. 42, 443–458. https://doi.org/10.1139/t04-106

Cremeans, M.M., Devlin, J.F., McKnight, U.S., Bjerg, P.L., 2018. Application of new point measurement device to quantify groundwater-surface water interactions. J. Contam. Hydrol. 211, 85–93. https://doi.org/10.1016/j.jconhyd.2018.03.010

Davis, N.S., De Wiest, R.J.M., 1966. Hydrogeology. Wiley, New York.

De Marsily, G., 1986. Quantitative Hydrogeology for Engineers. Paris School of Mines, Fontainebleau.

Dehghan, M., Jamal-Abad, M.T., Rashidi, S., 2014a. Analytical interpretation of the local thermal non-equilibrium condition of porous media imbedded in tube heat exchangers. Energy Convers. Manag. 85, 264–271. https://doi.org/10.1016/j.enconman.2014.05.074

Dehghan, M., Valipour, M.S., Saedodin, S., 2014b. Perturbation Analysis of the Local Thermal Non-equilibrium Condition in a Fluid-Saturated Porous Medium Bounded by an Iso-thermal Channel. Transp. Porous Media 102, 139–152. https://doi.org/10.1007/s11242-013-0267-2

Diersch, H.J.G., 2014. FEFLOW: Finite element modeling of flow, mass and heat transport in porous and fractured media, FEFLOW: Finite Element Modeling of Flow, Mass and Heat Transport in Porous and Fractured Media. https://doi.org/10.1007/978-3-642-38739-5

Djibrilla Saley, A., Jardani, A., Soueid Ahmed, A., Raphael, A., Dupont, J.P., 2016. Hamiltonian Monte Carlo algorithm for the characterization of hydraulic conductivity from the heat tracing data. Adv. Water Resour. 97, 120–129. https://doi.org/10.1016/j.advwatres.2016.09.004

Domenico, P.A., Schwartz, F.W., 1998. Physical and Chemical Hydrogeology, 2nd ed. Wiley, New York, NY.

References

Dullien, F.A.L., 1979. Porous media: fluid transport and pore structure. Academic Press, New York, NY. https://doi.org/10.1016/0300-9467(81)80049-4

Epting, J., García-Gil, A., Huggenberger, P., Vázquez-Suñe, E., Mueller, M.H., 2017. Development of concepts for the management of thermal resources in urban areas – Assessment of transferability from the Basel (Switzerland) and Zaragoza (Spain) case studies. J. Hydrol. 548, 697–715. https://doi.org/10.1016/j.jhydrol.2017.03.057

Fathi-kelestani, A., Nazari, M., Mahmoudi, Y., 2020. Pulsating flow in a channel filled with a porous medium under local thermal non-equilibrium condition: an exact solution. J. Therm. Anal. Calorim. https://doi.org/10.1007/s10973-020-09843-0

Ferguson, G., 2009. Unfinished business in geothermal energy. Ground Water 47, 167. https://doi.org/10.1111/j.1745-6584.2008.00528.x

Findlay, S., 1995. Importance of surface-subsurface exchange in stream ecosystems: The hyporheic zone. Limnol. Oceanogr. 40, 159–164. https://doi.org/10.4319/lo.1995.40.1.0159

Furbo, S., 2015. Using water for heat storage in thermal energy storage (TES) systems, in: Cabeza, L.F. (Ed.), Advances in Thermal Energy Storage Systems: Methods and Applications. Elsevier B.V, pp. 31–47. https://doi.org/10.1533/9781782420965.1.31

Ganguly, S., Mohan Kumar, M.S., Date, A., Akbarzadeh, A., 2017. Numerical investigation of temperature distribution and thermal performance while charging-discharging thermal energy in aquifer. Appl. Therm. Eng. 115, 756–773. https://doi.org/10.1016/j.applthermaleng.2017.01.009

Garabedian, S.P., LeBlanc, D.R., Gelhar, L.W., Celia, M.A., 1991. Large-scale natural gradient tracer test in sand and gravel, Cape Cod, Massachusetts: 2. Analysis of Spatial Moments for a Nonreactive Tracer. Water Resour. Res. 27, 895–910. https://doi.org/10.1029/91WR00241

García-Gil, A., Goetzl, G., Kłonowski, M.R., Borovic, S., Boon, D.P., Abesser, C., Janza, M., Herms, I., Petitclerc, E., Erlström, M., Holecek, J., Hunter, T., Vandeweijer, V.P., Cernak, R., Mejías Moreno, M., Epting, J., 2020. Governance of shallow geothermal energy resources. Energy Policy 138. https://doi.org/10.1016/j.enpol.2020.111283

Gossler, M.A., Bayer, P., Rau, G.C., Einsiedl, F., Zosseder, K., 2020. On the Limitations and Implications of Modeling Heat Transport in Porous Aquifers by Assuming Local Thermal Equilibrium. Water Resour. Res. https://doi.org/10.1029/2020wr027772

Gossler, M.A.M.A., Bayer, P., Zosseder, K., 2019. Experimental investigation of thermal retardation and local thermal non-equilibrium effects on heat transport in highly permeable, porous aquifers. J. Hydrol. 578, 1–14. https://doi.org/10.1016/j.jhydrol.2019.124097

Gunn, D.J., 1978. Transfer of heat or mass to particles in fixed and fluidised beds. Int. J. Heat Mass Transf. 21, 467–476. https://doi.org/10.1016/0017-9310(78)90080-7

Gunn, D.J., De Souza, J.F.C., 1974. Heat transfer and axial dispersion in packed beds. Chem. Eng. Sci. 29, 1363–1371. https://doi.org/10.1016/0009-2509(74)80160-0

Haehnlein, S., Bayer, P., Blum, P., 2010. International legal status of the use of shallow geothermal energy. Renew. Sustain. Energy Rev. 14, 2611–2625. https://doi.org/10.1016/j.rser.2010.07.069

References

Hähnlein, S., Bayer, P., Ferguson, G., Blum, P., 2013. Sustainability and policy for the thermal use of shallow geothermal energy. Energy Policy 59, 914–925. https://doi.org/10.1016/j.enpol.2013.04.040

Halloran, L.J.S., Rau, G.C., Andersen, M.S., 2016. Heat as a tracer to quantify processes and properties in the vadose zone: A review. Earth-Science Rev. 159, 358–373. https://doi.org/10.1016/j.earscirev.2016.06.009

Hamidi, S., Heinze, T., Galvan, B., Miller, S., 2019. Critical review of the local thermal equilibrium assumption in heterogeneous porous media: Dependence on permeability and porosity contrasts. Appl. Therm. Eng. 147, 962–971. https://doi.org/10.1016/j.applthermaleng.2018.10.130

Hecht-Méndez, J., Molina-Giraldo, N., Blum, P., Bayer, P., 2010. Evaluating MT3DMS for heat transport simulation of closed geothermal systems. Ground Water 48, 741–756. https://doi.org/10.1111/j.1745-6584.2010.00678.x

Heinze, T., Blöcher, J.R., 2019. A model of local thermal non-equilibrium during infiltration. Adv. Water Resour. 132, 103394. https://doi.org/10.1016/j.advwatres.2019.103394

Heinze, T., Hamidi, S., 2017. Heat transfer and parameterization in local thermal non-equilibrium for dual porosity continua. Appl. Therm. Eng. 114, 645–652. https://doi.org/10.1016/j.applthermaleng.2016.12.015

Heinze, T., Hamidi, S., Galvan, B., 2017. A dynamic heat transfer coefficient between fractured rock and flowing fluid. Geothermics 65, 10–16. https://doi.org/10.1016/j.geothermics.2016.08.007

Herbert, A., Arthur, S., Chillingworth, G., 2013. Thermal modelling of large scale exploitation of ground source energy in urban aquifers as a resource management tool. Appl. Energy 109, 94–103. https://doi.org/10.1016/j.apenergy.2013.03.005

Hermans, T., Nguyen, F., Klepikova, M. V., Dassargues, A., Caers, J., 2018. Uncertainty Quantification of Medium-Term Heat Storage From Short-Term Geophysical Experiments Using Bayesian Evidential Learning. Water Resour. Res. 54, 2931–2948. https://doi.org/10.1002/2017WR022135

Hoehn, E., Cirpka, O.A., 2006. Assessing hyporheic zone dynamics in two alluvial flood plains of the Southern Alps using water temperature and tracers. Hydrol. Earth Syst. Sci. Discuss. 3, 335–364. https://doi.org/10.5194/hessd-3-335-2006

Hopmans, J.W., Šimunek, J., Bristow, K.L., 2002. Indirect estimation of soil thermal properties and water flux using heat pulse probe measurements: Geometry and dispersion effects. Water Resour. Res. 38, 7-1-7–14. https://doi.org/10.1029/2000wr000071

Houben, G.J., 2015. Review: Hydraulics of water wells - flow laws and influence of geometry. Hydrogeol. J. 23, 1633–1657. https://doi.org/10.1007/s10040-015-1312-8

Huber, M.L., Perkins, R.A., Friend, D.G., Sengers, J. V., Assael, M.J., Metaxa, I.N., Miyagawa, K., Hellmann, R., Vogel, E., 2012. New International Formulation for the Thermal Conductivity of H2O. J. Phys. Chem. Ref. Data 41. https://doi.org/10.1063/1.4738955

Iooss, B., Janon, A., Pujol, G., Broto, B.-T., Boumhaout, K., Da Veiga, S., Delage, T., Fruth, J., Gilquin, L.-R., Guillaume, J., Le Gratiet, L., Lemaitre, P., Marrel, A., Mey-Naoui, A., Nelson, B.L., Monari,

References

F.-I., Oomen, R., Rakovec, O., Ramos, B., Roustant, O., Song, E.-H., Staum, J., Sueur, R., Touati, T., Weber, F., 2019. Package "sensitivity" Title Global Sensitivity Analysis of Model Outputs.

Irvine, D.J., Briggs, M.A., Lautz, L.K., Gordon, R.P., McKenzie, J.M., Cartwright, I., 2017. Using Diurnal Temperature Signals to Infer Vertical Groundwater-Surface Water Exchange. Groundwater 55, 10–26. https://doi.org/10.1111/gwat.12459

Irvine, D.J., Cranswick, R.H., Simmons, C.T., Shanafield, M.A., Lautz, L.K., 2015a. The effect of streambed heterogeneity on groundwater-surface water exchange fluxes inferred from temperature time series. Water Resour. Res. 51, 198–212. https://doi.org/10.1002/2014WR015769

Irvine, D.J., Kurylyk, B.L., Briggs, M.A., 2020. Quantitative guidance for efficient vertical flow measurements at the sediment–water interface using temperature–depth profiles. Hydrol. Process. 34, 649–661. https://doi.org/10.1002/hyp.13614

Irvine, D.J., Lautz, L.K., 2015. High resolution mapping of hyporheic fluxes using streambed temperatures: Recommendations and limitations. J. Hydrol. 524, 137–146. https://doi.org/10.1016/j.jhydrol.2015.02.030

Irvine, D.J., Lautz, L.K., Briggs, M.A., Gordon, R.P., McKenzie, J.M., 2015b. Experimental evaluation of the applicability of phase, amplitude, and combined methods to determine water flux and thermal diffusivity from temperature time series using VFLUX 2. J. Hydrol. 531, 728–737. https://doi.org/10.1016/j.jhydrol.2015.10.054

Irvine, D.J., Simmons, C.T., Werner, A.D., Graf, T., 2013. Heat and Solute Tracers: How Do They Compare in Heterogeneous Aquifers? Groundwater 53, 10–20. https://doi.org/10.1111/gwat.12146

Kaguei, S., Shiozawa, B., Wakao, N., 1976. Dispersion-concentric packed bed heat. Chem. Eng. Sci. 32, 507–513.

Kaviany, M., 1995. Principles of Heat Transfer in Porous Media, Mechanical Engineering Series, Mechanical Engineering Series. Springer New York, New York, NY. https://doi.org/10.1007/978-1-4612-4254-3

Khashan, S.A., Al-Amiri, A.M., Pop, I., 2006. Numerical simulation of natural convection heat transfer in a porous cavity heated from below using a non-Darcian and thermal non-equilibrium model. Int. J. Heat Mass Transf. 49, 1039–1049. https://doi.org/10.1016/j.ijheatmasstransfer.2005.09.011

Khashan, S.A., Al-Nimr, M.A., 2005. Validation of the local thermal equilibrium assumption in forced convection of non-Newtonian fluids through porous channels. Transp. Porous Media 61, 291–305. https://doi.org/10.1007/s11242-004-8305-8

Kim, S.J., Jang, S.P., 2002. Effects of the Darcy number, the Prandtl number, and the Reynolds number on local thermal non-equilibrium. Int. J. Heat Mass Transf. 45, 3885–3896. https://doi.org/10.1016/S0017-9310(02)00109-6

Klepikova, M. V., Wildemeersch, S., Hermans, T., Jamin, P., Orban, P., Nguyen, F., Brouyère, S., Dassargues, A., 2016. Heat tracer test in an alluvial aquifer: Field experiment and inverse modelling. J. Hydrol. 540, 812–823. https://doi.org/10.1016/j.jhydrol.2016.06.066

References

Klotz, D.K., Maloszewski, P.M., Moser, H., 1988. Mathematical Modeling of Radioactive Tracer Migration in Water Flowing through Saturated Porous Media. Radiochim. Acta 44–45, 373–380. https://doi.org/10.1524/ract.1988.4445.2.373

Kolditz, O., Görke, U.J., Shao, H., Wang, W., 2012. Thermo-hydro-mechanical-chemical processes in fractured porous media, Lecture Notes in Computational Science and Engineering. https://doi.org/10.1007/978-3-642-27177-9_1

Kunii, D., Smith, J.M., 1961. Heat transfer characteristics of porous rocks: II. Thermal conductivities of unconsolidated particles with flowing fluids. AIChE J. 7, 29–34. https://doi.org/10.1002/aic.690070109

Kurylyk, B.L., Irvine, D.J., 2019. Heat: An Overlooked Tool in the Practicing Hydrogeologist's Toolbox. Groundwater 57, 517–524. https://doi.org/10.1111/gwat.12910

Kurylyk, B.L., Irvine, D.J., Bense, V.F., 2019. Theory, tools, and multidisciplinary applications for tracing groundwater fluxes from temperature profiles. Wiley Interdiscip. Rev. Water 6, e1329. https://doi.org/10.1002/wat2.1329

Kurylyk, B.L., Irvine, D.J., Carey, S.K., Briggs, M.A., Werkema, D.D., Bonham, M., 2017. Heat as a groundwater tracer in shallow and deep heterogeneous media: Analytical solution, spreadsheet tool, and field applications. Hydrol. Process. 31, 2648–2661. https://doi.org/10.1002/hyp.11216

Kurylyk, B.L., Macquarrie, K.T.B., Linnansaari, T., Cunjak, R.A., Curry, R.A., 2015. Preserving, augmenting, and creating cold-water thermal refugia in rivers: Concepts derived from research on the Miramichi River, New Brunswick (Canada). Ecohydrology 8, 1095–1108. https://doi.org/10.1002/eco.1566

Kuznetsov, A. V., 1998. Thermal Nonequilibrium Forced Convection in Porous Media, in: Ingham, D.B., Pop, I. (Eds.), Transport Phenomena in Porous Media. pp. 103–129. https://doi.org/10.1016/b978-008042843-7/50005-2

Langevin, C.D., Thorne Jr., D.T., Dausman, A.M., Sukop, M.C., Guo, W., 2008. SEAWAT Version 4: A Computer Program for Simulation of Multi-Species Solute and Heat Transport, Techniques and Methods. https://doi.org/10.3133/tm6A22

Laws, B. V., Dickenson, E.R.V., Johnson, T.A., Snyder, S.A., Drewes, J.E., 2011. Attenuation of contaminants of emerging concern during surface-spreading aquifer recharge. Sci. Total Environ. 409, 1087–1094. https://doi.org/10.1016/j.scitotenv.2010.11.021

Lee, D.Y., Vafai, K., 1998. Analytical characterization and conceptual assessment of solid and fluid temperature differentials in porous media. Int. J. Heat Mass Transf. 42, 423–435. https://doi.org/10.1016/S0017-9310(98)00185-9

Leibundgut, C., Maloszewski, P., Külls, C., 2009. Tracers in Hydrology, Tracers in Hydrology. Wiley-Blackwell, West Sussex. https://doi.org/10.1002/9780470747148

Lenda, A., Zuber, A., 1970. Tracer dispersion in groundwater experiments. Isot. Hydrol. 1970, Proc Symp 129, 619–636.

Levec, J., Carbonell, R.G., 1985a. Longitudinal and lateral thermal dispersion in packed beds. Part I:

References

Theory. AIChE J. 31, 581–590. https://doi.org/10.1002/aic.690310408

Levec, J., Carbonell, R.G., 1985b. Longitudinal and lateral thermal dispersion in packed beds. Part II: Comparison between Theory and Experiment. AIChE J. 31, 591–602. https://doi.org/https://doi.org/10.1002/aic.690310409

Lewandowski, J., Angermann, L., Nützmann, G., Fleckenstein, J.H., 2011. A heat pulse technique for the determination of small-scale flow directions and flow velocities in the streambed of sand-bed streams. Hydrol. Process. 25, 3244–3255. https://doi.org/10.1002/hyp.8062

Lewandowski, J., Arnon, S., Banks, E., Batelaan, O., Betterle, A., Broecker, T., Coll, C., Drummond, J.D., Garcia, J.G., Galloway, J., Gomez-Velez, J., Grabowski, R.C., Herzog, S.P., Hinkelmann, R., Höhne, A., Hollender, J., Horn, M.A., Jaeger, A., Krause, S., Prats, A.L., Magliozzi, C., Meinikmann, K., Mojarrad, B.B., Mueller, B.M., Peralta-Maraver, I., Popp, A.L., Posselt, M., Putschew, A., Radke, M., Raza, M., Riml, J., Robertson, A., Rutere, C., Schaper, J.L., Schirmer, M., Schulz, H., Shanafield, M., Singh, T., Ward, A.S., Wolke, P., Wörman, A., Wu, L., 2019. Is the hyporheic zone relevant beyond the scientific community? Water (Switzerland) 11. https://doi.org/10.3390/w11112230

Littman, H., Barile, R.G., Pulsifer, A.H., 1968. Gas-particle heat transfer coefficients in packed beds at low reynolds numbers. Ind. Eng. Chem. Fundam. 7, 554–561. https://doi.org/10.1021/i160028a005

Lo Russo, S., Taddia, G., Cerino Abdin, E., Verda, V., 2016. Effects of different re-injection systems on the thermal affected zone (TAZ) modelling for open-loop groundwater heat pumps (GWHPs). Environ. Earth Sci. 75, 1–14. https://doi.org/10.1007/s12665-015-4822-8

Lu, W., Xiang, Y., 2012. Analysis of the instantaneous local thermal equilibrium assumption for heat exchange between rock matrix and fracture water. Adv. Mater. Res. 594–597, 2430–2437. https://doi.org/10.4028/www.scientific.net/AMR.594-597.2430

Ma, R., Zheng, C., 2010. Effects of Density and Viscosity in Modeling Heat as a Groundwater Tracer. Ground Water 48, 380–389. https://doi.org/10.1111/j.1745-6584.2009.00660.x

Ma, R., Zheng, C., Zachara, J.M., Tonkin, M., 2012. Utility of bromide and heat tracers for aquifer characterization affected by highly transient flow conditions. Water Resour. Res. 48, 1–18. https://doi.org/10.1029/2011WR011281

Maier, F., Schaffer, M., Licha, T., 2015. Temperature determination using thermo-sensitive tracers: Experimental validation in an isothermal column heat exchanger. Geothermics 53, 533–539. https://doi.org/10.1016/j.geothermics.2014.09.007

Markle, J.M., Schincariol, R.A., 2007. Thermal plume transport from sand and gravel pits - Potential thermal impacts on cool water streams. J. Hydrol. 338, 174–195. https://doi.org/10.1016/j.jhydrol.2007.02.031

Metzger, T., Didierjean, S., Maillet, D., 2004. Optimal experimental estimation of thermal dispersion coefficients in porous media. Int. J. Heat Mass Transf. 47, 3341–3353. https://doi.org/10.1016/j.ijheatmasstransfer.2004.02.024

Mills, R.T., Lu, C., Lichtner, P.C., Hammond, G.E., 2007. Simulating subsurface flow and transport on

References

ultrascale computers using PFLOTRAN. J. Phys. Conf. Ser. 78. https://doi.org/10.1088/1742-6596/78/1/012051

Minkowycz, W.J., Haji-Sheikh, A., Vafai, K., 1999. On departure from local thermal equilibrium in porous media due to a rapidly changing heat source: The Sparrow number. Int. J. Heat Mass Transf. 42, 3373–3385. https://doi.org/10.1016/S0017-9310(99)00043-5

Moeck, C., Radny, D., Popp, A., Brennwald, M., Stoll, S., Auckenthaler, A., Berg, M., Schirmer, M., 2017. Characterization of a managed aquifer recharge system using multiple tracers. Sci. Total Environ. 609, 701–714. https://doi.org/10.1016/j.scitotenv.2017.07.211

Molina-Giraldo, N., Bayer, P., Blum, P., Cirpka, O.A., 2011. Propagation of seasonal temperature signals into an aquifer upon bank infiltration. Ground Water 49, 491–502. https://doi.org/10.1111/j.1745-6584.2010.00745.x

Muela Maya, S., García-Gil, A., Garrido Schneider, E., Mejías Moreno, M., Epting, J., Vázquez-Suñé, E., Marazuela, M.Á., Sánchez-Navarro, J.Á., 2018. An upscaling procedure for the optimal implementation of open-loop geothermal energy systems into hydrogeological models. J. Hydrol. 563, 155–166. https://doi.org/10.1016/j.jhydrol.2018.05.057

Nagano, K., Mochida, T., Ochifuji, K., 2002. Influence of natural convection on forced horizontal flow in saturated porous media for aquifer thermal energy storage. Appl. Therm. Eng. 22, 1299–1311. https://doi.org/10.1016/S1359-4311(02)00056-X

Naghash, M., Fathieh, F., Besant, R.W., Evitts, R.W., Simonson, C.J., 2016. Measurement of convective heat transfer coefficients in a randomly packed bed of silica gel particles using IHTP analysis. Appl. Therm. Eng. 106, 361–370. https://doi.org/10.1016/j.applthermaleng.2016.06.027

Nelson, P.A., Galloway, T.R., 1975. Particle-to-fluid heat and mass transfer in dense systems of fine particles. Chem. Eng. Sci. 30, 1–6. https://doi.org/10.1016/0009-2509(75)85109-8

Nie, X., Evitts, R.W., Besant, R., Bolster, J., 2011. A new technique to determine convection coefficients with flow through particle beds. J. Heat Transfer 133, 1–8. https://doi.org/10.1115/1.4002945

Nield, D.A., Bejan, A., 2017. Convection in porous media, 5th ed. Springer International Publishing, Cham. https://doi.org/10.1007/978-3-319-49562-0

Nouri-Borujerdi, A., Noghrehabadi, A.R., Rees, D.A.S., 2007. The effect of local thermal non-equilibrium on conduction in porous channels with a uniform heat source. Transp. Porous Media 69, 281–288. https://doi.org/10.1007/s11242-006-9064-5

Novak, M.D., 2019. Validity of Assuming Equilibrium Between Liquid Water and Vapor for Simulating Evaporation. Water Resour. Res. 55, 9858–9872. https://doi.org/10.1029/2019WR025113

Obembe, A.D., Abu-Khamsin, S.A., Hossain, M.E., 2016. A Review of Modeling Thermal Displacement Processes in Porous Media. Arab. J. Sci. Eng. 41, 4719–4741. https://doi.org/10.1007/s13369-016-2265-5

Olver, P.J., 2016. Introduction to Partial Differential Equations, 2nd ed. Springer, London. https://doi.org/10.1016/S0079-8169(08)60768-0

References

Özgümüš, T., Mobedi, M., Özkol, Ü., Nakayama, A., 2013. Thermal dispersion in porous media - A review on the experimental studies for packed beds. Appl. Mech. Rev. 65, 1–19. https://doi.org/10.1115/1.4024351

Pan, M., Huang, Q., Feng, R., Xu, X., Xiong, Y., Huang, G., 2019. Improving the Estimation of Hydraulic and Thermal Properties of Heterogeneous Media via the Addition of Heat Loss. Vadose Zo. J. 18, 1–12. https://doi.org/10.2136/vzj2018.08.0149

Park, B.H., Bae, G.O., Lee, K.K., 2015. Importance of thermal dispersivity in designing groundwater heat pump (GWHP) system: Field and numerical study. Renew. Energy 83, 270–279. https://doi.org/10.1016/j.renene.2015.04.036

Park, B.H., Lee, B.H., Lee, K.K., 2018. Experimental investigation of the thermal dispersion coefficient under forced groundwater flow for designing an optimal groundwater heat pump (GWHP) system. J. Hydrol. 562, 385–396. https://doi.org/10.1016/j.jhydrol.2018.05.023

Perlmutter, N.M., Lieber, M., 1970. Dispersal of Plating Wastes and Sewage Contaminants in Ground Water and Surface Water, South Farmingdale - Massapequa Area, Nassau County, New York. https://doi.org/10.3133/wsp1879G

Peterson, R.A., Cavanaugh, J.E., 2019. Ordered quantile normalization: a semiparametric transformation built for the cross-validation era. J. Appl. Stat. 0, 1–16. https://doi.org/10.1080/02664763.2019.1630372

Pophillat, W., Bayer, P., Teyssier, E., Blum, P., Attard, G., 2020. Impact of groundwater heat pump systems on subsurface temperature under variable advection, conduction and dispersion. Geothermics 83, 101721. https://doi.org/10.1016/j.geothermics.2019.101721

Pruess, K., Oldenburg, C.M., Moridis, G.J., 1999. TOUGH2 User's Guide Version 2. https://doi.org/10.2172/751729

Quintard, M., 2015. Transfers in porous media. Spec. Top. Rev. Porous Media 6, 91–108. https://doi.org/10.1615/SpecialTopicsRevPorousMedia.2015013158

Quintard, M., Kaviany, M., Whitaker, S., 1997. Two-medium treatment of heat transfer in porous media: Numerical results for effective properties. Adv. Water Resour. 20, 77–94. https://doi.org/10.1016/s0309-1708(96)00024-3

Quintard, M., Whitaker, S., 1995. Local thermal equilibrium for transient heat conduction: theory and comparison with numerical experiments. Int. J. Heat Mass Transf. 38, 2779–2796. https://doi.org/10.1016/0017-9310(95)00028-8

Ranz, W., Marshall, W.R., 1952. Evaporation from drops 1. Chem. Engng. Prog. 48, 173–180.

Rau, G.C., Andersen, M.S., Acworth, R.I., 2012a. Experimental investigation of the thermal time-series method for surface water-groundwater interactions. Water Resour. Res. 48, 1–18. https://doi.org/10.1029/2011WR011560

Rau, G.C., Andersen, M.S., Acworth, R.I., 2012b. Experimental investigation of the thermal dispersivity term and its significance in the heat transport equation for flow in sediments. Water Resour. Res. 48, 1–21. https://doi.org/10.1029/2011WR011038

References

Rau, G.C., Andersen, M.S., McCallum, A.M., Acworth, R.I., 2010. Analytical methods that use natural heat as a tracer to quantify surface water-groundwater exchange, evaluated using field temperature records. Hydrogeol. J. 18, 1093–1110. https://doi.org/10.1007/s10040-010-0586-0

Rau, G.C., Andersen, M.S., McCallum, A.M., Roshan, H., Acworth, R.I., 2014. Heat as a tracer to quantify water flow in near-surface sediments. Earth-Science Rev. 129, 40–58. https://doi.org/10.1016/j.earscirev.2013.10.015

Rau, G.C., Halloran, L.J.S., Cuthbert, M.O., Andersen, M.S., Acworth, R.I., Tellam, J.H., 2017. Characterising the dynamics of surface water-groundwater interactions in intermittent and ephemeral streams using streambed thermal signatures. Adv. Water Resour. 107, 354–369. https://doi.org/10.1016/j.advwatres.2017.07.005

Reddy, J.N., Gartling, D.K., 2010. The Finite Element Method in Heat Transfer and Fluid Dynamics. Taylor & Francis Group, Bosa Roca, UNITED STATES, UNITED STATES.

Rees, D.A.S., Bassom, A.P., Siddheshwar, P.G., 2008. Local thermal non-equilibrium effects arising from the injection of a hot fluid into a porous medium. J. Fluid Mech. 594, 379–398. https://doi.org/10.1017/S0022112007008890

Rees, D.A.S., Pop, I., 2005. Local Thermal Non-Equilibrium in Porous Medium Convection, in: Ingham, D.B., Pop, I. (Eds.), Transport Phenomena in Porous Media III. Elsevier, pp. 147–173. https://doi.org/10.1016/B978-008044490-1/50010-7

Reeves, J., Hatch, C.E., 2016. Impacts of three-dimensional nonuniform flow on quantification of groundwater-surface water interactions using heat as a tracer. Water Resour. Res. 52, 6851–6866. https://doi.org/10.1002/2016WR018841

Ren, J., Cheng, J., Yang, J., Zhou, Y., 2018. A review on using heat as a tool for studying groundwater–surface water interactions. Environ. Earth Sci. 77, 1–13. https://doi.org/10.1007/s12665-018-7959-4

Rose, P.E., Benoit, W.R., Kilbourn, P.M., 2001. The application of the polyaromatic sulfonates as tracers in geothermal reservoirs. Geothermics 30, 617–640. https://doi.org/10.1016/S0375-6505(01)00024-4

Rosenberry, D.O., Lewandowski, J., Meinikmann, K., Nützmann, G., 2015. Groundwater - the disregarded component in lake water and nutrient budgets. Part 1: Effects of groundwater on hydrology. Hydrol. Process. 29, 2895–2921. https://doi.org/10.1002/hyp.10403

Roshan, H., Cuthbert, M.O., Andersen, M.S., Acworth, R.I., 2014. Local thermal non-equilibrium in sediments: Implications for temperature dynamics and the use of heat as a tracer. Adv. Water Resour. 73, 176–184. https://doi.org/10.1016/j.advwatres.2014.08.002

Runkel, R.L., 1996. Solution of the Advection-Dispersion Equation: Continous Load of Finite Duration. J. Environ. Eng. 122, 830–832. https://doi.org/https://doi.org/10.1061/(ASCE)0733-9372(1996)122:9(830)

Russo, S. Lo, Taddia, G., 2010. Advective heat transport in an unconfined aquifer induced by the field injection of an open-loop groundwater heat pump. Am. J. Environ. Sci. 6, 253–259. https://doi.org/10.3844/ajessp.2010.253.259

References

Saltelli, A., 2002. Making best use of model evaluations to compute sensitivity indices. Comput. Phys. Commun. 145, 280–297. https://doi.org/10.1016/S0010-4655(02)00280-1

Sarris, T.S., Close, M., Abraham, P., 2018. Using solute and heat tracers for aquifer characterization in a strongly heterogeneous alluvial aquifer. J. Hydrol. 558, 55–71. https://doi.org/10.1016/j.jhydrol.2018.01.032

Schärli, U., Rybach, L., 2001. Determination of specific heat capacity on rock fragments. Geothermics 30, 93–110. https://doi.org/10.1016/S0375-6505(00)00035-3

Schincariol, R.A., Schwartz, F.W., 1990. An experimental investigation of variable density flow and mixing in homogeneous and heterogeneous media. Water Resour. Res. 26, 2317–2329. https://doi.org/10.1029/WR026i010p02317

Schneidewind, U., van Berkel, M., Anibas, C., Vandersteen, G., Schmidt, C., Joris, I., Seuntjens, P., Batelaan, O., Zwart, H.J., 2016. LPMLE3: A novel 1-D approach to study water flow in streambeds using heat as a tracer. Water Resour. Res. 52, 6596–6610. https://doi.org/doi:10.1002/2015WR017453

Schwarz, G., 1978. Estimating the dimension of a model. Ann. Stat. 6, 461–464. https://doi.org/doi:10.1214/aos/1176344136

Seibert, S., Prommer, H., Siade, A., Harris, B., Trefry, M., Martin, M., 2014. Heat and mass transport during a groundwater replenishment trial in a highly heterogeneous aquifer. Water Resour. Res. 50, 9463–9483. https://doi.org/10.1002/2013WR015219

Seibertz, K.S.O., Chirila, M.A., Bumberger, J., Dietrich, P., Vienken, T., 2016. Development of in-aquifer heat testing for high resolution subsurface thermal-storage capability characterisation. J. Hydrol. 534, 113–123. https://doi.org/10.1016/j.jhydrol.2015.12.013

Shaik, A.R., Rahman, S.S., Tran, N.H., Tran, T., 2011. Numerical simulation of Fluid-Rock coupling heat transfer in naturally fractured geothermal system. Appl. Therm. Eng. 31, 1600–1606. https://doi.org/10.1016/j.applthermaleng.2011.01.038

Shent, J., Kaguei, S., Wakao, N., 1981. Measurements of particle-to-gas heat transfer coefficients from one-shot thermal responses in packed beds. Chem. Eng. Sci. 36, 1283–1286. https://doi.org/10.1016/0009-2509(81)80162-5

Shook, G.M., 2001. Predicting thermal breakthrough in heterogeneous media from tracer tests. Geothermics 30, 573–589. https://doi.org/10.1016/S0375-6505(01)00015-3

Singh, C., Tathgir, R.G., Muralidhar, K., 2006. Experimental validation of heat transfer models for flow through a porous medium. Heat Mass Transf. und Stoffuebertragung 43, 55–72. https://doi.org/10.1007/s00231-006-0091-0

Singhal, A., Cloete, S., Radl, S., Quinta-Ferreira, R., Amini, S., 2017a. Heat transfer to a gas from densely packed beds of cylindrical particles. Chem. Eng. Sci. 172, 1–12. https://doi.org/10.1016/j.ces.2017.06.003

Singhal, A., Cloete, S., Radl, S., Quinta-Ferreira, R., Amini, S., 2017b. Heat transfer to a gas from densely packed beds of monodisperse spherical particles. Chem. Eng. Sci. 172, 1–12.

References

https://doi.org/http://dx.doi.org/10.1016/j.cej.2016.12.12

Skeel, R.D., Berzins, M., 1990. A Method for the Spatial Discretization of Parabolic Equations in One Space Variable. SIAM J. Sci. Stat. Comput. 11, 1–32. https://doi.org/10.1137/0911001

Smart, P.L., Laidlaw, I.M.S., 1977. An evaluation of some fluorescent dyes for water tracing. Water Resour. Res. 13, 15–33. https://doi.org/10.1029/WR013i001p00015

Smith, S.A., Pretorius, W.A., 2002. The conservative behaviour of fluorescein. Water SA 28, 403–406. https://doi.org/10.4314/wsa.v28i4.4913

Somogyvári, M., Bayer, P., 2017. Field validation of thermal tracer tomography for reconstruction of aquifer heterogeneity. Water Resour. Res. 53, 1–15. https://doi.org/doi:10.1002/2017WR020543

Somogyvári, M., Bayer, P., Brauchler, R., 2016. Travel-time-based thermal tracer tomography. Hydrol. Earth Syst. Sci. 20, 1885–1901. https://doi.org/10.5194/hess-20-1885-2016

Sözen, M., Vafai, K., 1990. Analysis of the non-thermal equilibrium condensing flow of a gas through a packed bed. Int. J. Heat Mass Transf. 33, 1247–1261. https://doi.org/10.1016/0017-9310(90)90255-S

Stauffer, F., Bayer, P., Blum, P., Molina-Giraldo, N., Kinzelbach, W., 2013. Thermal use of shallow groundwater, Thermal Use of Shallow Groundwater. CRC Press, Boca Raton. https://doi.org/10.1201/b16239

Stonestrom, D.A., Constantz, J., 2003. Heat as a tool for studying the movement of ground water near streams, US Geological Survey Circular. https://doi.org/10.3133/cir1260

Stopa, J., Wojnarowski, P., 2006. Analytical model of cold water front movement in a geothermal reservoir. Geothermics 35, 59–69. https://doi.org/10.1016/j.geothermics.2005.11.002

Sun, B., Tenneti, S., Subramaniam, S., 2015. Modeling average gas-solid heat transfer using particle-resolved direct numerical simulation. Int. J. Heat Mass Transf. 86, 898–913. https://doi.org/10.1016/j.ijheatmasstransfer.2015.03.046

Taniguchi, M., Sharma, M.L., 1990. Solute and heat transport experiments for estimating recharge rate. J. Hydrol. 119, 57–69. https://doi.org/10.1016/0022-1694(90)90034-U

Tavassoli, H., Kriebitzsch, S.H.L., van der Hoef, M.A., Peters, E.A.J.F., Kuipers, J.A.M., 2013. Direct numerical simulation of particulate flow with heat transfer. Int. J. Multiph. Flow 57, 29–37. https://doi.org/10.1016/j.ijmultiphaseflow.2013.06.009

Tavassoli, H., Peters, E.A.J.F., Kuipers, J.A.M., 2015. Direct numerical simulation of fluid-particle heat transfer in fixed random arrays of non-spherical particles. Chem. Eng. Sci. 129, 42–48. https://doi.org/10.1016/j.ces.2015.02.024

Taylor, K., Banks, D., Watson, I., 2016. Heat as a natural, low-cost tracer in mine water systems: The attenuation and retardation of thermal signals in a Reducing and Alkalinity Producing Treatment System (RAPS). Int. J. Coal Geol. 164, 48–57. https://doi.org/10.1016/j.coal.2016.03.013

References

Toride, N., Leij, F.J., van Genuchten, M.T., 1995. The CXTFIT Code for Estimating Transport Parameters from Laboratory or Field Tracer Experiments. Transport.

Toze, S., Bekele, E., Page, D., Sidhu, J., Shackleton, M., 2010. Use of static Quantitative Microbial Risk Assessment to determine pathogen risks in an unconfined carbonate aquifer used for Managed Aquifer Recharge. Water Res. 44, 1038–1049. https://doi.org/10.1016/j.watres.2009.08.028

Tsagarakis, K.P., Efthymiou, L., Michopoulos, A., Mavragani, A., Anđelković, A.S., Antolini, F., Bacic, M., Bajare, D., Baralis, M., Bogusz, W., Burlon, S., Figueira, J., Genç, M.S., Javed, S., Jurelionis, A., Koca, K., Ryżyński, G., Urchueguia, J.F., Žlender, B., 2018. A review of the legal framework in shallow geothermal energy in selected European countries: Need for guidelines. Renew. Energy 147, 2556–2571. https://doi.org/10.1016/j.renene.2018.10.007

Urich, C., Sitzenfrei, R., Möderl, M., Rauch, W., 2010. Einfluss der Siedlungsstruktur auf das thermische Nutzungspotential von oberflächennahen Aquiferen. Osterr. Wasser- und Abfallwirtschaft 62, 113–119. https://doi.org/10.1007/s00506-010-0188-z

Urumović, K., Urumović, K., 2014. The effective porosity and grain size relations in permeability functions. Hydrol. Earth Syst. Sci. Discuss. 11, 6675–6714. https://doi.org/10.5194/hessd-11-6675-2014

Van Antwerpen, W., Du Toit, C.G., Rousseau, P.G., 2010. A review of correlations to model the packing structure and effective thermal conductivity in packed beds of mono-sized spherical particles. Nucl. Eng. Des. 240, 1803–1818. https://doi.org/10.1016/j.nucengdes.2010.03.009

van Genuchten, M.T., Alves, W.J., 1982. Analytical Solutions of the One-Dimensional Convective-Dispersive Solute Transport Equation. Tech. Bull. - United States Dep. Agric. 1661. https://doi.org/10.1016/0378-3774(84)90020-9

Vandenbohede, A., Louwyck, A., Lebbe, L., 2009. Conservative solute versus heat transport in porous media during push-pull tests. Transp. Porous Media 76, 265–287. https://doi.org/10.1007/s11242-008-9246-4

Vandenbohede, A., Van Houtte, E., 2012. Heat transport and temperature distribution during managed artificial recharge with surface ponds. J. Hydrol. 472–473, 77–89. https://doi.org/10.1016/j.jhydrol.2012.09.028

VDI, 2013. VDI-Wärmeatlas, VDI-Wärmeatlas. https://doi.org/10.1007/978-3-642-19981-3

Vienken, T., Dietrich, P., 2011. Field evaluation of methods for determining hydraulic conductivity from grain size data. J. Hydrol. 400, 58–71. https://doi.org/10.1016/j.jhydrol.2011.01.022

Virto, L., Carbonell, M., Castilla, R., Gamez-Montero, P.J., 2009. Heating of saturated porous media in practice: Several causes of local thermal non-equilibrium. Int. J. Heat Mass Transf. 52, 5412–5422. https://doi.org/10.1016/j.ijheatmasstransfer.2009.07.003

Wagner, V., Li, T., Bayer, P., Leven, C., Dietrich, P., Blum, P., 2014. Thermal tracer testing in a sedimentary aquifer:Field experiment (Lauswiesen, Germany) and numerical simulation. Hydrogeol. J. 22, 175–187. https://doi.org/10.1007/s10040-013-1059-z

Wakao, N., Kaguei, S., 1982. Heat and mass transfer in packed beds. Gordon and Breach Science

References

Publishers, New York.

Wakao, N., Kaguei, S., Funazkri, T., 1979. Effect of fluid dispersion coefficients on particle-to-fluid heat transfer coefficients in packed beds. Correlation of nusselt numbers. Chem. Eng. Sci. 34, 325–336. https://doi.org/10.1016/0009-2509(79)85064-2

Weatherill, J.J., Atashgahi, S., Schneidewind, U., Krause, S., Ullah, S., Cassidy, N., Rivett, M.O., 2018. Natural attenuation of chlorinated ethenes in hyporheic zones: A review of key biogeochemical processes and in-situ transformation potential. Water Res. 128, 362–382. https://doi.org/10.1016/j.watres.2017.10.059

Whitaker, S., 1999. The Method of Volume Averaging, Theory and Applications of Transport in Porous Media, Theory and Applications of Transport in Porous Media. Springer, Dordrecht. https://doi.org/10.1007/978-94-017-1114-2

Whitaker, S., 1991. Improved Constraints for the Principle of Local Thermal Equilibrium. Ind. Eng. Chem. Res. 30, 983–997. https://doi.org/10.1021/ie00053a022

Whitaker, S., 1980. Heat and mass transfer in granular porous media, in: Mujumdar, A.S. (Ed.), Advances in Drying I. Hemisphere Publishing Corporation, Washington, pp. 23–61.

Wildemeersch, S., Jamin, P., Orban, P., Hermans, T., Klepikova, M., Nguyen, F., Brouyère, S., Dassargues, A., 2014. Coupling heat and chemical tracer experiments for estimating heat transfer parameters in shallow alluvial aquifers. J. Contam. Hydrol. 169, 90–99. https://doi.org/10.1016/j.jconhyd.2014.08.001

Wong, K.F., Dybbs, A., 1976. An experimental study of thermal equilibrium in liquid saturated porous media. Int. J. Heat Mass Transf. 19, 234–235. https://doi.org/10.1016/0017-9310(76)90120-4

Woods, A.W., Fitzgerald, S.D., 1997. The vaporization of a liquid front moving through a hot porous rock. Part 2 Slow injection. J. Fluid Mech. 3443, 303–316. https://doi.org/https://doi.org/10.1017/S0022112097005855

Woods, A.W., Fitzgerald, S.D., 1993. The vaporization of a liquid front moving through a hot porous rock. J. Fluid Mech. 251, 563–579. https://doi.org/10.1017/S0022112093003520

Yagi, S., Kunii, D., Wakao, N., 1960. Studies on axial effective thermal conductivities in packed beds. AIChE J. 6, 543–546. https://doi.org/10.1002/aic.690060407

Yang, K., Vafai, K., 2011. Restrictions on the validity of the thermal conditions at the porous-fluid interface - An exact solution. J. Heat Transfer 133, 112601. https://doi.org/10.1115/1.4004350

Yang, K., Vafai, K., 2010. Analysis of temperature gradient bifurcation in porous media - An exact solution. Int. J. Heat Mass Transf. 53, 4316–4325. https://doi.org/10.1016/j.ijheatmasstransfer.2010.05.060

Yokoyama, T., Higashiura, M., Hirose, K., Iida, T., 1997. Treatment of transient heat transfer among fluids and particles in free aquifers. JSME Int. Journal, Ser. B Fluids Therm. Eng. 40, 415–421. https://doi.org/10.1299/jsmeb.40.415

Zanoni, M.A.B., Torero, J.L., Gerhard, J.I., 2017. Determination of the interfacial heat transfer coefficient

References

between forced air and sand at Reynold's numbers relevant to smouldering combustion. Int. J. Heat Mass Transf. 114, 90–104. https://doi.org/10.1016/j.ijheatmasstransfer.2017.06.020

Zhang, X., Liu, W., Liu, Z., 2009. Criterion for local thermal equilibrium in forced convection flow through porous media. J. Porous Media 12, 1103–1111. https://doi.org/10.1615/JPorMedia.v12.i11.60

Zhou, X., Gao, Q., Chen, X., Yu, M., Zhao, X., 2013. Numerically simulating the thermal behaviors in groundwater wells of groundwater heat pump. Energy 61, 240–247. https://doi.org/10.1016/j.energy.2013.09.020

Zhu, L.T., Liu, Y.X., Luo, Z.H., 2019. An enhanced correlation for gas-particle heat and mass transfer in packed and fluidized bed reactors. Chem. Eng. J. 374, 531–544. https://doi.org/10.1016/j.cej.2019.05.194

Appendix A Mesh and model domain independency

To investigate the mesh independency and possible boundary effects of our results we set up a parameter grid of the four most sensitive parameters as shown in Table A 1 resulting in $3^4 =$ 81 parameter sets.

Table A 1: Parameter setting of the simulations used to investigate the influence of the nodal distance.

Parameter	Values	Unit
Thermal conductivity solid λ_s:	1.5; 4.75; 8	W m-1 K-1
Seepage velocity v_a:	1; 15.5; 30	m d-1
Particle size d_p:	0.1; 7.5; 15	cm
Porosity n:	0.1; 0.275; 0.45	-

The remaining model input parameters are random values within the investigated ranges (see main document Table 7 for ranges). The spatial discretization was changed in the following procedure. First in nine steps from 0.002 m to 0.2 m with equal distances in the whole domain. Then in a second approach with increasing nodal distances in the model domain. Exemplary thermal BTCs for different equal distance spatial discretization are shown in Fig. A 1: While a finer mesh does not influence the thermal BTCs, the numerical model can show instability at nodal distances of 0.04 m and larger (Fig. A 1) for some parameter combinations.
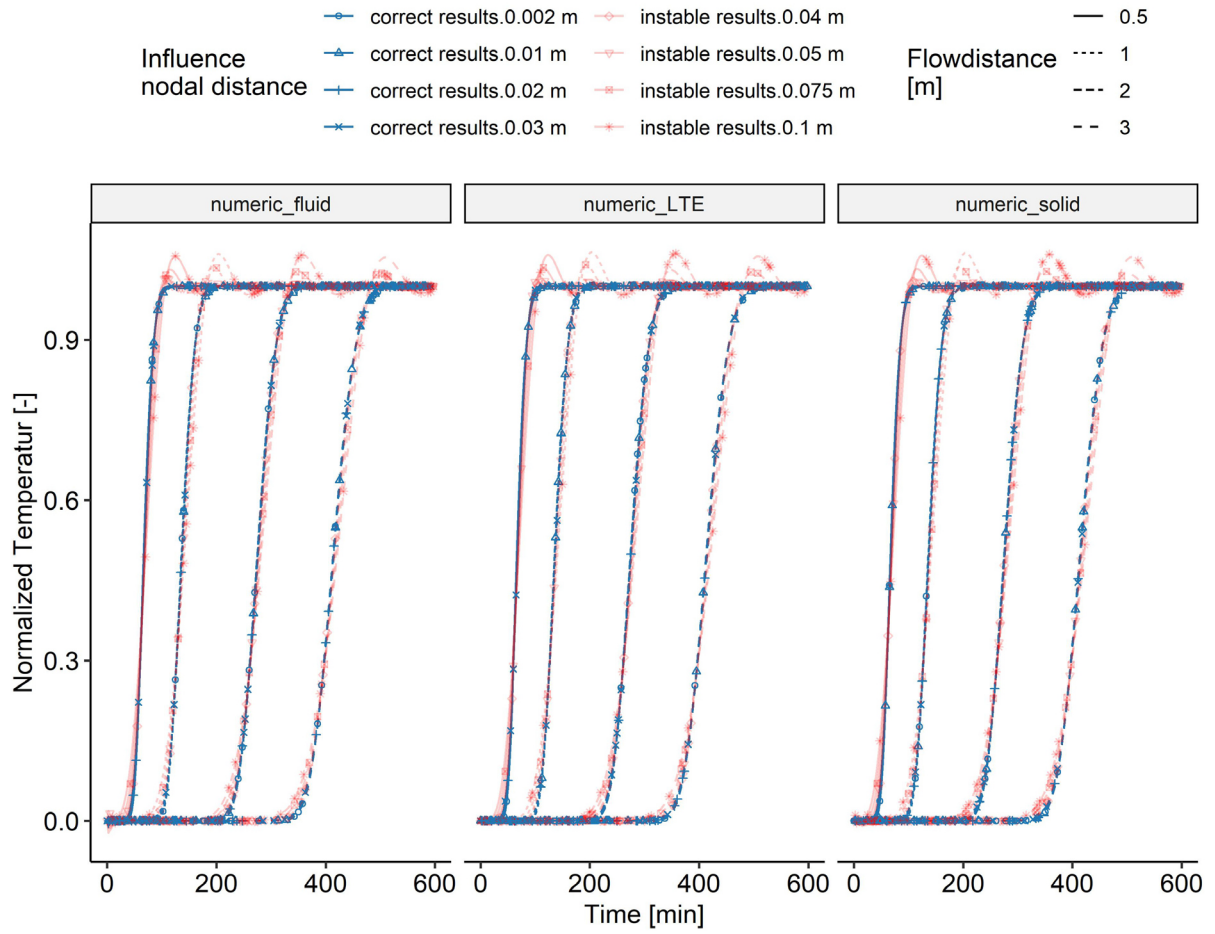
Appendix A Mesh and model domain independency

Fig. A 1: Thermal breakthrough curves of the LTNE fluid, LTNE solid and LTE model for different spatial discretization and flow distances. Up to a nodal distance of 0.01 m the resulting breakthrough curves are identical indicating the mesh independency up to this spatial discretization. Beginning with the nodal distance of 0.1 m the numerical model starts to show instability.

If one considers a deviation of up to 5 % of $LTNE_{method1,D_l}$ acceptable, the nodal distance could be increased up to 0.03 m (Fig. A 2) with an equal distance mesh. The results for a nodal distance lower than 0.01 m are identical, proving that the chosen nodal distance of 0.0025 m does not influence our results.
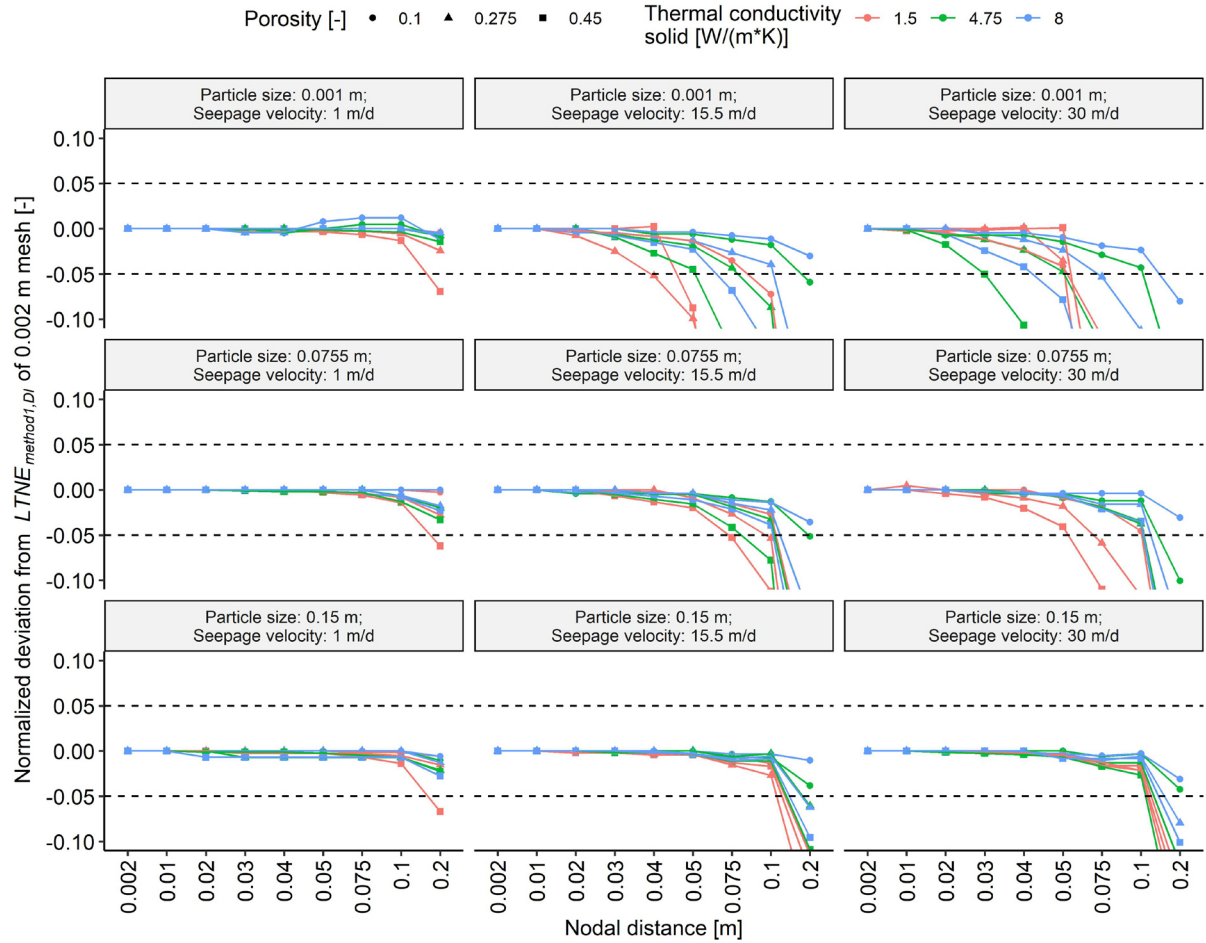
Fig. A 2: Influence of the nodal distance of the numerical model on the results. At a spatial discretization of 0.04 m and higher the values start to deviate from the expected value for more than 5 % for some parameter combinations. At nodal distances of 0.03 m and smaller the simulation results are very similar (deviation <5 %). At a nodal distance of < 0.01 m the results are identical, proofing the mesh independency of our chosen nodal distance of 0.0025 m.

When relating the nodal distance to the particle size (Fig. A 3) one can see that the results for the small particle size (upper row Fig. A 3) do not deviate for ratios up to a factor of 35 of nodal distance to particle size. This proves that the deviation at a spatial discretization larger than 0.03 m is based on numerical instability and not on the relationship between particle size and nodal distance. The deviations for larger particle sizes are therefore a result of the numerical instability due to the spatial discretization.

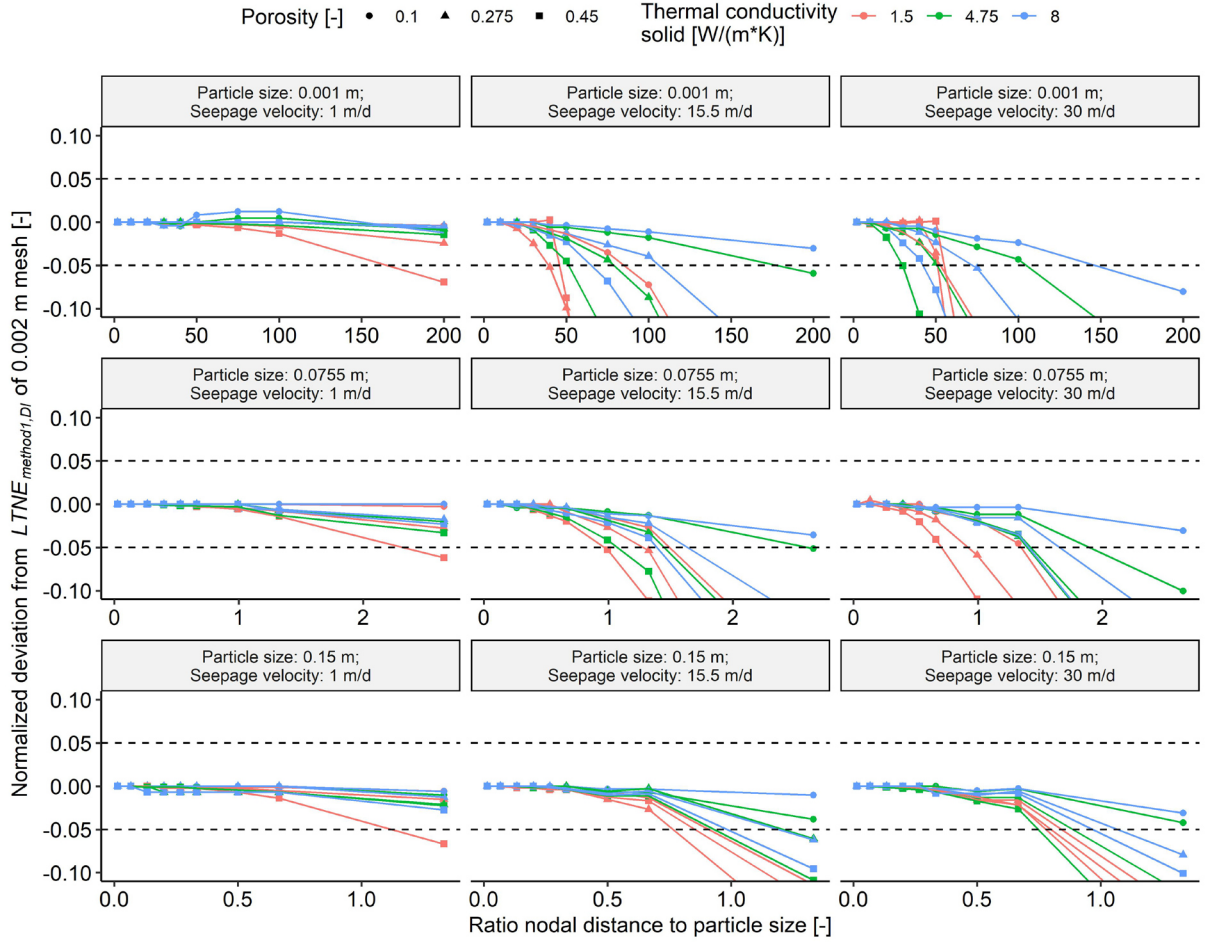# Appendix A Mesh and model domain independency

Fig. A 3: Influence of the ratio of the nodal distance to the particle size on the numerical model on the results. At higher spatial discretization, the simulations with larger particle sizes and higher seepage velocities start to deviate from the expected results due to numerical instabilities.

To further demonstrate this, we used a second approach constantly increasing the nodal distance in the model domain, which improves the numerical stability while allowing larger nodal distances with increasing flow distances. The nodal distance x_{mesh} was increased using the following function

$$x_{mesh;i} = x_{mesh;i-1} + x_{mesh;i-1} \cdot k \qquad (A1)$$

with four values of k (0.01; 0.025; 0.05; 0.1) and an initial step length $x_{mesh,i=1}$ of 0.01 m. The resulting nodal distances x_{mesh} versus the flow distance are shown in Fig. A 4. This approach allows a higher nodal distance at higher flow distances due to a higher numerical stability. Fig. A 5 shows the influence of the ratio of nodal distance to particle size at a flow distance of 5 m.

For the finer particle sizes, the nodal distance can be increased until the ratio between nodal distance and particle size reaches around 50. At larger nodal distances, the numerical model becomes instable. The results are not influenced by the mesh size up to this factor. For medium and large grain sizes, a ratio of nodal distance to particle size of around 2 can be reached until the numerical model becomes instable. This again shows that our results are not influenced by the choice 0.0025 m as a nodal distance.
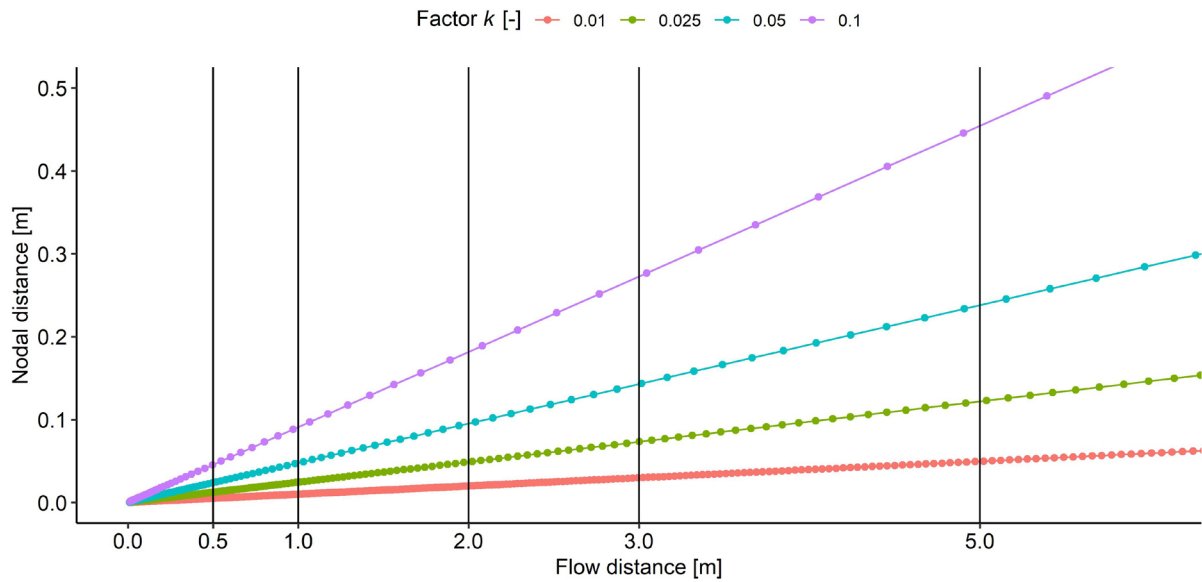
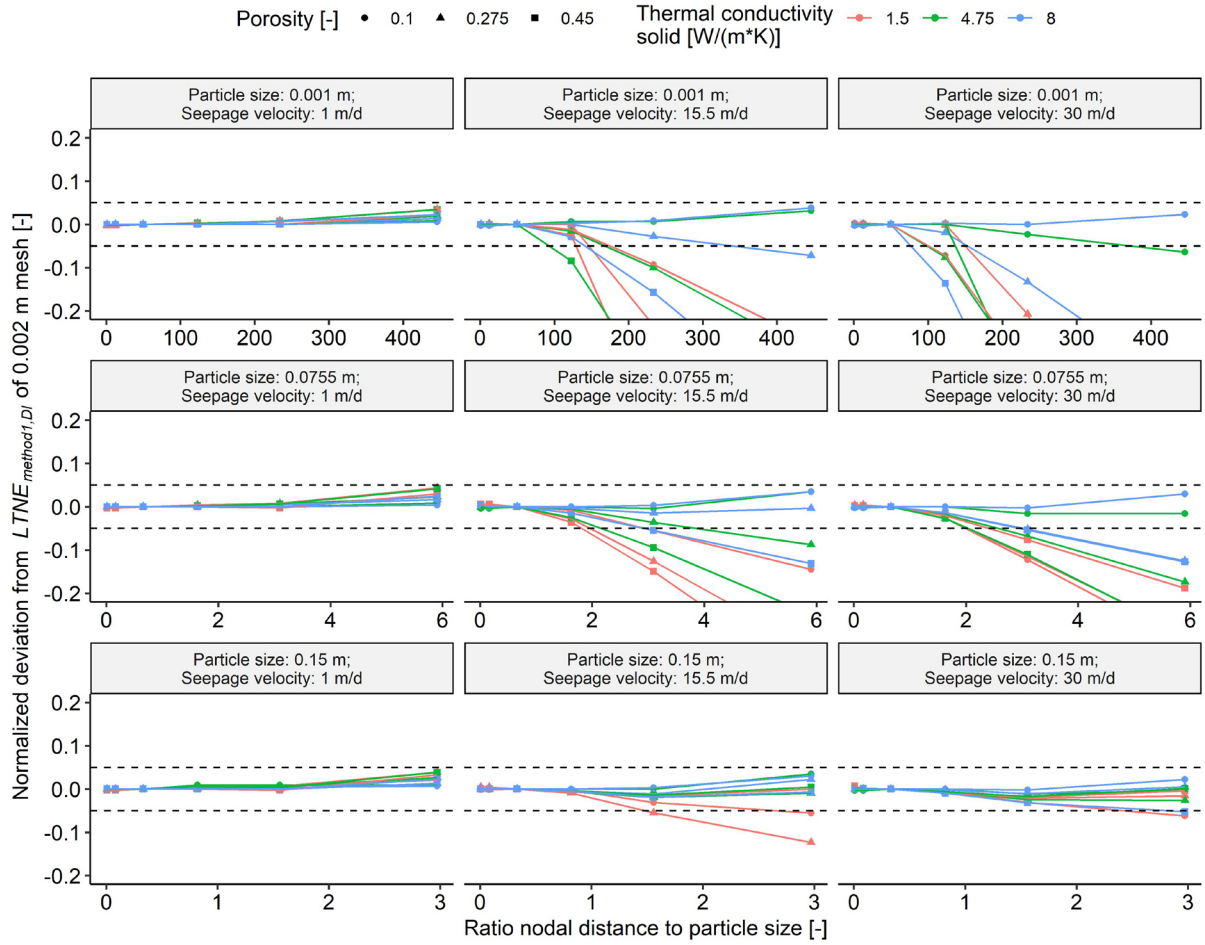Fig. A 4: Increasing nodal distance for different values of *k* with increasing flow distance.

Fig. A 5: Influence of the ratio of the nodal distance to the particle size at a flow distance of 5 m on the results of $LTNE_{method1,DI}$.

Investigation of possible boundary effects

The model domain length of 15 m was chosen to assure that boundary effects can be avoided. To verify that the results are not influenced by boundary effects, the same 81 parameter settings as explained above (Table A 1) were used. The model domain length was varied between 5 m and 15 m. The breakthrough curves (Fig. A 6) and results (Fig. A 7) are identical for all investigated model domain lengths. This demonstrates that the model domain length is sufficiently large to avoid any influence of boundary effects.
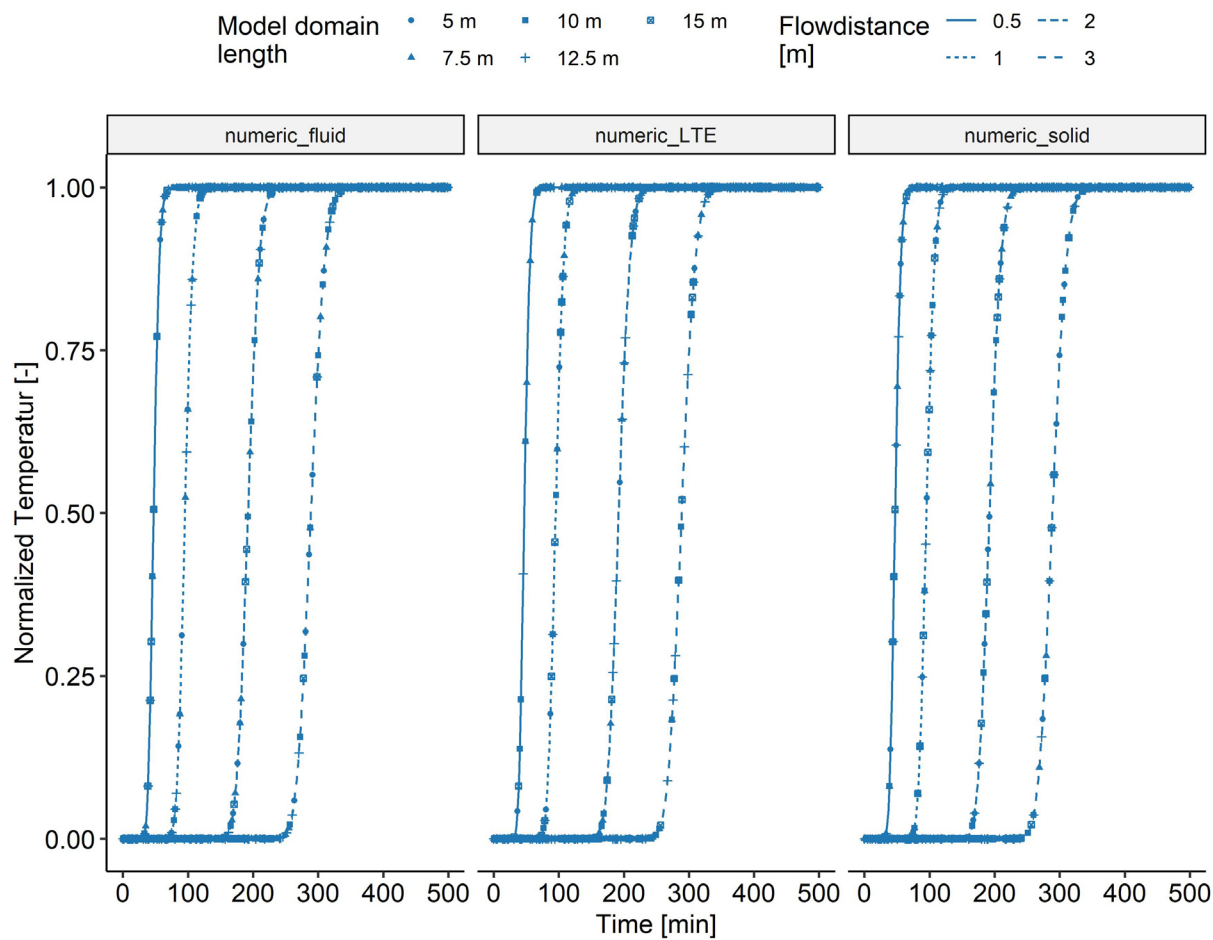
Fig. A 6: Thermal breakthrough curves for different model domain lengths. The resulting breakthrough curves are identical for all investigated model domain lengths.
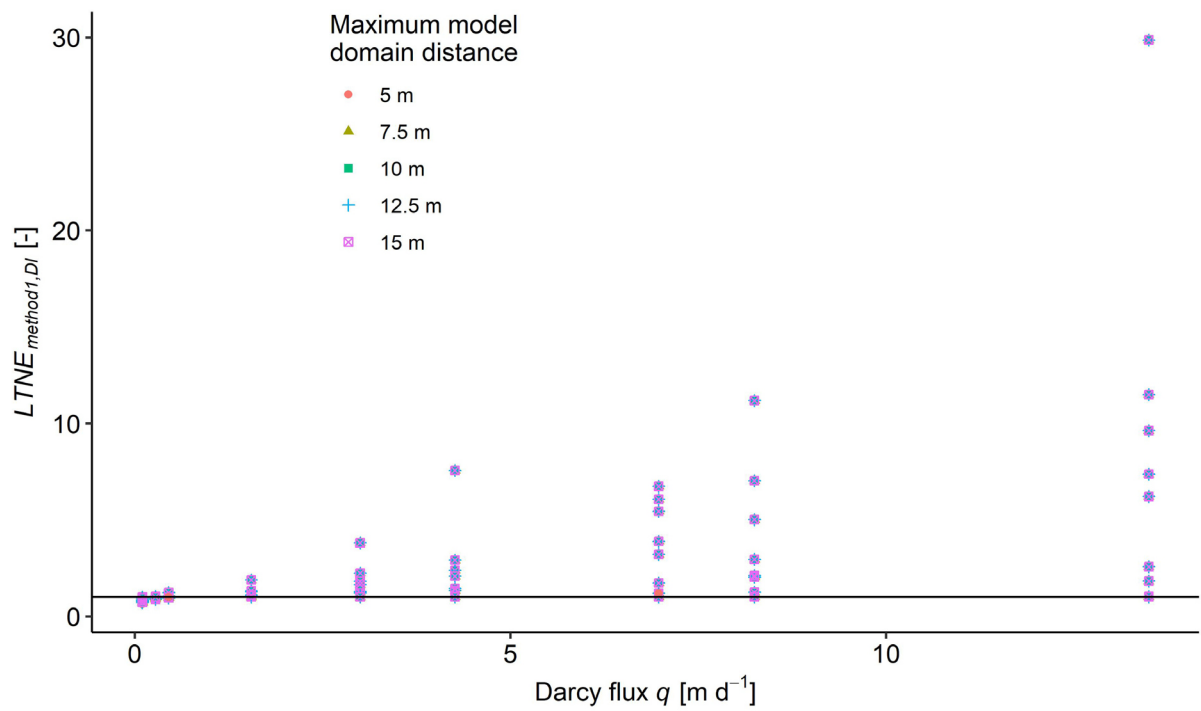
Fig. A 7: Influence of the model domain length on the results. All simulations results are identical showing that the model domain length can be decreased to 5 m without influencing the results.

Appendix B Calibratrion curve of uranine

$R^2 = 0.99995$, $p = 4.5462e\text{-}07$
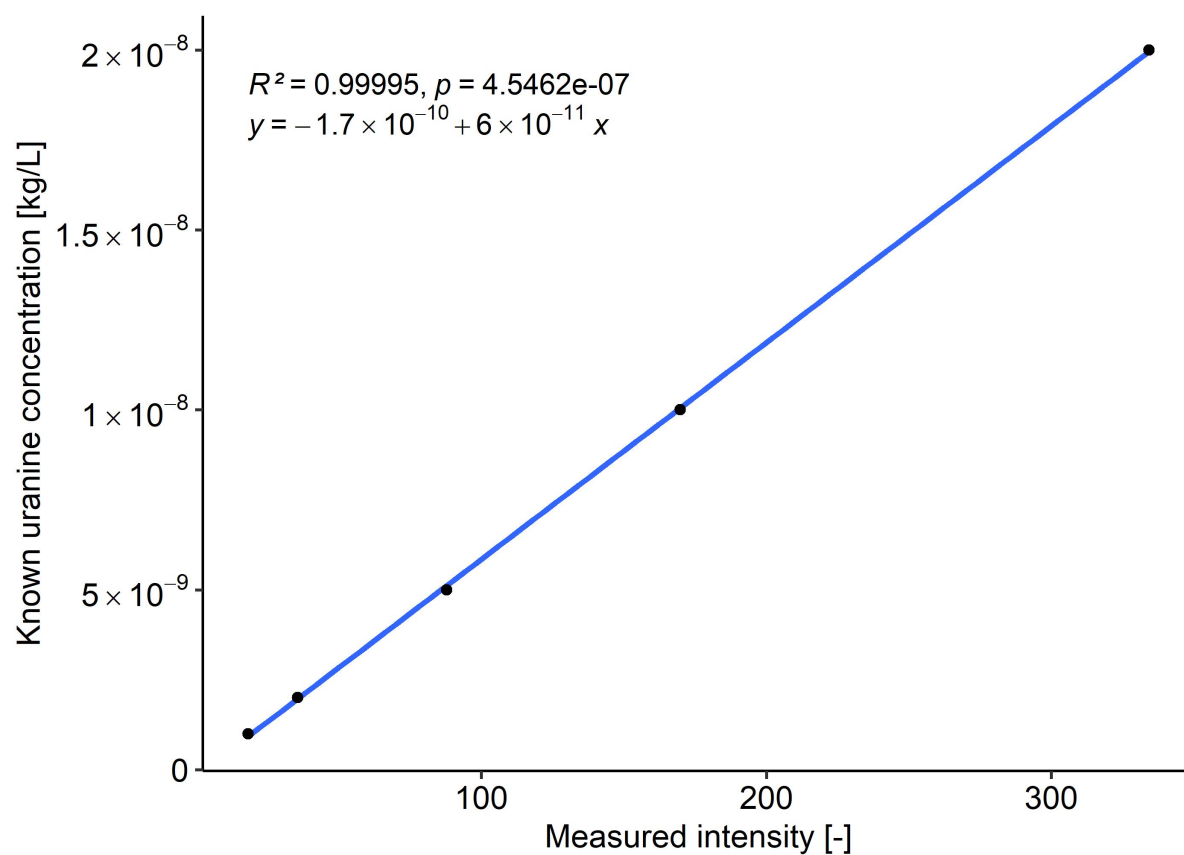$y = -1.7 \times 10^{-10} + 6 \times 10^{-11}\, x$

Fig. B 1: Linear regression of the calibration curve to determine the uranine concentration from the measured intensity.